



POLITECNICO
MILANO 1863

SCUOLA DI INGEGNERIA INDUSTRIALE
E DELL'INFORMAZIONE

Frequency stability analysis of low inertia power systems facing interactions among power electronics interfaced generators and loads equipped with frequency response capabilities

TESI DI LAUREA MAGISTRALE IN
ENERGY ENGINEERING
INGEGNERIA ENERGETICA

Author: **Lucio Radaelli**

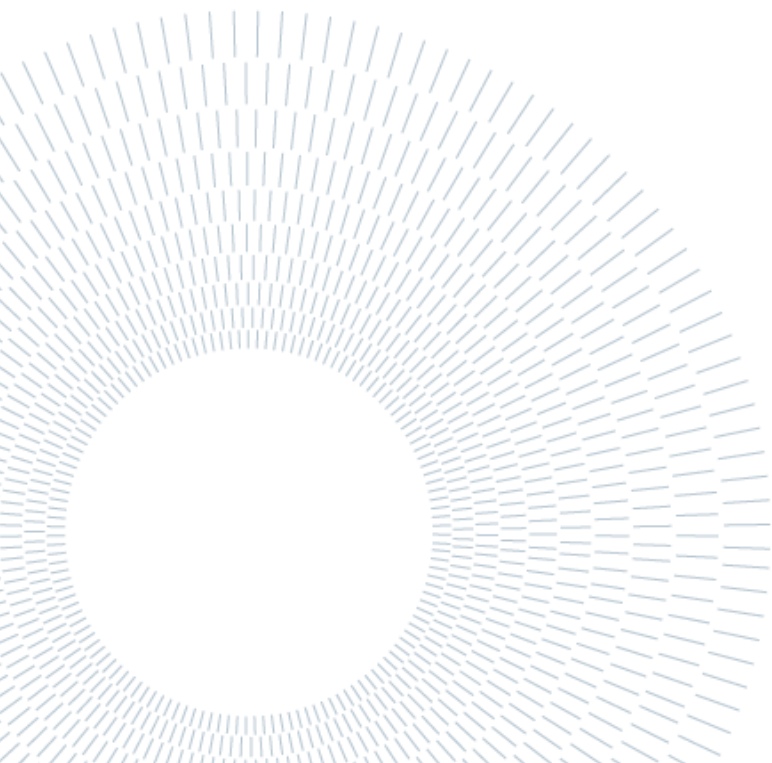
Student ID: 10560272

Advisor in Politecnico di Milano: Prof. Marco Merlo

Advisor in Universidad Politécnica de Madrid: Prof. Sergio Martínez

Academic Year: 2021-2022

This master's thesis is part of the research project "Support for frequency control of low inertia power systems through actions that complement energy storage (LowInertiaPS)", funded by the Spanish national research agency "Agencia Estatal de Investigación" within the National R&D&i Program Oriented to the Challenges of Society, of the Spanish National Plan for Scientific and Technical Research and Innovation 2017-2020, with reference PID2019-108966RB-I00 / AEI / 10.13039/501100011033.



EXTENDED SUMMARY

Introduction

In the last decades the world started perceiving the effects of the Global Warming, which is strictly linked to the greenhouse gases emissions from a plenty of sources. The most important of them, accounting for the 41.8% of the equivalent CO₂ emissions, is the energy sector [1]. It is undeniable that the energy provision to as much people as possible is a target to spread higher quality of life to everyone in the world [2], but at the same time this objective has to be met in the cleanest and most environmental friendly way to preserve our planet.

This is why, in last years, a lot of targets have been set to guide the world through a decarbonization process, and the energy sector is of course one of the centres for the attention. In particular, the shift from fossil fuelled plants to renewable generators will be a milestone along this path [3].

Actually, while talking about conventional generators displacement and their consequent substitution with renewables often some issues are not mentioned, but they are technically fundamental. This paper focuses on one of these aspects, that is crucial to ensure the proper operation of a power system, which is the frequency stability. In fact, before allowing the displacement of fossil fuelled plants, all the actions that they operate for the power system stability have to be performed by the renewable ones.

The task analysed in this work is the frequency control. It is fundamental in a power system to prevent faults, and, nowadays, it is almost completely worked by conventional power plants. Indeed, in each time instant, the active power injected and absorbed from the grid have to be equal, otherwise the frequency will oscillate from its nominal value (which is 50 or 60 Hz, depending on the location) [4]. The renewables, as conceived today, are not able to modulate their active power to counter a frequency variation, and consequently they are useless for this target. This need of covering the features of traditional plants with renewables pushed the research in developing ways to make them (and in particular the non-programmable ones) more flexible and controllable.

Before proposing a model in which they do coexist wind and photovoltaic generators equipped with innovative active power control strategies, a work of literature review has been performed, aiming to understand which approaches are recommended in research environment.

While variable-speed wind turbines have an inertia but it cannot be exploited due to the presence of power electronic converters which interconnects them with the grid [5], photovoltaics are totally without inertia.

In both cases some methods have been developed to control them in an updated way, enabling their participation in the frequency control, and, to be more centred on the aim of this paper, on the primary one. For what concerns PV technology, [6] proposes an advanced algorithm for the control of the DC-DC converter of the PV systems allowing their operation in a curtailed mode and the consequent possibility to furnish a reserve for the system's frequency regulation. It introduced a least-square curve fitting procedure for the MPP estimation in real-time, which became one of the most used techniques. However, it is able to operate just on the right side of the P-V curve, which is steeper and more subjected to environmental conditions changes. Indeed, the basis for working in curtailed mode is imposing a voltage to the module (that is different from the MPP one) for which it produces the desired power output. For example, [7] and [8] propose the operation on the left side, which is more stable in case of fluctuating irradiance due to the lower slope of the P-V curve, while [9] works on the right side. Actually, the literature does not agree on which side is the better one. This is due to the fact that the best side depends on the situation. For rapidly changing irradiance the left side is advised, while if big changes of power are required in short times, it is way better the right one. For this reason, [10] proposes a method to be able to adapt the operational side to the occurring situation. This kind of solution, which has been evaluated as optimal, is adopted also in the model presented in this work.

Concerning wind plants, a lot of methods have been proposed, both to emulate the inertia of the wind turbine with a virtual or synthetic one and to operate a primary frequency control. As explained in [11], to realize the inertia emulation an additional control loop is required. It has the function to drive the exploitation of the kinetic energy stored in the rotor of the wind turbine to model its power output as a function of the frequency deviation. This control loop can be based simply on the frequency deviation Δf , as in [12] and [13], or on both the frequency deviation and the frequency time-derivative, as shown in [14] and [15]. In the second case, the control can be seen as an inertial-droop control, meaning that it works both as inertial control and as primary frequency control. Another way to implement the primary

control is through a deloaded operation, which consists in working in a suboptimal condition to be able, in case of requirement, to increase the power output to balance a frequency deviation. This kind of control is implemented in [16].

Starting from this literature review, a customized model has been implemented, to understand how the innovative controls for PV and wind system interact each other and sustain the synchronous generators in their primary control task. The aim of this work is not just to model two renewable generators controlled in an innovative way, but rather observing how they support the system frequency stability when different perturbations occur both in the load or in the environmental conditions and in a future scenario in which they will displace a large portion of the conventional synchronous generators fleet. Furthermore, this study is set on a generic small island power system, modelled through the LFC method, which represents a critical environment due to its small size and the lack of interconnections with other power systems.

Developed model

As stated in the introduction, the developed model joins together three kinds of generators, which constitute the generation fleet of the small island power system, and a load. The system is modelled using a LFC logic, which means that it is not modelled node by node, but just using a transfer function that describes its behaviour as a whole regarding the frequency response. In this sense, the generators have not to be seen in absolute terms (i.e., in terms of power), but the focus is on their relative weights. Indeed, all the power variations (both of the generators and of the load) are expressed in per unit with respect to a common basis, and not in absolute value.

This kind of approach makes this study maybe less specific and more simplified, but at the same time the results are more general and can be extended to a large variety of situations.

It is appropriate to frame the model by showing its fundamental components, as in Figure 1.

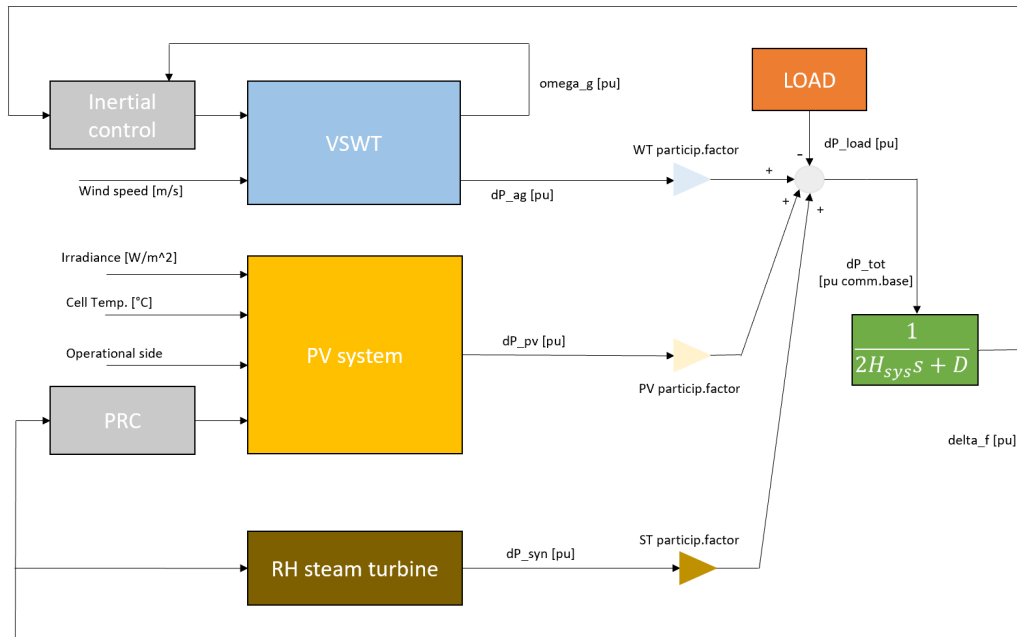


Figure 1: layout of the overall model

The two renewable generators are equipped with two additional control loops which enable their frequency response. In particular, VSWT system uses an Extended OPPT Method which implements the virtual inertia control, while the PV system is able to modulate its active power through a Power Reserve Control (PRC). Each variation of power of the i -th generator is weighted using a participation factor.

If an active power unbalance between generation and load happens, a non-null signal is generated. This, through the transfer function which models the equivalent inertia of the synchronous generators and the load damping constant, calculates the frequency deviation from the nominal value (50 Hz).

Before going in detail in the subsystems block description, it is important to state the simplifying assumptions of this work, which are quite usual in this kind of study. They are mainly related to the ambient conditions: in the simulations, they are accounted the effects of variable wind speed, variable irradiance and ambient temperature. To make the model simpler, the non-uniform distribution of the wind resource among different wind turbines is neglected, since they are considered as an aggregate; the same happens for photovoltaic modules, which work under the assumption of uniform radiation and shading is neglected.

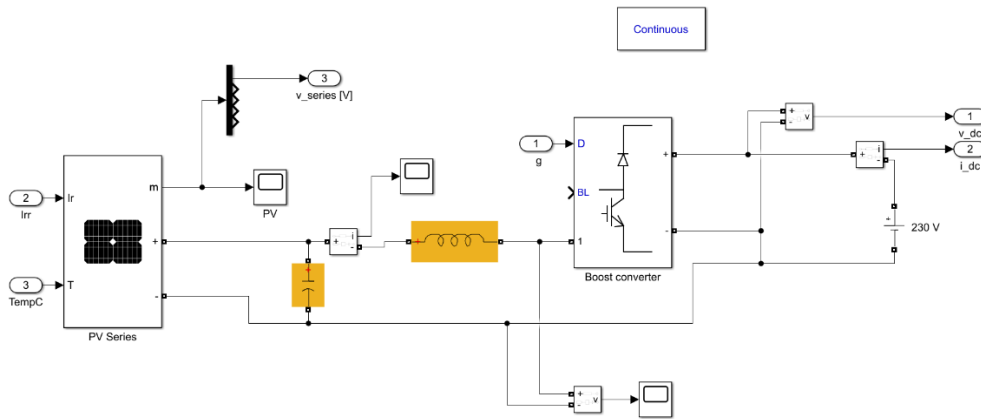


Figure 2: PV electrical subsystem block scheme

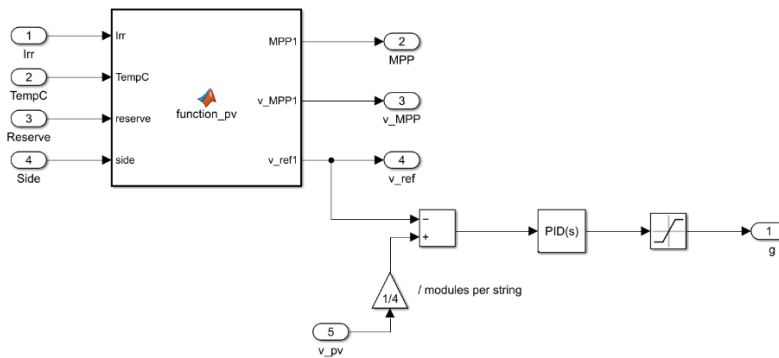


Figure 3: voltage control block scheme

The PV system is composed by two subsystems: the electrical one (Figure 2), which models it under an electrical point of view, and the voltage control subsystem (Figure 3). Schematically, the voltage control subsystem receives the irradiance and temperature measurements, as well as the required reserve command coming from the PRC block and the operational side signal (which imposes the operation on the left or on the right of the P-V curve). Starting from the ambient conditions measurements, it estimates in real-time the P-V curve using a five parameters single diode model (implemented in a MATLAB function), and then it calculates the duty cycle to be imposed to the DC-DC converter of the electrical subsystem block to operate the PV modules at the desired voltage (power) level. The electrical subsystem, on the other hand, is constituted by a predefined Simulink PV array block, which has been imposed to be a series of 4 modules of the model SOLARTECH POWER SPM210P, a capacitor in parallel with the array and a boost converter.

The PRC block is required to produce a reserve signal for the PV system block. It receives the signal of frequency deviation and adapts the reserve level using a droop

of 5%, which is identical to the value of droop of the equivalent synchronous generator present in the model. This value has been found as a compromise: if the droop is smaller (ex. 1-2%) the reserve deploys too fast and the PV system is not anymore able to participate to the primary frequency control until the signal is not externally re-initialized, while if it is too large the adaptation of power does not support the other generators in their frequency control action in a significant manner.

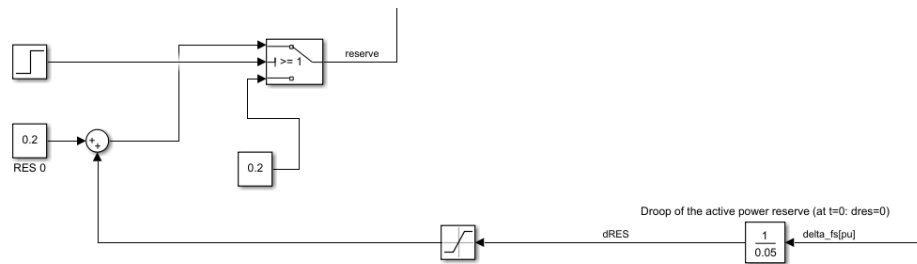


Figure 4: PRC subsystem block scheme

Concerning the wind turbine system, it has been modelled as proposed in [17]. This layout is formed by five subsystems interacting each other that compose the wind turbine system. Following a conceptual path from the wind speed to the output power, they are met in sequence: a predefined Simulink wind turbine block, which receives the wind speed, the low-speed shaft rotational speed and the pitch angle signals and calculates the mechanical torque applied to that shaft; this torque signal is compared in the mechanical system (which represents the gearbox mechanisms) with the torque applied to the DFIG generator, and, through a first-order dynamics represented by a transfer function the rotational speeds of the two shafts are calculated; the high-speed shaft signal is used in the speed governor block to calculate the new power setup, compared in the same block with the actual power to calculate the reference generator torque; in the DFIG, simply modelled through another first-order dynamics, the reference torque is imposed to the generator; a pitch control block adapts the pitch angle, if necessary, as a function of the high-speed shaft rotational speed, to limit the output power to the maximum value for wind speeds higher than the nominal one.

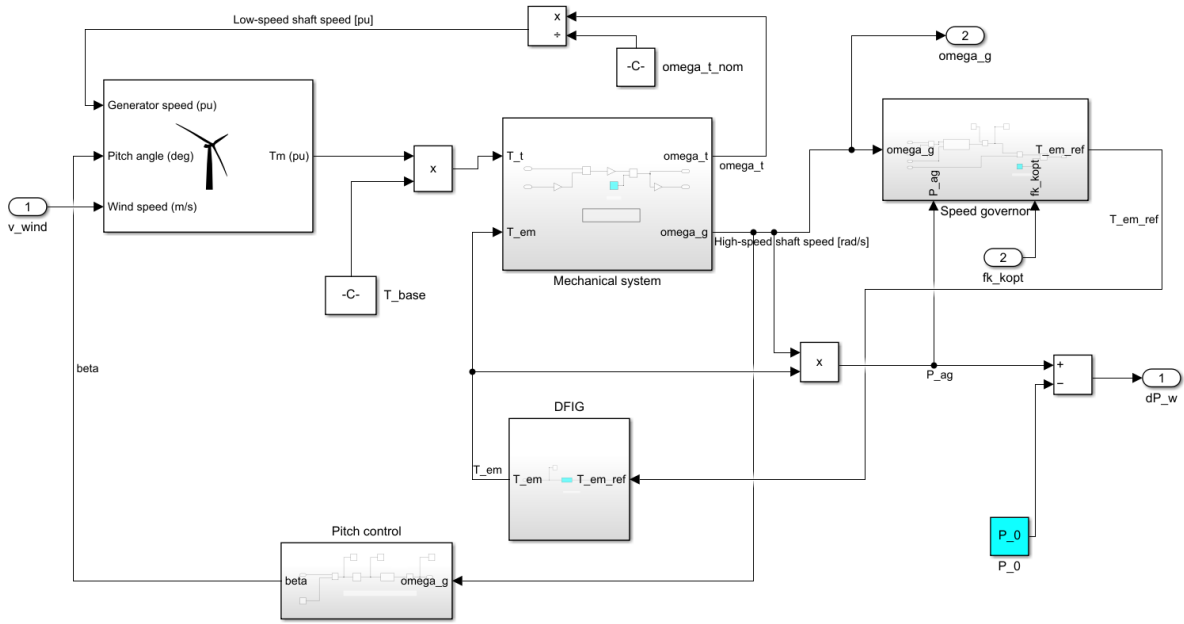


Figure 5: wind turbine system block scheme

The inertia control is grafted in this model inside the speed-governor block. In particular, a multiplication factor $f_{k,opt}$ (which is calculated in the inertial control block) called *signal for the optimization zone* is used to shift the operation of the wind turbine from the MPPT curve to other curves by exploiting the kinetic energy of the rotor (Figure 6). This method is called Extended OPPT Method [18]. The control function of the method is shown in Equation. As can be observed, $f_{k,opt}$ depends both on the frequency deviation and on the time derivative of the frequency. Indeed, the effectiveness of this virtual inertia algorithm depends both on the magnitude of the frequency disturbance (through Δf_s and df_s/dt) and on the initial kinetic energy stored in the rotor before the disturbance.

$$f_{k,opt} = \left(\frac{\omega_{g0}[pu]}{\omega_{g0}[pu] + k_{vir}\Delta f_s[pu]} \right)^3 - W_{vir} \frac{k_0}{K_{opt}\omega_{g0}^3[pu]} f_s[pu] \frac{df_s[pu]}{dt} \quad (1)$$

where:

$$K_0 = 2 \frac{\omega_{g0}[pu]}{\omega_{s0}[pu]} k_{vir} H_{WT} \quad (2)$$

with $\omega_{s0}[pu]$ that is the pre-disturbance rotational speed corresponding to the system frequency, that in per unit is equal to 1.

The inertia control block simply implements these equations in a block scheme, providing as final output the $f_{k,opt}$ signal, which, has already mentioned, is used to shift the operating point of the turbine.

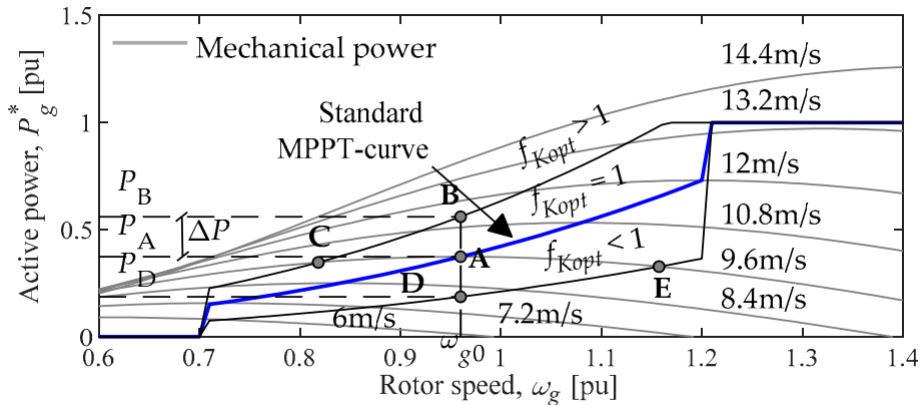


Figure 6: Extended OPPT method [18]

Looking at the P - ω chart in Figure 6, it is possible to understand the functioning of the OPPT algorithm. Under the hypothesis of constant wind speed and normal operating conditions, the generator will deliver a power P_A , associated with a rotational speed ω_{g0} . If it happens an underfrequency event, caused for example by a mismatch between the injected and the consumed power in the system, it will be required an increase in the power output of the turbine to reduce as much as possible the frequency oscillation. In particular, the non-null value of Δf_s and df_s/dt will activate the inertial response emulation of the wind turbine, with a consequent shift of the MPPT curve upwards ($A \rightarrow B$). The higher the severity of the underfrequency event (and so the magnitude of Δf_s and df_s/dt), the higher will be the value assumed by P_B . In this situation, the unbalancing between the active power extracted from the electric generator and the mechanical power delivered at the turbine shaft will cause a deceleration of the rotating masses of the turbine, testifying the exploitation of the turbine kinetic energy. This deceleration moves the operational point on the left ($B \rightarrow C$), reaching a new equilibrium condition when P_C coincides with P_A , situation that corresponds to a balance between the mechanical power delivered by the turbine and the active power extracted by the generator (P_C). When the support is not anymore necessary, the system returns to the initial state ($C \rightarrow A$), preparing it for future requirements [18].

Putting together these two renewable generators with a reheated steam turbine (modelled as in [4] it is obtained the scheme proposed before in Figure 1. On this scheme various simulations have been performed in four different scenarios: with primary frequency control operated only by conventional generators, by PV and conventional, by wind and conventional and by all the generators. They have been studied different situations, as load active power variations (both sinusoidal and step

change), wind speed and irradiance profiles and different participation factor combinations.

Simulations results

A first outlook on the effectiveness of the implemented algorithms can be observed in a test in which a step variation of the load power is introduced. In particular, the model has been tested with steps of different magnitudes, obtaining the same shape of frequency response in all the cases, but of course with different entities.

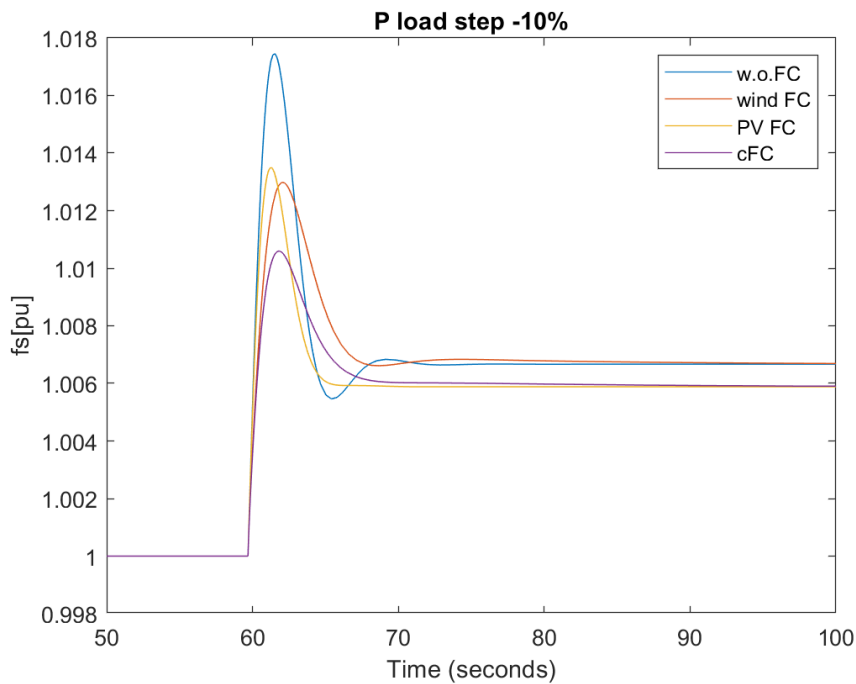


Figure 7: frequency response after a load power step of -10%

Figure 7 reports the response in case of a sudden reduction of the load power of the 10%. It can be clearly observed how the introduced updated controls help the system in improving its frequency stability by significantly reducing the frequency nadir. They operate in a satisfying manner both individually and together, situation in which they act in synergy to further increase the effectiveness of the primary frequency control.

It is interesting to consider also a more realistic load perturbation: a continuous small variation of the load active power (modelled through a sinusoid with the amplitude equal to 0.5%) followed by the same sudden step. This implies that a part of the reserve is already used to compensate the small oscillation, so it is not anymore available in contributing against the step power reduction. The resulting frequency trend (Figure 8) testifies that the updated control algorithms are able to follow and

react also to such a small and periodic variations of the load power, as well as to a step that follows them. Also in this situation the participation of the two renewables to the primary frequency control helps significantly the synchronous generator in limit the frequency deviation.

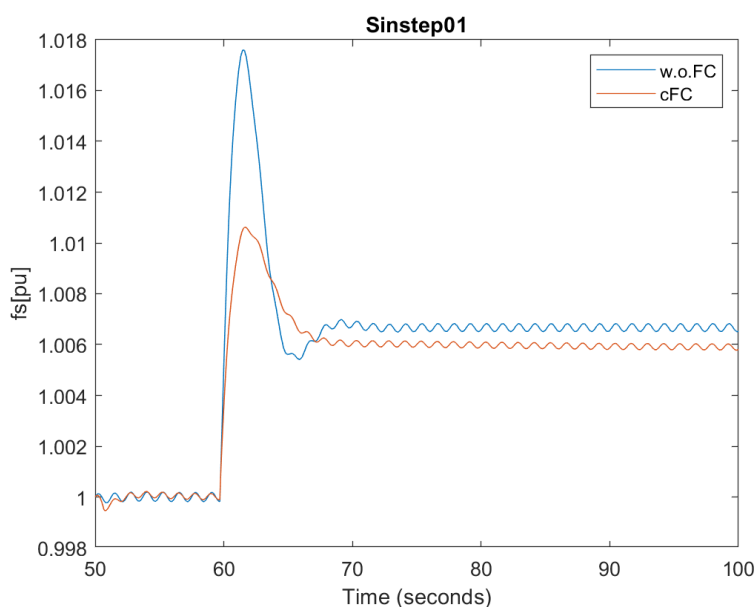


Figure 8: frequency response to small sinusoidal oscillations of load power

Other perturbations that are particularly interesting in the time frame in which the primary frequency control is activated are the ambient conditions variations. In particular, the more critical are the faster ones related to a wind speed variation, while in case of irradiance and temperature changes they are slower and less intense. This means that the renewables controls need to be ready to face also this kind of condition. The wind variability can be even more critical if combined with a large step variation as the one already presented and with a large renewables penetration. In Figure 9 can be seen the result of such a critical condition on the frequency in case of a large renewable penetrated system (which can easily be imagined as a future power system of a small island) both with and without the updated algorithms for the control of PV and VSWT.

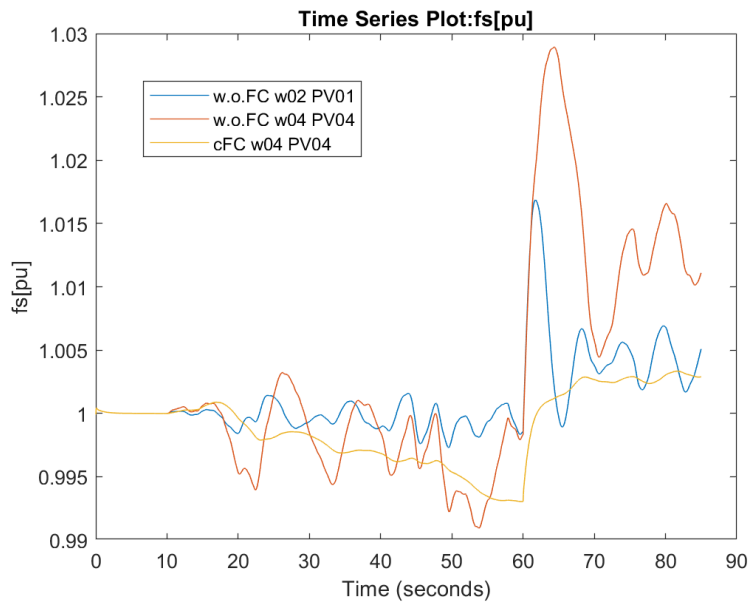


Figure 9: frequency trend for real wind profile and step variation of load power in a largely penetrated system

It is clear that the help of these algorithms is huge, particularly if considering the RoCoF reduction and the smoothing effect on the frequency profile.

Conclusions and proposals for future developments

Looking ahead to a future in which renewables will be more and more relevant in the energy mix, they have been implemented two strategies starting from the literature proposed models to make them able to help (or substitute) conventional generators in keeping the power system stable. In particular, Power Reserve Control and Extended OPPT Method have been adopted in this work aiming in allowing respectively photovoltaic modules and variable-speed wind turbines to participate to the primary frequency control. In this sense, the results obtained in this work, especially when the two controls coexist, are encouraging. Indeed, even if the Power Reserve Control introduces a very small increase of the RoCoF in the very few instants after a strong and sudden perturbation, the frequency nadir is reduced with respect to the case in which the frequency is not supported by renewables, especially in a future scenario in which they are massively present in the power system.

The model and the results rely on some simplifications, which make them general but at the same time lacking in detail. For this reason, there is open field for future developments of the present work in some areas.

One of the possible fields of improvement is the modelling of the photovoltaic system, in particular for what concerns the shading conditions and the inequality in the sun resource distribution among the modules. Indeed, this would allow a deeper study about the capability of photovoltaic systems in supporting the system's frequency in more realistic situations.

Another possible improvement regards the modelling of the load. Indeed, it could be really interesting to better characterize its active power demand profile in case of a small island, to make the study even more realistic and fitted on real field situations.

The last and more challenging proposal for future developments would be to model node by node a small system as the one studied in an overall way with the LFC approach in this work. This of course will make it completely fitted to a specific practical situation, allowing to catch some details that for sure with a general approach are invisible; at the same time, the adaptation to a very specific contest removes one of the biggest advantages of the LFC approach, which is the generality and the versatility of the developed model. Nevertheless, since the results obtained are promising, such improvements are for sure interesting and can add a lot of cues to go deeper in the knowledge of this argument that in the future will be at the centre of the scientific focus.

Key-words: primary frequency control, load frequency control, photovoltaic power curtailment, variable-speed wind turbine virtual inertia.

Abstract in italiano

Una delle linee di azione per limitare il riscaldamento globale prevede la progressiva sostituzione di generatori “convenzionali” con generatori rinnovabili. E’ dunque fondamentale riuscire a dare continuità alle azioni di stabilizzazione del sistema elettrico che questi ultimi svolgono, sviluppando strategie per fornirli anche con fonti rinnovabili non programmabili.

In questo lavoro l’attenzione è posta sul controllo primario di frequenza che, per via del rimpiazzamento di turbine a vapore e a gas, è indebolito da una diminuzione dell’inerzia totale del sistema e alla contestuale riduzione dei generatori che sono in grado di operarlo. Sono dunque stati adottati due algoritmi per controllare la potenza attiva rispettivamente di fotovoltaico ed eolico (Power Reserve Control e Extended OPPT Method), studiando i benefici che ne conseguono in vari scenari. E’ stato scelto di ambientare questo studio su un sistema elettrico di una piccola isola, schematizzato tramite la logica Load Frequency Control, che rappresenta il caso più critico per la sua piccola taglia e mancanza di interconnessioni con altri sistemi elettrici.

I test e le simulazioni, svolti sul software Simulink, prevedono la sottoposizione del sistema a differenti perturbazioni, come riduzione a gradino del carico, piccole oscillazioni sinusoidali, variazioni nelle condizioni ambientali e incremento della penetrazione di rinnovabili, con lo scopo di dimostrare che questi algoritmi avanzati per il controllo dei generatori rinnovabili possono portare enormi benefici per stabilità di frequenza, e sono altresì in grado di fronteggiare agilmente diversi tipi di perturbazione che possono investire il sistema.

Parole chiave: controllo primario di frequenza, controllo della potenza attiva di impianti fotovoltaici, inerzia virtuale di turbine eoliche.

Contents

EXTENDED SUMMARY	i
Abstract in italiano	xiii
Contents.....	xv
Introduction	1
1 Introduction about frequency stability, inertia and primary frequency control of a power system	5
1.1. Frequency stability	5
1.2. The concept of power system inertia.....	7
1.3. Primary frequency control.....	8
1.4. Boundary conditions of the primary frequency control.....	11
1.5. Remuneration for primary frequency control.....	14
2 Active power control of a photovoltaic system	17
2.1. Problems related to a large PV penetration.....	17
2.2. New functionalities required to PV plants.....	19
2.3. PV system integrated with battery energy storage systems (BESS)	22
2.4. Overview of the algorithms for PV active power control proposed in literature	24
3 Active power control of wind turbines.....	29
3.1. Primary frequency control provision with wind turbines.....	30
3.1.1. Inertial control with wind turbines.....	31
3.1.2. De-loaded operation of VSWTs.....	32
4 Developed model for small island power system with renewable generators participating to the primary frequency control.....	35
4.1. Assumptions of the model.....	36
4.2. Overview of the general model.....	37
4.3. Photovoltaic generators model	39
4.3.1. Voltage control subsystem	41
4.3.2. Electrical model of the PV module subsystem.....	47
4.3.3. Reserve adaptation to frequency changes	50

4.4.	Variable Speed Wind Turbine participating to primary frequency control model	51
4.4.1.	VSWT model.....	51
4.4.2.	Inertia control subsystem	61
4.5.	Steam turbine model.....	63
4.6.	Initialization procedure	65
4.6.1.	PV system initialization	65
4.6.2.	Wind turbine system initialization.....	69
4.6.3.	Complete model initialization	71
5	Simulations summary and metrics to evaluate the results	73
5.1.	List of the performed simulations.....	73
5.2.	Tips to reduce the simulation time	78
5.3.	Metrics to evaluate the primary frequency control adequacy	80
5.4.	Solver selection	81
6	Simulation results	83
6.1.	Load active power step up/down	83
6.2.	Small sinusoidal oscillations and step down load active power.....	88
6.3.	Variable environmental conditions	89
6.4.	Increasing renewables penetration.....	93
7	Conclusions and future developments proposals	99
	Bibliography	103
	List of Figures	109
	List of Tables	113
	List of symbols	115
	Acknowledgments.....	117

Introduction

In the last decades decarbonization targets have been set in order to face and to limit the global warming. On a timeline, the last milestone of this challenge has been set with the Paris Agreement in 2015, which established the goal of keeping the global warming well below 2°C, and possibly under 1.5°C, with respect to the pre-industrial level [19] [20]. In this scenario, one of the most important layers of intervention is the energy sector, that in 2019 accounted for the 41.8% of the CO₂ emissions in the world, consequently representing their major contributor [1]. An outlined solution to reduce its impact is the increase in renewable energies utilization. In this sense, for example, the EU set the target of covering the 32% of its energy consumptions with renewable energies in 2030 [21].

These ambitious targets are inducing deep changes in the energy mix, leading to equally difficult technological challenges. In particular, renewable generators are displacing conventional fossil-fueled ones, leading to a variety of issues mainly related to their non-dispatchability and inability in providing ancillary services.

A potential future scenario is presented in report [3]. It offers an immediate idea of the modification that will hit the electric system in less than thirty years: if the world will adopt measures in order to accomplish with the Paris agreement (“REmap Case”), the share of renewable energies in power generation sector could reach the 86%, while the one of variable renewables such as solar and wind would be about 60%, with an annual addition of capacity respectively up to 360 GW/yr for photovoltaic plants and up to 240 GW/yr for wind plants in 2050.

Starting from this estimation, it is clear how important it will be in the future to make renewable generators able to provide the services that nowadays are responsibility of the traditional ones. According to this, regulators and System Operators (SO) are starting to ask for some of these services also to renewable plants in the updated versions of grid codes, to face the system developing and keep ensuring its safety and reliability [22]. For variable renewable sources the implementation of techniques to meet these requirements is asking huge research efforts due to their nature. In fact, they are used to be connected with the grid through power electronic devices, which have no rotational parts, making them actually not contributing to the total inertia of the power system.

Inertia is a fundamental concept while analyzing a power system. Indeed, transient stability and frequency stability are strongly related to the kinetic energy present in

the system, which amount in turn is correlated to the inertia constant. A reduction of the total inertia constant is reflected in a stability decrease [23].

Focusing on the frequency stability problem, inertia constant impact can be appreciated in Equation (0.1) [23]:

$$\frac{df}{dt} = \frac{1}{2} f_0 \frac{P_{gen} - P_{load}}{S_{tot} H_{tot}} \quad (0.1)$$

where f is the frequency of the system, f_0 is the nominal frequency, P_{gen} is the total generated power in a certain time instant and P_{load} the total consumed one, S_{tot} is the sum of the rated power of all the generators and H_{tot} is the equivalent inertia constant of the system as a whole. It is evident that, if H_{tot} decreases, given a certain active power unbalance between generation and load the frequency variation will be larger.

To contain the frequency variations and keeping the frequency as close as possible to its nominal value it is thus necessary to make available certain levels of reserve at different timescales.

The spread of variable renewable energies (VRE) mentioned above impacts on the reserve problem in more than one way: the uncertainty of the primary source availability, and so of the power production, requires additional reserve in the system; the participation in the system of the conventional units that are able to provide reserves reduces, and so the stability of the system.

All the technical reasons that have been exhibited underline once again the importance of developing strategies to provide services to ensure system stability also with renewable sources.

This work is focused on the first seconds immediately after an unbalance, in which the primary reserve activates to contain as much as possible the initial oscillation of frequency after a perturbation. In particular, it will be faced the issue of acting the primary reserve with renewable generators as photovoltaic modules and wind turbines, that traditionally are not technically able to perform it, trying to understand how to implement it and whether the performances are acceptable.

In particular, Chapter 1 provides a general overview of inertia and primary control concepts; Chapter 2 and Chapter 3 respectively offer an overview of the algorithms proposed in the literature to perform primary control with photovoltaic and wind technologies; Chapter 4 describes accurately the models adopted in this work to implement the primary control on the two technologies, as well as the overall model in which they are present simultaneously; in Chapter 5 they are defined the metrics to evaluate the performances of the primary control, and they are summarized the different tests performed on the model; Chapter 6 shows the results of the tests; Chapter 7 explains the conclusions of the present work.

1 Introduction about frequency stability, inertia and primary frequency control of a power system

A power system is an extraordinarily complex entity. Its function is basically the conversion of energy from a certain naturally available source to the electrical form, which can be easily and efficiently transported to the points of consumption. This simple concept in reality hides a dense interconnections network, as well as a large generation portfolio and a huge number of points of consumption.

Reference [4] highlights how designing such a large interconnected system to ensure stable operation at minimum cost is difficult. Indeed, it is a highly non-linear system whose performances are influenced by a lot of devices with different behaviors and response characteristics. For this reason, the problem of the power system stability must not be seen as a unique problem, but rather as a combination of different ones.

This work focuses on one of these facets of the power system stability: the frequency stability.

1.1. Frequency stability

For a satisfactory operation of a power system, the frequency should remain nearly constant. Frequency stability is related to the instantaneous balance of active power demand and generation in the power grid: any unbalance will produce a frequency variation coherently with Equation (0.1).

Since frequency is common to all the system, if it is observed a change in the active power demand or production at one point, this will cause a frequency variation throughout the entire system.

[24] summarizes why it is extremely important to keep the frequency in a narrow band:

- The conventional power plants performances are strongly affected by the efficiency of the auxiliary electric motor drives. In case of low frequency their speed decreases, causing a reduction of the plant power output, leading to several cascade shutdowns of the power stations

- Frequencies lower than 47 Hz damage steam turbines; under 45 Hz lead to plants disconnection from the grid
- A deviation of frequency can overload the transformers, since they are sensitive to frequency level
- To drive at a constant speed the AC motors, used in a lot of consumer equipments, it is required a nearly constant frequency
- Frequency is often employed in electronics for timing various processes: its variation could lead to errors

Actually, the power system includes a large number of synchronous generators. They are formed by essentially two elements: the field, positioned on the rotor, and the armature, which is on the stator. In case of a turbine driving the rotor, the rotation of the field creates a rotating magnetic field which induces alternating voltages in the three-phase armature windings of the stator as well as a rotating magnetic field on the stator, which in steady-state conditions rotates with the same speed as the rotor one. However, the two fields are separated by an angular delay, which is a function of the power (torque) exchanged. The frequency of the induced voltage is synchronized with the rotor rotational speed, as well as with the grid one. The stator and rotor fields react with each other creating an electromagnetic torque opposite to the mechanical one that, in steady-state operation, balances it. If a disequilibrium between the two happens, the rotor will accelerate/decelerate.

If during an unbalance a generator runs for a certain time faster/slower with respect to the others, this will cause a relative variation of the angular shift between the rotors of different generators. If the shift is relatively small, this effect is spontaneously restored by the angular difference itself, that tends to charge more the faster machine, reducing its speed and so the angular separation; if the shift is beyond a certain limit, an increase in angular separation causes a decrease in power transferred, further increasing the separation and leading to instability. The situation just described leads the generator to a loss of synchronism with the rest of the system, since its rotor is not anymore able to generate a voltage at system frequency [4].

The ability of an interconnected synchronous machine to remain in synchronism after an unbalance is defined *Rotor Angle Stability*.

In the same way, *Frequency Stability* is defined as the ability of the power system to maintain steady state frequency after a severe system upset resulting in a significant imbalance between generation and load [25].

Since synchronous generator rotor speed is synchronized with the system frequency, the rotor angle stability is strictly correlated with the frequency stability. In fact, any change in system frequency is reflected in synchronous generator rotor speed [26].

The two are strongly impacted by the kinetic energy present in the system, that in turn is related to inertia constant of the production units powering the system. Inertia is

one the key concept to understand the influence of a large renewable penetration in power systems, and hence a more detailed explanation is given in the next section.

1.2. The concept of power system inertia

The inertia of a production unit is usually accounted between a parameter called inertia constant (H), which represents the ratio between the kinetic energy (Equation (1.1)) at nominal speed and the rated power of the unit (Equation (1.2)) [23]:

$$\varepsilon_{kin} = \frac{1}{2}J\omega^2 \quad (1.1)$$

$$H = \frac{\frac{1}{2}J\omega_0^2}{S_{nom}} \quad (1.2)$$

(J is the moment of inertia and ω the rotational speed of the mass; $\omega_0=2\pi f_0$ is the nominal rotational speed).

It is possible to calculate the total amount of kinetic energy present in a synchronous system as the sum of the kinetic energy of all the machines:

$$\varepsilon_{tot} = \sum_i \varepsilon_i = \sum_i S_i H_i \quad (1.3)$$

Formally, the right part of Equation (1.3) would hold just at the nominal frequency but, in practice, since the frequency variation is usually equal to few percent of the nominal value it can be considered a good approximation [23].

This definition of the total kinetic energy allows to calculate the total inertia constant for the system as a whole:

$$H_{tot} = \frac{\varepsilon_{tot}}{S_{tot}} = \frac{\sum_i S_i H_i}{S_{tot}} \quad (1.4)$$

in which the most appropriate value for S_{tot} is the actual active power of the load rather than the sum of the nominal power of the generators, since some of them are redundant and would lead to an underestimation of the actual constant.

This constant is particularly useful in order to understand the impact of the increase of the penetration of the variable renewable energies in the electric system. Since the renewable generators are interfaced with the system through power electronic devices they have H_i equal to zero, so they don't contribute at all to the inertia of the system.

Indeed, their spread is replacing conventional generation, reducing the total amount of kinetic energy and directly affecting the frequency stability.

After defining the concept of inertia constant, it is necessary to understand how it affects the frequency stability. By imagining to divide the response of the system to a sudden active power unbalance and represent it temporally, inertia would be the first control action that limits the frequency variation, followed by primary, secondary and tertiary control (explained in Subchapter 1.3).

In fact, since synchronous generators are directly coupled electromechanically to the grid, they naturally absorb or deliver kinetic energy in order to stabilize system frequency. This action is called *inertial response* [26]. A lower system inertia results in both larger frequency variations during normal operation and larger frequency drop due to the loss of a large production unit or the disconnection of a large load.

Some seconds after this initial and spontaneous containment of the frequency variation it becomes available the *primary reserve*.

1.3. Primary frequency control

According to the definition proposed in [27], primary control has the aim of stabilizing the system frequency at a stationary value after a disturbance in the time-frame of some seconds, but without restoring the system frequency at its original value before the event.

It is conventionally constituted by the “spinning reserve”, i.e. large production units able to very quickly vary their production by a small amount. This reserve should be spread all over the system, to be able to rapidly dab a frequency variation without stressing the transmission line and to properly dispose of reserve in all the portions of the system in case of its splitting [23].

The principle of the primary control is shown in Figure 1.1:

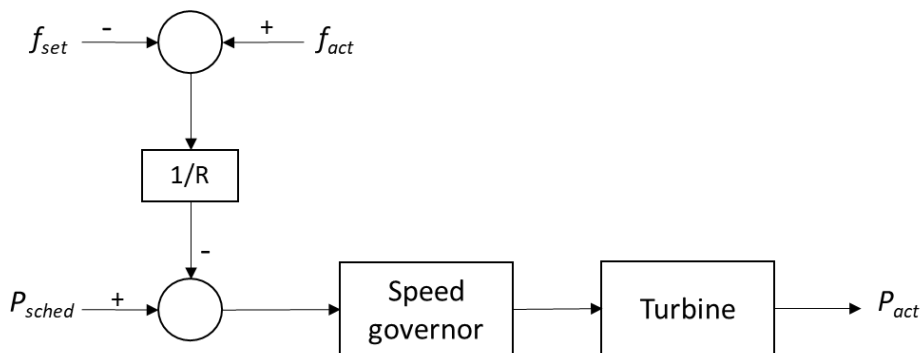


Figure 1.1: principle of primary frequency control

The difference between the actual frequency (f_{act}) and the frequency setpoint (f_{set}) (usually the nominal one, 50 Hz or 60 Hz) is used by a *droop setting* (R) to calculate how much it does vary the power with respect to the scheduled value (P_{sched}) to respond to that frequency deviation. The resulting signal arrives to the speed governor, which acts on steam valves (for a thermal power plant) or water inlet valves (for an hydropower plant) to regulate the amount of working fluid that reaches the turbine. In few seconds the turbine adapts its output power to this condition, actually performing the primary control by modulating it to contain the frequency variation.

The same principle can be adapted to distributed generation and variable renewable generators by substituting the speed governor with an electronic controller that modulates the power output. This will be treated for photovoltaic and wind technology in next chapters.

It can be pointed out that, to be able to increase the power output, during their normal operation the generators such as thermal units and hydropower plants must work under their maximum capacity. By reasoning in economic terms, they are not selling all the energy that could be sold. In a situation in which the electricity price is higher than the marginal cost for the unit, the owner of the plant is losing a profit to keep a reserve margin available. This fact highlights how they have to be properly set remuneration systems to give value to the service provided by the “spinning reserve” plants.

It can be useful to resume what said until now with an example. The reference situation is a system composed by three identical steam turbines with reheat and a load, that initially are balanced in terms of power. The reference model for the steam turbine used to perform this example as well as in the entire work is the one described in [4], which has been evaluated as appropriate for the aim of this work, that is not centered on the modeling of a synchronous generator but rather on implementing a technique to exploit renewable generators for primary frequency control.

After few seconds the equilibrium condition is perturbed by a sudden step reduction of the load with an amplitude of 0.02 pu.

The frequency response is studied at three different equivalent inertia constants of the system, namely 10 s, 7.5 s and 5 s, to observe the influence of this parameter on frequency stability.

The obtained results are shown in Figure 1.2:

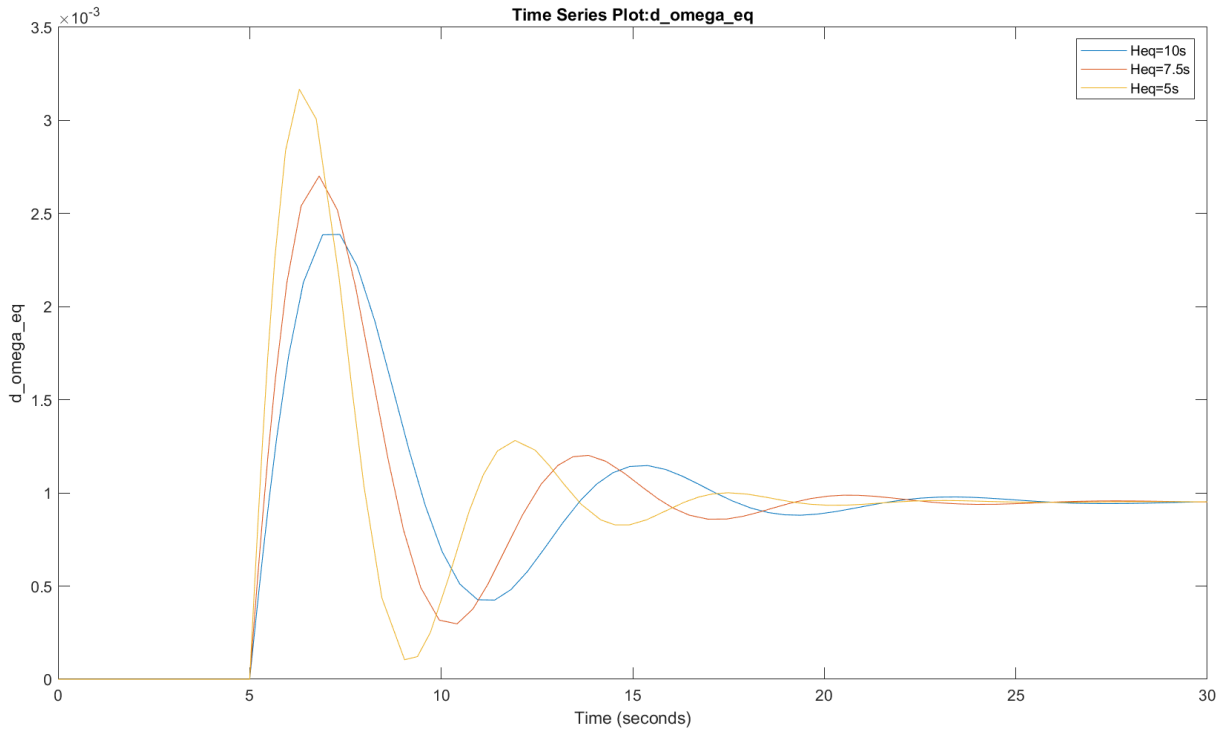


Figure 1.2: impact of system inertia on frequency response

When studying such a plot representing the frequency response to a demand variation they are usually assessed mainly two parameters: the *frequency nadir*, which is the maximum/minimum value of the frequency reached following a disturbance [28], and the rate of change of frequency (*RoCoF*).

The results of this example underline how a decrease of the system inertia worsens the primary frequency regulation during the transient, increasing both the frequency nadir and the RoCoF.

This simple example makes evident the importance of finding a way to face the system inertia reduction due to variable renewable generators spread making them able to support the remaining conventional spinning reserve during the frequency stabilization.

Before finishing this chapter, it is important to specify that in this work the attention is only posed on the primary control, so secondary and tertiary ones are neglected both in modelling and in the result analysis. Nevertheless, for the sake of completeness, they are reported the definitions of the two controls, provided another time by [27].

Secondary control has the aim of maintaining a balance between generation and consumption within a synchronous area, modifying the active power setpoints of the units forming the system. The timeframe in which it operates goes from some second up to fifteen minutes after the disturbance.

Tertiary control is usually activated manually by the TSO to free up the secondary control as soon as the balance is reached, but also to support it in case of a large disturbance.

Figure 1.3 summarizes the operational sequence of the three controls as well as the typical shape of the frequency response after a disturbance, helping to graphically fix what explained until now [26].

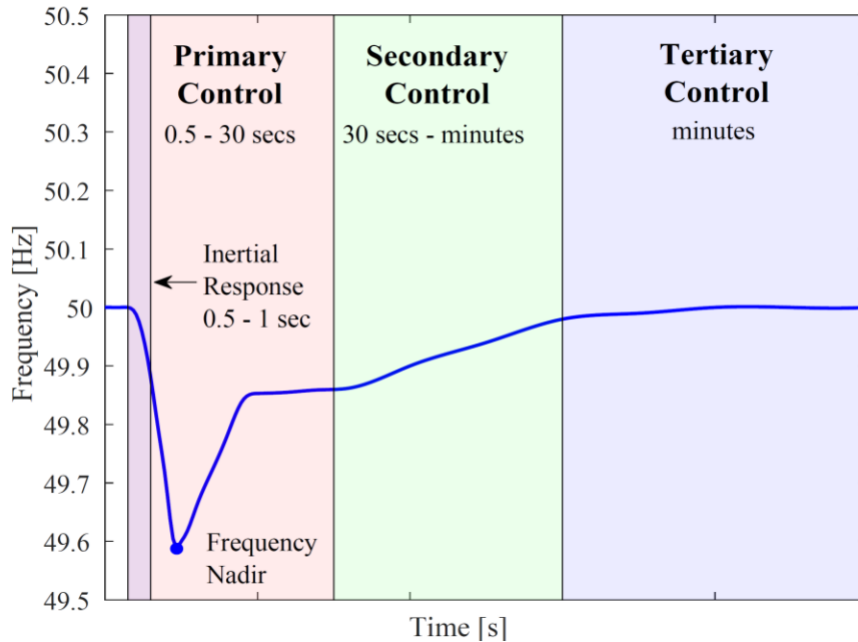


Figure 1.3: Primary, secondary, and tertiary frequency control response

1.4. Boundary conditions of the primary frequency control

In reality the primary frequency control is much more complex than a simple droop. Indeed, there are some boundary conditions to be respected and, not least, a market mechanism to remunerate the service offered to the system.

Since the model developed in this work has not a precise location and has to be intended as a study on the power system of a generic small island, and the boundary conditions are typical of each power system, they are presented only qualitatively.

In general, providing resources for the primary frequency control means to make available to the TSO a range of capacity of the plant in which the power output can be modulated by an automatic controller answering to a change in system frequency.

The amplitude of this power interval depends on the location of the plant. For example, in Italy, its amplitude has to be higher than the $\pm 1.5\%$ of the efficient power (maximum power that can be produced by a plant for a functioning time of 4 hours or more if all its parts work at their nominal efficiency [29]) of the plant in the mainland, while higher than $\pm 10\%$ of the efficient power for power plants located in Sardinia (and in Sicily when disconnected to the mainland) [30]. All the power plants that satisfy the

requirements are obliged to participate to the primary frequency control, accomplishing these mandatory rules.

Furthermore, there are other conditions to comply with, that can be distinguished for normal functioning or emergency functioning.

In normal functioning conditions, it can be calculated the amount of the power reserve interval (ΔP_e) to be produced as a function of the frequency variation (Δf) from its nominal value, as in Equation (1.5):

$$\Delta P_e = - \frac{\Delta f P_{eff}}{50 R} 100 \quad (1.5)$$

The two, as already mentioned in 1.3, are related by the droop constant, whose value is also prescribed in the grid codes. For example, in Italy, the droop has to be equal to 5% for thermoelectric units and to 4% for hydroelectric ones [31].

It does exist an interval of frequency centered in its nominal value, called *dead band*, in which the controller is not able to respond to a change in frequency. In grid codes it is established the maximum amplitude of this dead band in order to effectively answer to a frequency variation. In Italy the maximum amplitude of the dead band is ± 10 mHz for hydroelectric units and simple steam cycles, while ± 20 mHz for gas turbines and steam turbines in combined cycles [31].

Since for frequency variations lower than the dead band the power output is not adapted, if the oscillation is larger the controller has to recover the contribution in primary frequency control not yet provided by decreasing the droop in another interval around the dead band, as shown in Figure 1.4 [31].

It is usually also present a limit in terms of time to provide the amount of ΔP_e required. In Italy, at least a half of ΔP_e has to be provided in the first 15 s after the frequency variation event, and the entire ΔP_e has to be provided before 30 s. If the frequency deviation continues, the units have to go on in providing the regulation. When the unit reaches a new value of power according to ΔP_e , it has to be able to continuously keep that value for at least 15 minutes [31].

In emergency conditions a production unit that participates to the primary frequency control is asked to provide the service in a more challenging way. Indeed, usually the grid codes ask for making available all the power band ΔP_e with the higher gradient technically possible (i.e. the maximum gradient that allows the plant to operate continuously).

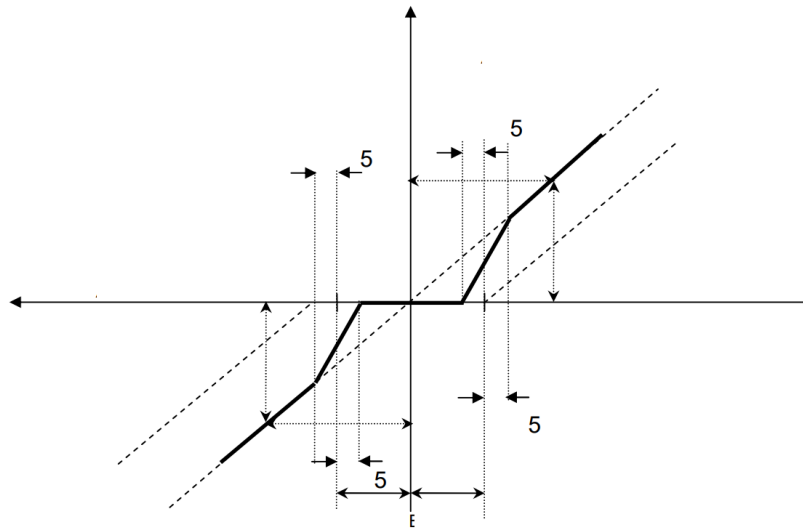


Figure 1.4: proper dead band compensation for droop controllers

To conclude, all the national grid codes ask for these actions in order to keep the frequency into a certain interval and ensure the safety operation of the system. Each state has its own limits, reviewed and grouped in [32]:

Country or Region	Steady state Range, Hz	Transient Range, Hz
Austria	49 - 50.5	47.5 - 51.5
Belgium	48.5 - 51	47.5 - 52.5
Bulgaria	48.75 - 51.25	No
Czech Republic	48.5 - 50.5	47.5 - 51.5
France	49.5 - 50.5	47 - 55
GB	49 - 51	47.5 - 51.5
Germany	49 - 50.5	47.5 - 51
Greece	49.5 - 50.5	47 - 53
Italy	49 - 51	47.5 - 52
Lithuania	No	No
Netherlands	49.85 - 50.15	48 - 51
Poland	49 - 51	47.5 - 52.5
Romania	49.5 - 50.5	49 - 52

Scandinavia	49 - 50.3	47.5 - 52
Spain	48 - 51.5	47 - 51.5
Austria	49 - 50.5	47.5 - 51.5

Table 1.1: European grid codes: frequency variation

In some nations they do exist also limits for the RoCoF:

Country or region	ROCOF (Hz/s)	Duration (seconds)
Austria	0.2 Hz/s	10 s
Germany	0.09 Hz/s	10
Greece	0.5 Hz/s	-
Ireland	1 Hz/s	-
Switzerland	0.09 Hz/s	10

Table 1.2: RoCoF limits

In the future the frequency ranges are expected to become tighter and tighter to improve the security of the system during disturbances, and, for the same reason, the RoCoF limit will decrease [33].

1.5. Remuneration for primary frequency control

Since ancillary services can be intended as a commodity, the creation of a market for their trading is important in order to resolve the conflict between buyers and sellers and reach a mutual benefit. Indeed, through an ancillary services market, the TSO is able to purchase the resources needed to ensure the system safety at the minimum cost, while the plant owners have another source of income by selling that resource. However, due to the complexity of the traded good, they have been developed in the years different options to trade them [34].

The TSO can purchase the services mainly through four procurement methods [34]:

A. COMPULSORY PROVISION

Through this mechanism a certain class of network users are asked to provide upon request of the TSO a certain amount of a given ancillary service up to a certain quantity. It is considered “fair”, since all the users of a class have to provide the same amount of service. On the other hand, it simplifies too much the problem. Indeed, the cost for the procurement is not minimized from the TSO, since the providers all treated in the same manner, not exploiting the fact that some of them could offer the service for a lower price; another problem is

that, since the quantities are not coincident with the actual amount needed, there are additional costs for the providers.

B. BILATERAL CONTRACTS

Through bilateral contracts the TSO negotiates quantity, quality and price of the service with the provider. This removes the simplifications of the previous mechanism, solving the two issues mentioned above. By the way, bilateral contracts also have some drawbacks: there is a lack of transparency, since there is no a third party certifying the conditions, and this is a problem when the buyer is a monopolist (TSO); negotiations are long, complex and costly, leading to long term contracts with fixed conditions, which, in case of a change in the market conditions, is detrimental for one of the two parties.

C. TENDERING PROCESS and SPOT MARKET

The differences between these two mechanisms are light, since both are characterized by the presence of a market. The first are usually considered for long-duration or less standardized products, while the second imply short-term standardized products.

Togther with the structure of the procurement method, another key aspect in the ancillary services provision is the remuneration method. Also in this case more options are available [34]:

A. NON-REMUNERATED SERVICE

This mechanism is convenient for the TSO, but is not economically optimal, since the providers charge other products on other markets with their costs to provide the services to the TSO.

B. REGULATED PRICE (RP)

With RP the regulatory agency (which is the figure necessary to limit monopolist power and to ensure fair conditions) establishes a price common for all the providers. This procedure does not take into account the rapidly changing conditions of the market as well as the different costs that each provider has to face to realize the service.

C. PAY AS BID PRICE (PBP)

In PBP mechanism the provider receives the value of its accepted offer for the service. It is particularly suitable for situations with highly differentiated products, in which the offers are not so easily comparable. However, since the offer value represents the remuneration obtained, the providers are not offering at their marginal cost, but at a higher price, to realize a profit.

D. COMMON CLEARING PRICE (CCP)

In a common clearing price system, all the successful providers are paid the price of the most expensive accepted or the least expensive rejected offer. This mechanism gives incentives to the providers to offer their marginal cost. Differently from PBP, it is suitable for standardized products, for which the offers are easily comparable simply looking at the price.

Furthermore, the remuneration for an ancillary service should take into account the different voices of cost that a provider has to face when making it available to the TSO, with additional components as an availability price, a utilization payment, a utilization frequency price, and a compensation for a possible opportunity cost [34].

2 Active power control of a photovoltaic system

The management of the energy system is very complex, and requires a lot of actions, not only operated by a central control but also at the generating units level. Historically the photovoltaic plants were not able to provide ancillary services, but their massive diffusion is driving through a change in this paradigm: it is becoming crucial to develop new PV systems modes of operation and control, to make them able to participate to the electric system stabilization. More specifically, in the following will be treated the problem of their active power control, a key feature to keep the electric grid balanced and allowing the frequency to remain as constant as possible.

In particular, the diverse needs in terms of active power control strategies of PV generating units could be conceptually derived from the problems related to their strong penetration in the electric system. For this reason, this chapter will be divided in the following parts: 2.1) problems related to a large penetration of PV systems in the energy mix; 2.2) new functionalities required to PV plants in order to face their increasing penetration; 2.3) batteries vs power curtailment methods; 2.4) overview of the algorithms for active power control proposed in the literature.

2.1. Problems related to a large PV penetration

In the last decade it has been observed an incredible growth of the photovoltaic technology application. Indeed, the large availability of sunlight and the cost reduction for its manufacturing pushed it from a niche to a significant role in the energy sector.

In Errore. L'origine riferimento non è stata trovata. can be observed the trend in PV installation of the last years, both in terms of accumulated installed capacity and yearly installed capacity [35].

This rate of growth putted the attention of the researchers on understanding the problems and the challenges introduced by a high penetration of photovoltaic generators in the power system.

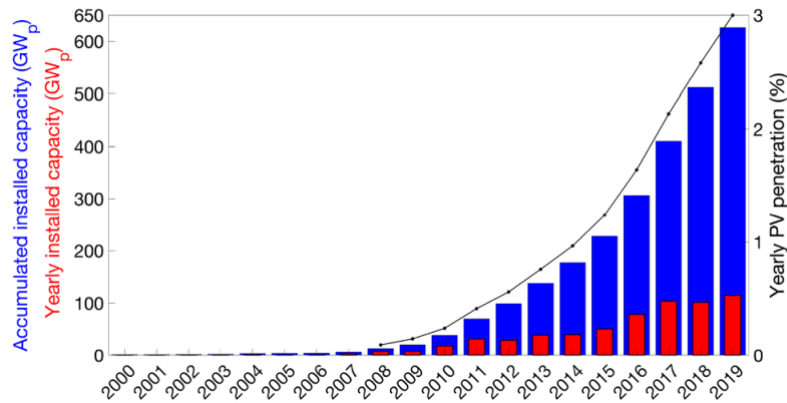


Figure 2.1: Historical PV accumulated installed capacity, PV yearly installed capacity and share of PV electricity production

[35] brings together and explains effectively the key features of the technology which can lead to problems for the system:

- *Distributed*: the modularity of the PV panels allows their installation in the vicinity of the load. If the modules are positioned behind the meter, the grid operator might not detect them, and so they are non-dispatchable. Furthermore, when they produce more than the load requirements and storage is not available, reverse power flow happens, leading to a problem for the distribution network.
- *Diurnal*: PV modules only produce power during daytime. This is positive in applications with load peak during the central hours of the day, but in the usual applications (i.e. residential) the peak is positioned in the evening, when PV production is very low.
- *Converter-based*: photovoltaic technology does not have rotating parts. Consequently, they are not able to store kinetic energy, and their inertia is null. As seen in Chapter 1, this lack of inertia could represent a problem in highly renewable-penetrated power systems, causing instability.
- *Intermittent*: the production of PV plants is strongly affected by the environmental conditions, such as irradiance and air temperature. In windy and sunny days with some clouds, the irradiance can vary suddenly, leading to strong variations in the production occurring in few seconds. This steep active power variation stresses the power system, especially when the penetration level is high.

These characteristics constitute the basis to understand the problems when a high PV penetration is reached in a power system. As part of this work, there is interest in

summarizing the ones that affect the primary frequency control and the inertial response, as in Figure 2.2:

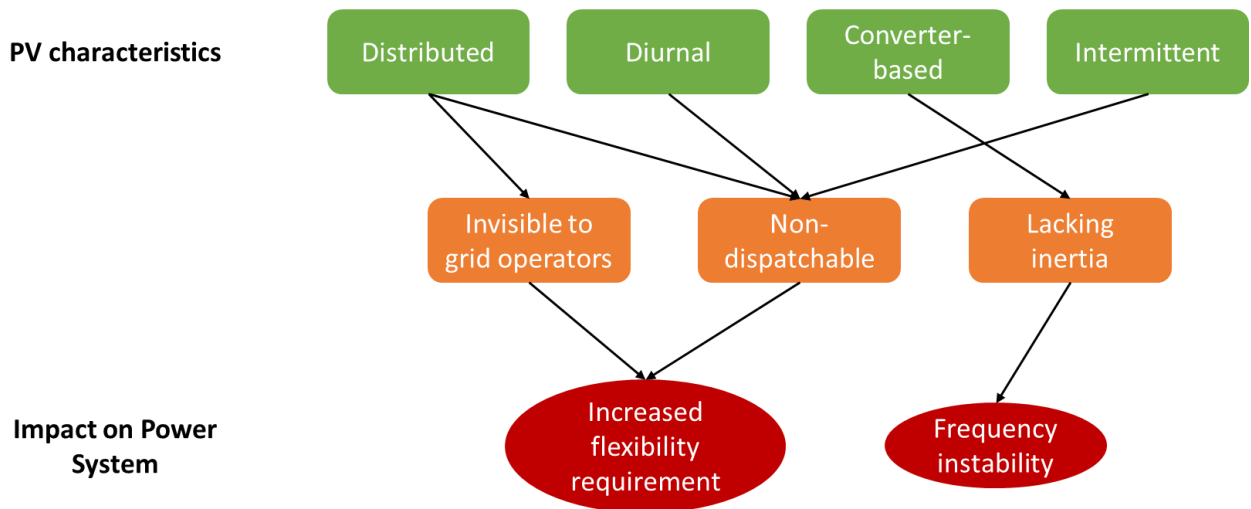


Figure 2.2: issues for high PV penetration related to this work topics

It has already been discussed the reduction of system inertia due to the displacement of conventional generators caused by the increased presence of the photovoltaic in the energy mix. Since the photovoltaic modules are nowadays operated always at their maximum power point, there is no margin for frequency regulation. These two facts combined lead to an important problem: the need of reserve is increased, since the PV is not flexible if operated at its MPP, but the reserve available is reduced due to the reduction of the conventional generation presence. The result is a potential reduction in frequency stability as photovoltaic technology increases its weight in the generation mix, in the shape of a RoCoF and frequency nadir increase.

2.2. New functionalities required to PV plants

In the scenario of a world with more and more renewable power plants, it is crucial to make them as flexible and system friendly as possible.

In particular, as explained in the previous subchapter, nowadays the photovoltaic plants are somewhat rigid and stressful for the system. Conceptually, it is possible to start from those key issues and develop strategies to progressively smooth and eliminate their drawbacks. The interest of this work is focused on the active power control, since is the characteristic that influences the frequency regulation, as explained in Chapter 1.

They do exist two main solutions to accomplish to the future requirements in terms of modulation of active power as a response to a frequency deviation: the use of a battery storage system or the implementation of innovative control schemes [36]. In this

subchapter it is conceptually explained the second option, which is the one implemented in this work, while in **Errore. L'origine riferimento non è stata trovata.** it is presented an overview of the BESS (*Battery Energy Storage System*) option and a qualitative comparison between the two.

If the choice is to modify the control algorithm of the photovoltaic module, they may be implemented three main functionalities [37]: *Power Limiting Control* (PLC), *Power Ramp-Rate Control* (PRRC) and *Power Reserve Control* (PRC), that are conceptually described in the following.

A. POWER LIMITING CONTROL (PLC)

The concept presented in the following is the basis for all the power curtailment methods. It is based on the imposition of a certain level of active power required from the plant (P_{res}), that has to be reached by modifying the voltage applied to the PV panels (v_{pv}^*), taking into account the P-V curve, having the characteristic shape in Figure 2.3:

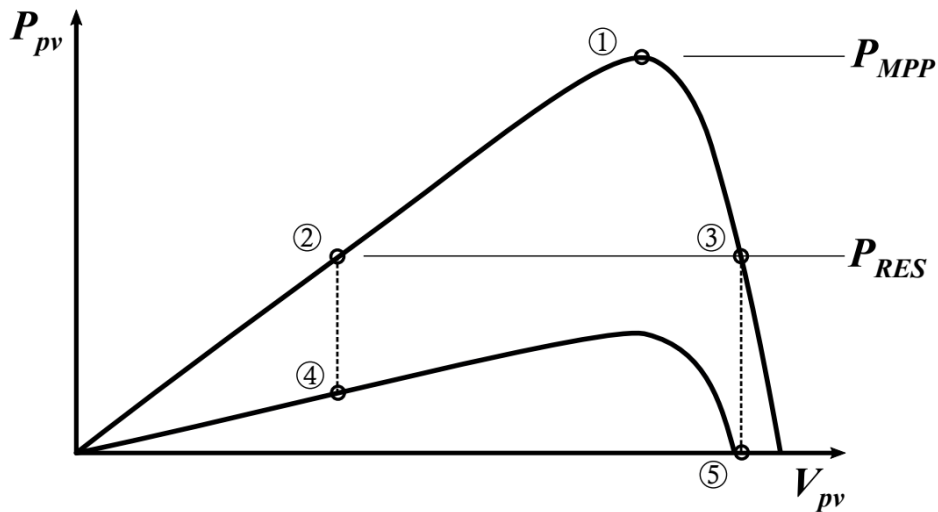


Figure 2.3: P-V curve for a photovoltaic module for two different values of irradiance

It is evident that, given a certain P_{res} , it is fundamental to characterize the irradiance (G) and the temperature (T) in order to establish the shape of the power curve. In this sense, here it grafts another problem: the choice of the method to obtain the power curve. They are available different solutions, for example the direct measurements of G and T , a Non-Linear Least-Square Curve Fitting or using solar forecasting methods. A more detailed explanation of the possible techniques is explained in Chapter 4, but it can be anticipated that it represents a trade-off between cost and accuracy, due to the fact that the most accurated methods are also the most expensive to be implemented.

Once determined the actual I-V curve (and so the P-V curve and the MPP) all the inputs required for the algorithm are available:

- If $P_{res} > P_{MPP} \rightarrow$ MPP operation: the PV system will operate at its maximum power point, so $v_{PV}^* = v_{MPP} / P_{PV} = P_{MPP}$
- If $P_{res} < P_{MPP} \rightarrow$ curtailed operation: the PV system will operate at a voltage $v_{PV}^* = v / P_{PV} = P_{res}$

It can be noticed that, in the curtailed case, two voltage levels are possible for the same P_{res} , respectively on the left and on the right of the MPP: it is yet not proved what is the optimal operation side of the P-V curve, since each of the two options has pros and cons. In fact, by operating on the right side (higher voltages) the inverter works at higher efficiency values, but the power output is extremely sensitive to irradiance variations, so in that condition (ex. cloudy days) the control becomes difficult on this side. On the other side the influence of irradiance variations on the power output is less important, but the range of regulation of power is limited [38]. This work is adopting an innovative approach proposed in [10], so a detailed explanation of the comparison between the operation on the two sides is given in Chapter 4.

B. POWER RAMP-RATE CONTROL (PRRC)

The aim of this strategy is to smooth the active power output oscillations of the PV system. In particular, the algorithm imposes a maximum rate of variation of the active power output when variations of irradiance occur. In this case the criterion to curtail the power does not come from the absolute value of the active power output but from its change rate with time [37].

The PV power ramp-rate can be calculated as in Equation (2.1):

$$R_r(t) = \frac{dP_{PV}}{dt} \quad (2.1)$$

If $R_r(t)$ is higher than the limit value required by the System Operator, the voltage v_{PV}^* is perturbed in order to reduce the change rate of the PV power to that value. This kind of control can be performed both by controlling the voltage (as just explained) or the power.

C. POWER RESERVE CONTROL (PRC)

This control logic can be seen as a particular case of the PLC algorithm. In fact, instead of imposing a certain constant power output level, in the PRC algorithm the PV output is regulated as a percentage of the maximum available power in each time instant. This dynamically changing fraction of the P_{MPP} is called *Power Reserve* (ΔP). The output power is then obtained as:

$$P_{res} = P_{MPP} - \Delta P \quad (2.2)$$

Also in this case the challenge is to estimate the MPP, since it is one of the inputs necessary for the controller. The detailed explanation of this algorithm as well as of the determination of the P-V curve (and so of the MPP) is provided in Chapter 4, where it is described the complete implementation of a model to control the active power output of photovoltaic modules in order to enable their capability to participate to the primary frequency control.

The combination of these three techniques provides one possible solution to allow the control of the active power output of the photovoltaic technology. In the next subchapter it is proposed a qualitative comparison between the power curtailment method just explained and the other possible solution for the problem: combining the photovoltaic with a battery energy storage system.

2.3. PV system integrated with battery energy storage systems (BESS)

In literature they have been developed a lot of strategies using BESS integrated with PV systems in order to provide primary frequency control, especially in small power systems of islands, which is the case studied in this work. Although the aim of this study is centered on power curtailment methods for photovoltaic application, it can be useful to present at least the major features of the BESS solution, in order to outline the differences between the two approaches.

The use of batteries to provide primary frequency control is conceptually easy: when the load power is higher than the generators power the frequency will decrease, so the batteries are asked to discharge to compensate the difference in power; on the other hand, when the frequency increases due to a generation that is higher than the absorption by the load, the batteries are charged, as described in Figure 2.4 [39]. Of course, the entity of the charge/discharge power has to be proportional to the entity of frequency deviation. This is why, qualitatively, the battery control could be seen as an emulation of the droop control of synchronous generators. By the way, the real operation of a battery is subjected to a lot of constraints, as a maximum discharge capacity, a C-ratio limit to avoid a fast degradation, a voltage limit to preserve the battery from faults. This gives at least an outlook on how difficult is to find a balance between all these aspects to realize an effective control system.

In fact, the real profile of frequency is very fluctuating, this means that they are asked to charge and discharge a lot of times in a day. This fact pushes to develop a very dynamic control to be able to follow these fluctuations.

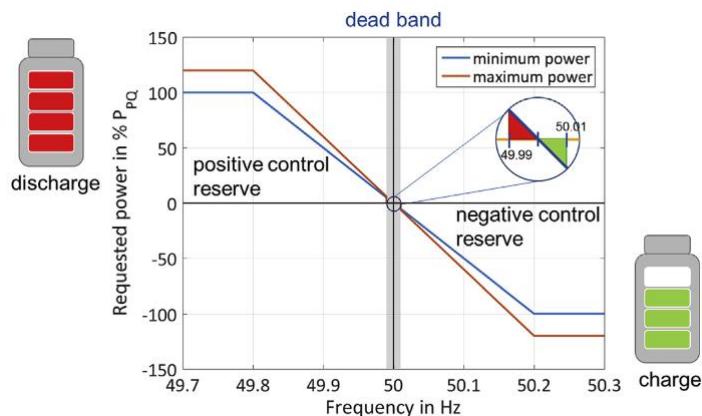


Figure 2.4: Power to frequency characteristic (P-f characteristics) for BESS providing FCR on the Central European market

The adoption of BESS for primary frequency control can potentially solve the issues in highly renewable penetrated systems, as the small island ones or the power systems of the future. The biggest advantage with respect to power curtailment methods is that no energy is wasted. Indeed, to keep always available a certain reserve level, renewable generators have to exploit just a certain amount of the producible energy. If the remuneration and the incentives for the participation to the primary control are not enough, the profitability of renewable plants decreases. In that case, adopting a BESS system integrated with the generators would allow a more flexible utilization without reducing the energy exploited. Another winning aspect of the batteries is that they are able to adapt the power with rapid ramp rates, which is one of the key targets for the future primary frequency control [40].

On the other hand, the BESS solution presents also some drawbacks, mainly related to investment cost and complexity. In fact, the BESS solution requires of course an additive investment to purchase the storage system itself, which requires advanced communication systems. Furthermore, the lifetime of the batteries is limited [36]. These negative aspects can lead to an increase of the cost for the PV electricity produced, which is in contrast with the expectations of cost reduction in the next decade [41].

It is also important to state that power curtailment and storage are not necessarily mutually exclusive solutions, since in some situations combining the two it is obtained the best option from the economic point of view [42].

In this work it is analyzed the impact of the second solution, which allows a simpler control and lower investment costs.

2.4. Overview of the algorithms for PV active power control proposed in literature

As stated before, one of the aims of this work is to develop a model to operate the power curtailment (in particular, the power reserve control) of a photovoltaic system as well as the virtual inertia method for wind turbines, in order to unlock the possibility to participate in primary frequency control also with this kind of renewable generators.

Before going through the developed model, it is extremely important to offer an overview of the methods and algorithms proposed in literature for the power reserve control of photovoltaic systems. This bibliographic analysis is very useful, since each one of the methods can have some issues and some advantages, which can be compared to the ones of the model developed in this work, understanding its effectiveness.

To organize this section, it has been decided to outline the differences between the various approaches under some key aspects that usually are the ones in which they do exist the main differences between the documents in the literature: PV plant model, estimation output, controlled variable, MPPT tracking method, operational side of the P-V curve. The summary of the paper reviewed is presented in Table 2.1:

N°	Authors	Reference
1	Batzelis et al.	[38]
2	Sangwongwanich et al.	[7]
3	Li et al.	[8]
4	Hoke et al.	[9]
5	Riquelme et al.	[10]

Table 2.1: reviewed models for PV power reserve control

The starting point of each work about the power reserve control of a photovoltaic grid-connected system is the model adopted for the plant itself. They can be used mainly two approaches: the most complete one is the two-stage model [43], which comprehends all the conversion stages between the modules and the grid (represented in Figure 2.5). It includes the boost converter to step up the voltage to the DC-link value, the full-bridge inverter and an LCL filter. However, since the actual power output control is operated on the DC-DC converter, usually in the literature it is used the single-stage model, represented in Figure 2.6, where the duty cycle command is

obtained by a control module. The main differences between all the reviewed methods are found in this control module.

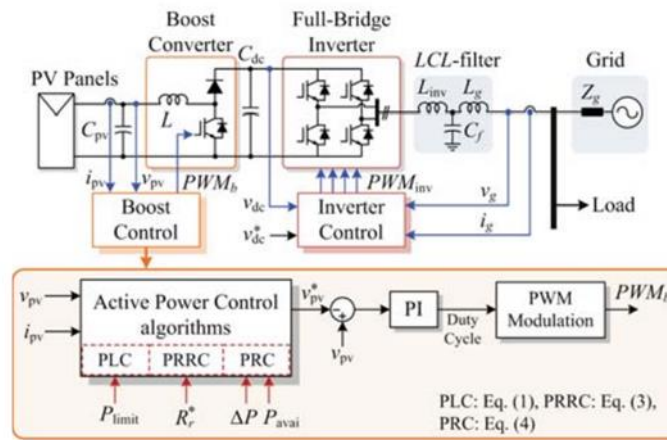


Figure 2.5: two-stage grid-connected PV system [37]

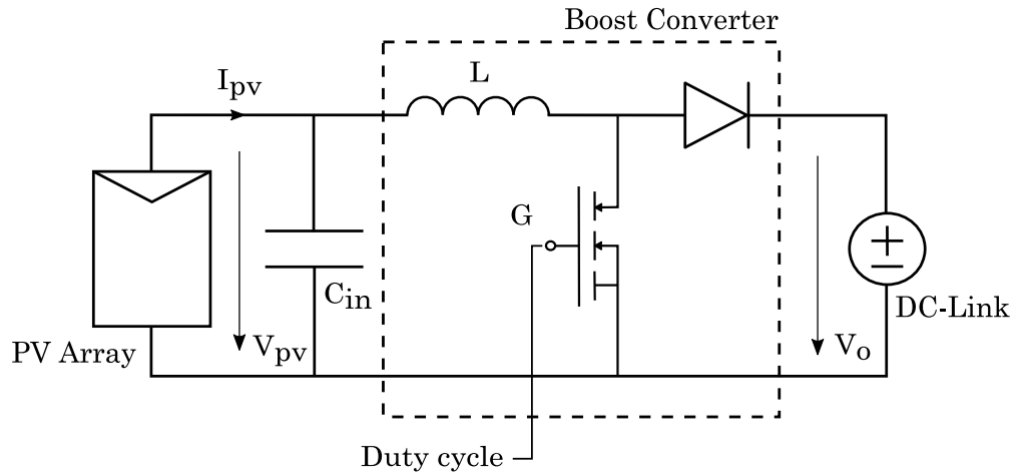


Figure 2.6: single-stage grid-connected PV system [36]

The logical process of the control block is a sequence of some key operations: first of all, the maximum power point is estimated in real-time. This calculation can be performed through a variety of techniques. The approach proposed in [38] is probably the more diffused: the P-V curve is estimated starting from past measurements of power and voltage in the current window close to the operating point through the equation for the P-V curve shown in Chapter 4. The measurements are referred to the last temperature value recorded, and fitted through a least-squares curve fitting method, whose output are the five characteristic parameters of the module, necessary to solve the module equations, as presented in Chapter 4. Qualitatively, without entering in the detail of the mathematical formulation which is not the focus of this paper, the least squares fitting consist in finding the P-V curve which better approximates the measurements, i.e. producing the lower difference between the measurements and the estimated values (Figure 2.7). In [7] it is used a similar approach, but with a combination of a linear and a quadratic approximation. The

interesting aspect of [7] is that, focusing on multi-string PV plants, one string called “master string” is operated at the MPP, while the others in the curtailed mode, but using the estimation of MPP of the master as reference to adapt their power. A non-linear least-squares fitting is also used in [10], proposing further and deeper observations about the possibility to follow the actual characteristic of the PV modules when temperature and irradiance change, and demonstrating that the non-linear least squares fitting works well also in changing ambient conditions if utilizes measurements close to the MPP or on its right. Since the I-V curves of PV modules are almost superposed for different temperatures on the left side, it is not possible to estimate the correct one if measurements are taken on that side. However, since the temperature dynamics are slower than the irradiance ones, it is by the way possible to operate with measurements on the left side at least for short periods. A different method is used in [9]: the MPP is found with a polynomial function of the irradiance and the temperature, which in this case, differently from the previous ones, are measured. The coefficients for the polynomial relation are found by calculating the value of module current (with Equation (4.6)) for all the expected irradiance, temperature and voltage values, then finding numerically the power maximums and interpolate them with a linear regression. It is also worthy to state that, in photovoltaic systems, another possibility to find the MPP are the Perturb and Observe methods [44], representing the traditional way of estimation, which in this case are not useful since the knowledge of the entire P-V curve is necessary.

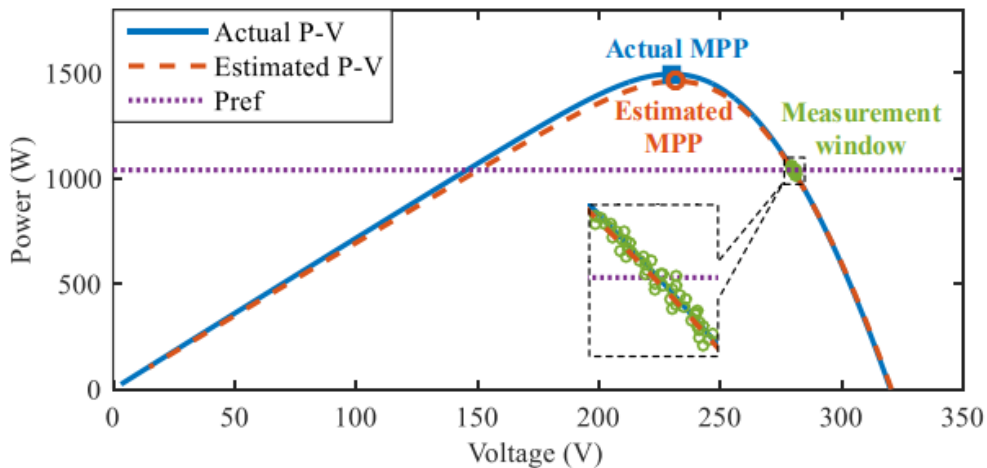


Figure 2.7: indicative scenario of least squares curve fitting MPP estimation

Once the MPP is known for the actual operating condition (so for an irradiance / temperature couple) it has to be calculated the required operating point to deliver the curtailed active power output desired. The most used control variable is the voltage: it is calculated the voltage level corresponding to the desired output power, and then it is compared with the actual voltage applied to the PV system to produce a duty cycle signal by means of a PI controller. This approach is used in [7], [9] and [10]. The same reasoning is adapted with the power as reference variable in [38] and [8], where the

desired value of power is compared with the actual value to produce a duty cycle signal for the boost converter.

It is also important to notice that, for a certain level of curtailed power desired, there are two options in terms of voltage, respectively on the left and on the right of the maximum power point in the P-V curve. The scientific literature does not agree on which is the best side of the power curve of the PV module to operate the power curtailment. All the existing algorithms are able to work only on one side: since the operating condition throughout the year can be very different, this can be limiting.

In fact, operating on the right side allows a bigger variation range of the power, but at the same time modest reductions of irradiance can lead to a drop in the power output. This behavior can be easily explained looking at the P-V curve: reasoning at fixed irradiance, a request of power reduction from the System Operator can be easily satisfied with small variations of the operational voltage. This is intrinsic to the high slope of the right part of the P-V curve. On the contrary, in a context in which the irradiance varies a lot, if a reduction of irradiance occurs at constant voltage the power output would immediately reduce, and even become null.

Instead, on the left part of the curve the pros and the cons are shifted due to the lower slope of the curve: there is a moderate insensitivity to the irradiance, but at the same time the range of variation of power is very restricted.

From these observations can be immediately pointed out how the choice of a single side of the P-V curve in which operate the power curtailment can influence the actual capability of the plant to participate to the frequency control. In this sense becomes crucial to develop an algorithm able to adapt the control strategy to the boundary conditions of the problem (i.e., meteorological conditions, level of power reserve demanded by the SO) [10]. This is why, also in the present work, it is adopted the approach proposed in [10] to be able to work on both sides of the P-V curve, exploiting the advantages of the operation on the two sides as a function of the situation.

After this brief review about the approaches to operate the power reserve control present in literature, in Chapter 4 it is explained in detail the model and the approach proposed in this work to operate it. In Chapter 3, instead, is performed a similar discussion to understand how to make wind turbines flexible and able to participate to the primary frequency control.

3 Active power control of wind turbines

As described in the introduction, the conventional synchronous generators are being progressively displaced by renewable generators. After photovoltaic technology, wind turbines are certainly the most exploited solution to drive the energy sector through the decarbonization.

Among all the positive outcomes of the production of electricity in a sustainable way in wind power plants, there are some problems that can affect their possible large penetration in the electric system in the future. Indeed, the wind generation management is complicated due the variable nature of the wind resource and to its difficult predictability, very often affected by a significant uncertainty [18]. When the power system begins to experience an important penetration level of wind generators, displacing synchronous ones, the inertial response that the remaining generators can provide could be seriously weakened. This is due to the fact that the usual control logic of wind turbines includes the adaptation of the rotational speed of the rotor to the incoming wind speed to maximize the power output of the system and its coefficient of performance (this happens in particular for wind speeds lower than the rated one), so the operational point is decoupled by the grid frequency. This decoupling explains why the wind turbines do not contribute to the equivalent inertia of the system [5].

The apparition of unintentional electrical islands is another problem of interest in literature due to the massification of distributed generators, particularly in weak or isolated systems and microgrids. In networks with these characteristics, wind turbines controllers must be able to detect an off-grid operation and disconnect to avoid safety hazards and damages to the electrical infrastructure [18].

These problems open the field to technical challenges aiming to use wind generators to help controlling the grid frequency and contributing to the system equivalent inertia, as well as to islanding detection algorithms. To replace to these, it is observed a large attention in the scientific literature on this argument, with a lot of interesting proposals that produced very promising results that justify the participation of wind turbines in grid frequency control tasks.

In the following subchapter are reviewed the different approaches proposed in the literature to allow wind turbines to participate to the primary frequency control.

3.1. Primary frequency control provision with wind turbines

If for photovoltaic systems the algorithms to control the active power output through the power reserve control are relatively similar each other in the logical sequence, for wind turbines this does not happen. Indeed, they are available different techniques to provide inertial control and, in particular, primary frequency control. The large variety of solution is well visible in Figure 3.1 [11]. Primary frequency control with wind turbines is an autonomous response to a change in system frequency that emulates the governor control of synchronous generators. More precisely, when a change in frequency is detected, the wind turbine modulates its power output to respond to this change and helping to balance the system.

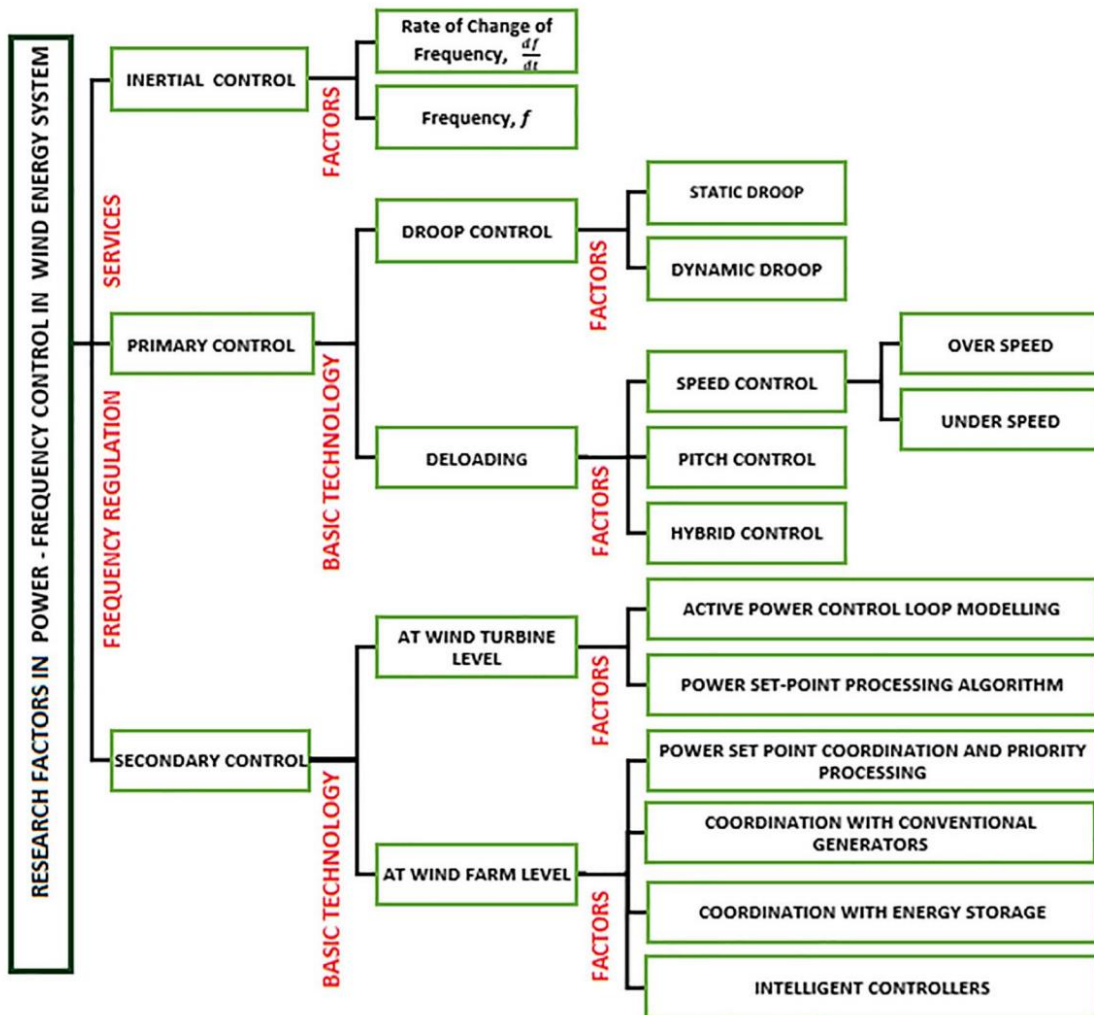


Figure 3.1: Active power frequency control research study line in wind based power plants [11]

It is possible to observe that, for inertial control and primary frequency control, they are available different methods, which are in turn implemented with different viable solutions.

In the following they are explained the main concepts of each of them, underlining also the different models presented in the literature to implement these control techniques.

3.1.1. Inertial control with wind turbines

First of all, it is important to offer an overview of the different types of wind turbines present in the market. In general, they do exist fixed speed wind turbines, semi-fixed speed wind turbines and variable speed wind turbines [11].

Fixed and semi fixed speed ones have an inertia constant but is smaller with respect to the conventional synchronous generators one, due to the lower coupling of induction generator with the grid frequency. This makes their inertial response lower and slower compared to the conventional generation [11].

On the other hand, as already mentioned, variable speed wind turbines (which are dominant in the market due to their higher efficiency) are decoupled from grid frequency due to the presence of the power electronics converter, so their contribution to the system inertia is null. However, it is possible to achieve from VSWTs a short-term inertial response, by introducing an additional control loop in their control system which modifies the operation, allowing the turbine to exploit the kinetic energy of its rotating mass to modulate the electrical power output of the system and so to contribute to participate to the inertial control.

The functioning principle is simple: if the control detects a frequency variation, a signal is sent to the turbine speed governor or torque governor, temporarily modifying the power setup accordingly to the entity of the frequency variation and enabling the possibility to exploit an amount of the kinetic energy of the rotor. For example, if an increase of power output is required to balance a frequency decay, the kinetic energy stored in the rotor is temporarily released. In this case, an unbalance between the electrical power injected into the grid and the mechanical power extracted from the wind is created, causing a deceleration of the rotor (i.e., a decrease of kinetic energy). This slowing down reduces the lift, discharging aerodynamically the blades, and increasing the stall risk at the bottom sections of the blade. To avoid stalling, the overproduction period has to be followed by an underproduction period in which the rotational speed of the rotor is increased [11].

They do exist different models for the inertial control in the literature, but they can be conceptually divided in two main categories: a “simple” inertial control which takes into account just one between the absolute value of the frequency deviation Δf and the frequency derivative df/dt , or an inertial-droop control which takes into account both.

The first category is presented for example in [12] and [13], while the second is adopted in [15] and [18]. Between the two, the inertial-droop approach allows to perform a very fast inertial control as well as an active power support more extended in time. An extended explanation of this kind of control is given in Chapter 4, since is the one adopted in the present work. The droop concept for VSWTs is analogous to the synchronous generators one. They do exist two types of droop control: fixed or variable droop value. The second is of course more accurate in responding to frequency deviations, since it depends on wind and power reserve conditions [45] or on the RoCoF [18] [46]. Indeed, it ensures improved system stability and avoids reserve exhaustion.

The drawbacks of this kind of control are intrinsic to the physical behavior of the rotor during the frequency oscillation. In fact, when the rotor slows down, it has always to respect aero-mechanical limits and avoiding stall, keeping a safety margin, and consequently the control is limited, especially for low wind speeds. Furthermore, while the operational life in normal functioning has been tested a lot at industrial level, the operation with inertial control enabled has not, leading to the prescription of practical utilization of this kind of control just in few situation by the grid codes [11].

Another issue is related to the fact that, to re-accelerate to optimal speed, the power released to the grid has to be lower than the one exchanged with the wind. This implies that, for a certain time interval, the power output of the turbine is lowered to recover kinetic energy delaying frequency recovery and, in some situations, requiring an extra amount of reserves to prevent a “double-dip” in system frequency, increasing the risk of triggering protective relays at the substation level and causing blackouts [47].

3.1.2. De-loaded operation of VSWTs

In normal operation wind turbines follow the MPP to extract the maximum energy available from the wind, achieving the highest aerodynamic efficiency possible. However, if an underfrequency event happens (i.e., the load increases its power), with such an operation there is no margin to respond to the frequency variation. On the other hand, through de-loading, the operation is shifted from the maximum power point to a sub-optimal one, keeping a power margin to face that event [48].

To work in de-loaded condition is sufficient to reduce the coefficient of performance of the turbine (C_p), which is a function of the tip-speed ratio (λ) and of the pitch angle (β). The tip-speed ratio is proportional to the rotor rotational speed (ω_r). Consequently, it is immediate to derive the two possibilities to de-load the wind turbine: working in a rotational overspeed condition (as in [16]) or through a pitching control (Figure 3.2).

In case of rotational overspeed de-loading, if the maximum power and the rotational speed are known, the power setpoint can be determined as [11]:

$$P_{ref-del} = \frac{\omega_{del} - \omega_{meas}}{\omega_{del} - \omega_{opt}} (P_{max} - P_{del}) + P_{del} \quad (3.1)$$

$$P_{del} = K_{del} P_{max} \quad (3.2)$$

$$K_{del} = 1 - \frac{del\%}{100} \quad (3.3)$$

$$P_{max} = K_{opt} \omega_{opt}^3 \quad (3.4)$$

$$K_{opt} = \frac{1}{2} \rho \frac{C_{p,opt}}{\lambda_{opt}^3} \pi R^5 \quad (3.5)$$

In case of pitch controlled de-loading, an offset of pitch angle ($\Delta\beta$) is applied to the actual pitch (β_0) to decrease the C_p of the turbine.

Usually, rotor overspeeding is applied when the rotor speed is low, while for rotor speed equal or higher than the rated one the pitch control technique is used [5].

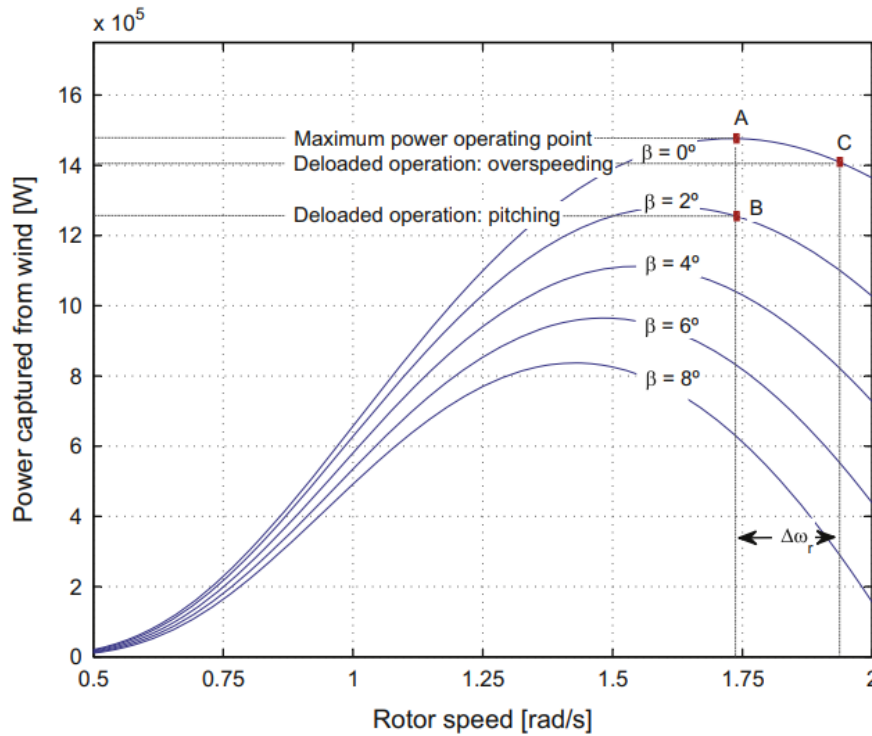


Figure 3.2: Power rotor-speed curves for different values of pitch angle and de-loaded options for a 1.5 MW wind turbine (wind speed: 10 m/s) [5]

De-loading of wind turbines has some limitations which historically confined it to very few practical applications. First of all, similarly for what happens for power curtailment of photovoltaic plants, the de-loading leads to a reduction of the annual capacity factor of the turbine. At the same time, overspeeding can reduce the turbine life. To determine power set-point it is crucial to arrange accurate wind speed

measurements, otherwise incorrect or rough estimations can highly affect power output and turbine life [11].

4 Developed model for small island power system with renewable generators participating to the primary frequency control

After an introduction about the issues and the possibilities deriving from highly renewable penetrated power systems, as well as an overview of the techniques to allow them participating to the inertial and primary frequency control, it is important to go through the model developed in this work.

It is demonstrated how the negative effects on stability due to a massive presence of variable renewable sources are more severe in small and isolated power systems, due to lack of interconnections with other systems and to their limited inertia. For this reason, many studies have assessed the impact on the frequency stability in small islands power system [16] [49].

This study selected a generic small island power system, i.e. the most challenging situation, to evaluate the coordinated effect on frequency stability of photovoltaic modules equipped with power reserve control and wind turbines with inertial control enabled.

The models described in the following have been developed using the Simulink software, which allows to easily observe and study a large variety of scenarios.

This chapter starts with an overview of the complete final model to offer a general introduction to the problem. Then, since it is composed by several blocks, they are studied individually in detail, highlighting their components, their features, the challenges found during their development and of course the literature documents which have been helpful to build them.

Once all the blocks have been studied, returning to the complete model, they are described the interactions between them, the initialization procedure and some useful tips in order to work on them and to perform simulations.

4.1. Assumptions of the model

The general Simulink model is presented in Figure 4.2.

Before starting to describe it, it is important to state the fundamental assumptions on which it is based, which are necessary to understand the work and its main objectives.

The most important observation regards the power system representation: in primary frequency control studies, i.e. in the time frame from 1 to 100 seconds, it is a common practice to schematize it using the *Load Frequency Control* (LFC) approach. In fact, in such problems, the time constants of the electromechanical variables are smaller and smaller with respect to the ones representing the dynamics of the mechanical variables of synchronous generation prime movers [4]. Furthermore, also the time constants of the wind turbines and photovoltaic converters are very small, justifying this approach. This kind of consideration is well represented in Figure 4.1.

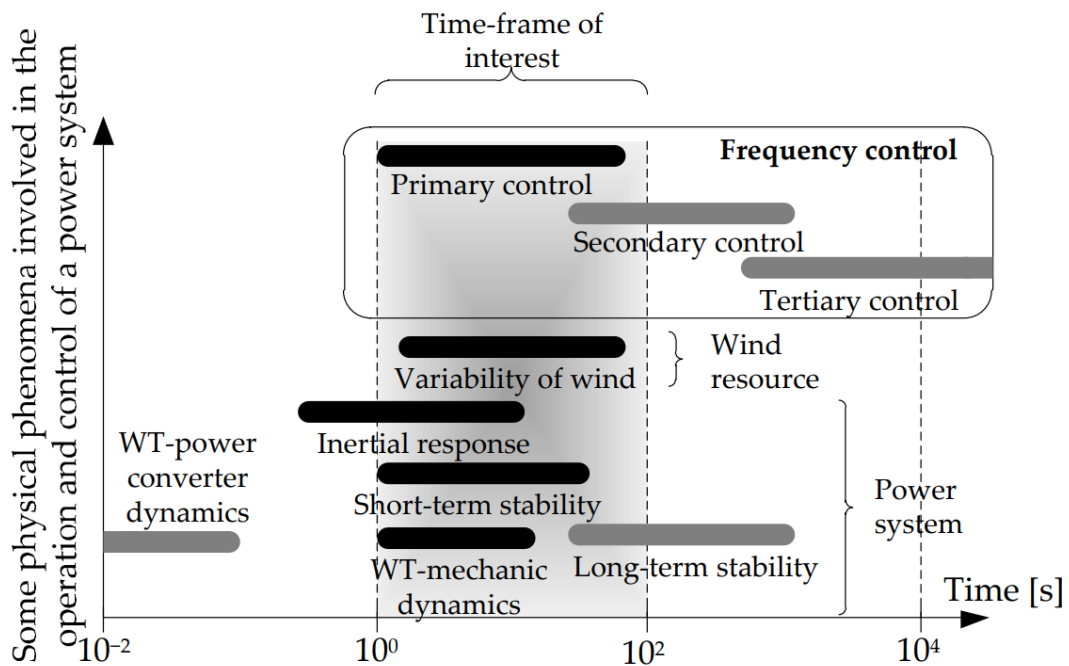


Figure 4.1: Typical time ranges in which the phenomena involved in the operation and control of a power system take place [18]

Due to this reasoning, the equivalent inertia constant of the system is the key parameter to obtain the dynamic frequency characteristics [50], together with the load damping constant, which describes the sensitivity of load power to the frequency variations [4]. This allows to represent the entire system response just through a transfer function block, making the problem at the same time easier to be modelled (the system is not modelled node by node) and more general.

A similar kind of reasoning is related to the generation blocks. Indeed, since the only aim of this work is to observe the inertial response and the primary frequency one, it has been chosen not to schematize the single generating units, but to aggregate them in equivalent generating units. This is valid in particular for the variable speed wind turbines and for photovoltaics. The same principle is applied to the load, which is schematized as a unique block.

The main advantages of this approach are the simplicity and the versatility of the results to a lot of practical cases, while the main drawback is the losing of detail.

To account the penetration of the different generating sources in the energy system it is used a participation factor (p_i), which represents the fraction of the total power of the system which is generated by the i -th source.

Other assumptions, which are quite usual in this kind of study, are related to the ambient conditions. In the simulations, they are accounted the effects of variable wind speed, variable irradiance and ambient temperature. At the same time, the non-uniform distribution of the wind resources among different wind turbines is neglected, since they are considered as an aggregate; the same happens for photovoltaic modules, which work under the assumption of uniform radiation and shading is neglected.

4.2. Overview of the general model

In Figure 4.2 it is shown the model for the system under study. It represents a small isolated power system, comprehending three kind of generating plants: a reheated steam turbine, wind turbines and photovoltaic units.

It has to be specified that the total generated power (that in equilibrium condition equals the load power), as well as the power of the three generating blocks, vary with the entity of the participation factors. In fact, in this kind of study, the importance is related to the relative weight of the three generating blocks rather than to the absolute magnitude of the system, since it is based on per unit variations in a reference common basis. This concept is particularly relevant for simulations at different participation factors, as the ones presented in Chapter 5. In that context it is explained in detail how to define the weight in terms of power of each unit, while in this chapter the aim is just to study the developed model, the equations that govern it, the connections and the features of each block.

Before going in detail of the characteristics of the different subsystems present in the model, it can be useful at least to understand the main connections between them, to facilitate their study.

Each of the three generation blocks produces a signal of variation of power in per unit with respect to the regime value (dP_i), which is the power corresponding to the initial condition:

$$P_{i_0} : \sum_i^3 P_{i_0} = P_{load_0} \quad (4.1)$$

Indeed, all the simulation are initialized to have a dP_i [pu] = dP_{load} [pu] = 0, corresponding to a frequency value equal to the nominal one, which is 50 Hz (i.e. $\Delta f = 0$).

The three signals of variation of power of the generating blocks are initially in per unit with respect to the generator nominal power, so they require to be weighted to obtain the equivalent variation on a common basis (the sum of the nominal powers of the three generators blocks): each of them passes through a gain block in which it is multiplied to its participation factor, as in Equation (4.2). The dP_{load} , on the contrary, is already defined in per unit common basis.

$$dP_i[pu \text{ common basis}] = p_i dP_i[pu] \quad (4.2)$$

For simplicity, from now on, in the equations it is omitted “common basis”.

Then, the four dP signals are summed up to obtain the instantaneous power unbalance of the entire system:

$$dP_{tot}[pu] = \sum_i^3 dP_i[pu] - dP_{load}[pu] \quad (4.3)$$

A non-negative power unbalance leads, through a transfer function, to a frequency deviation from the nominal value.

The transfer function describes the frequency response behaviour of the system. The meaning is captured by two parameters: H_{eq} is the equivalent inertia constant of the synchronous generator present in the system, while D is the damping constant of the load, which represents the sensitivity of the load power to the frequency variations.

The function output is the signal representing the frequency variation in per unit with respect to the nominal value, which is also one of the metrics to evaluate the developed model in the analysis presented in Chapter 5.

The frequency variation signal is also the main input for the controllers of the three generators. Indeed, the synchronous one is traditionally able to respond to a change in system frequency adapting its power, but in this study also photovoltaics and wind turbines are, thanks to the presence of the power reserve control block (PRC) and the inertial control block, respectively.

After this brief introduction, a more detailed analysis of each block is required, to understand the modelling of the generators as well as the functioning of the above-mentioned controllers.

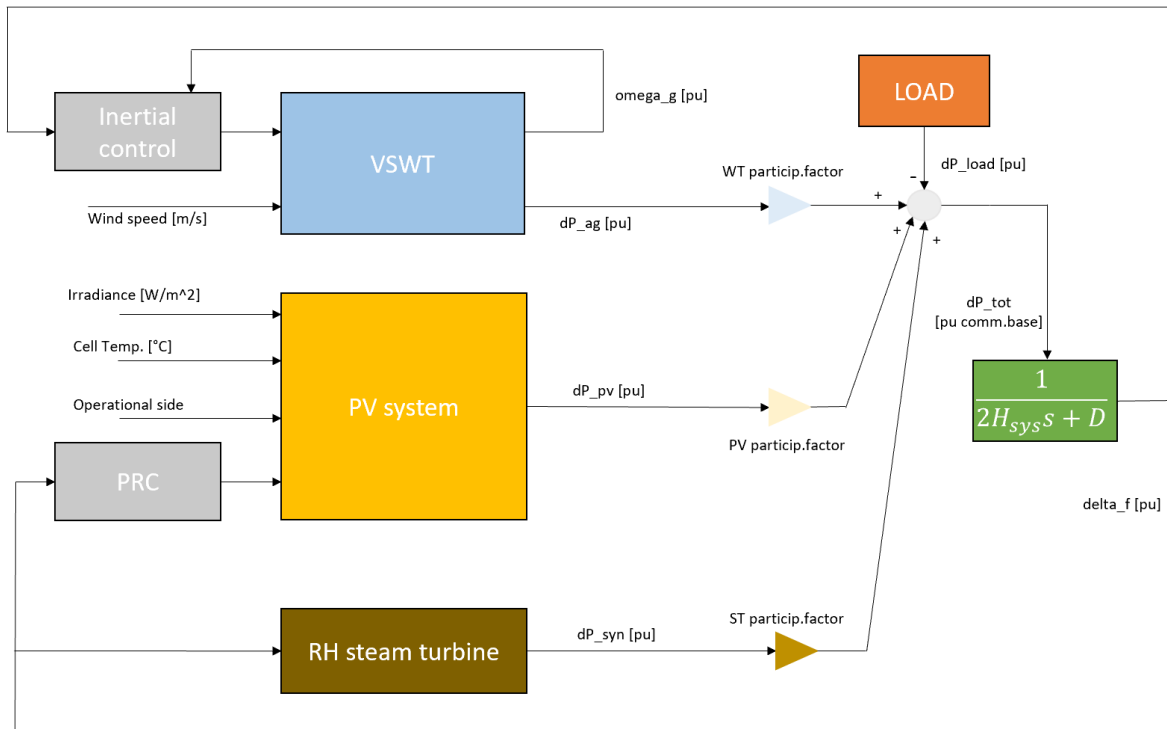


Figure 4.2: developed model simplified scheme

4.3. Photovoltaic generators model

One of the three generating blocks represents the photovoltaic modules present in the system. The modelling of this block has been quite challenging, requiring a lot of different literature sources as well as customized solutions to improve its functioning.

Firstly, Figure 4.3 gives an overview of the model.

The model is divided into two subsystems: the upper one contains the electrical model of a photovoltaic string, while the lower block represents the control system of the PV string, modified to operate the power reserve control.

Observing the inputs, some observations can be done:

- Irradiance and cell temperature are the two ambient conditions that mainly influence the performances of the photovoltaic modules. They are assumed to be measured in real time: this is a strong assumption, which implies for sure higher costs with respect to other solutions, as non-linear least squares fitting methods. This assumption comes from the fact that the aim of this work is

centred on the control logic, not on the determination of the irradiance and cell temperature.

- The reserve signal is produced by another subsystem which is presented in the following. It is sensible to frequency variation: if the frequency is at its nominal value, reserve level is fixed at a certain value imposed for the regime condition. When the frequency oscillates, the reserve level is adapted automatically to face this variation. Of course, this signal is required by the control system to calculate the operating PV string voltage corresponding to a curtailed operation.
- The last external input, indicated with *Side*, represents the desired operational side of the P-V curve in which operate the reserve control. Indeed, in this work it has been adopted the innovative approach proposed in [10], which allows, as a function of the requirements, to operate on both sides of the power curve, simply switching this input value, which is a Boolean type.

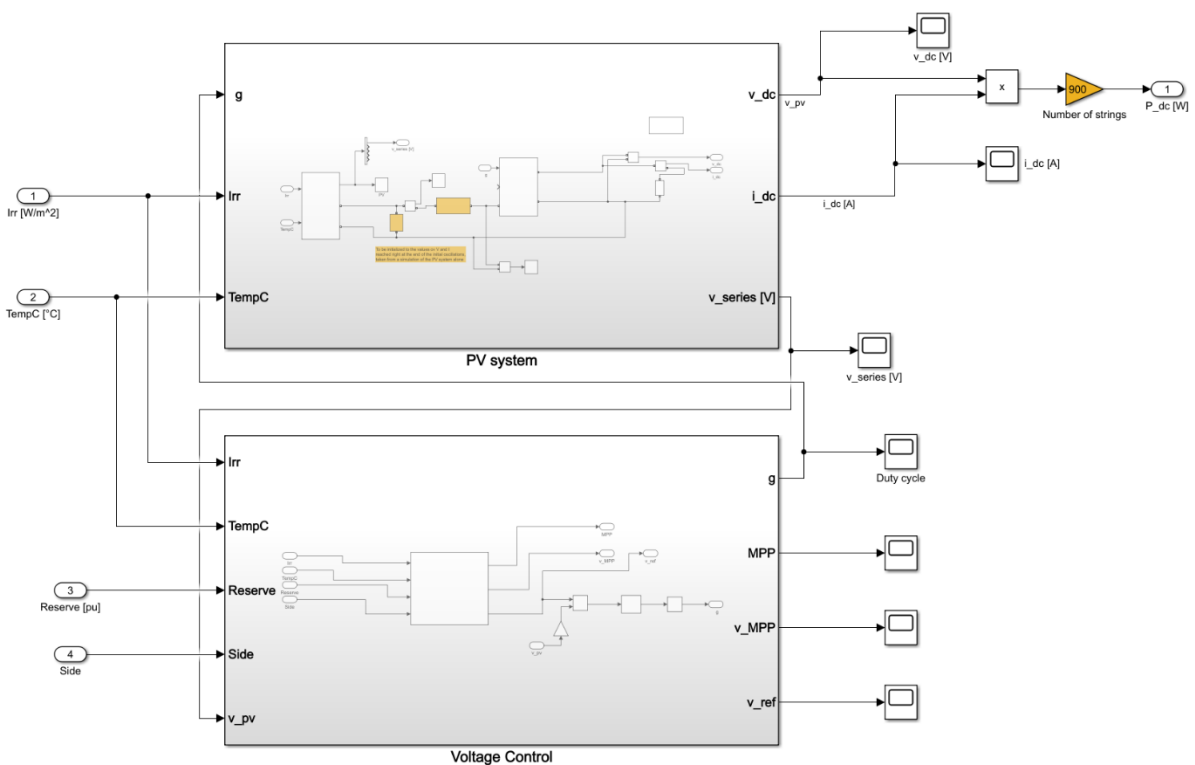


Figure 4.3: photovoltaic system model, including the electrical model (upper subsystem) and the voltage control (bottom subsystem)

The control system receives these four inputs, as well as the measurement of the actual voltage applied to the PV string, and calculates the maximum power point, the corresponding voltage, the reference voltage to operate in the desired curtailed

condition and, above all, a duty cycle signal for the boost converter necessary to impose that desired operation to the PV string.

4.3.1. Voltage control subsystem

The layout of the voltage control subsystem is shown in Figure 4.4.

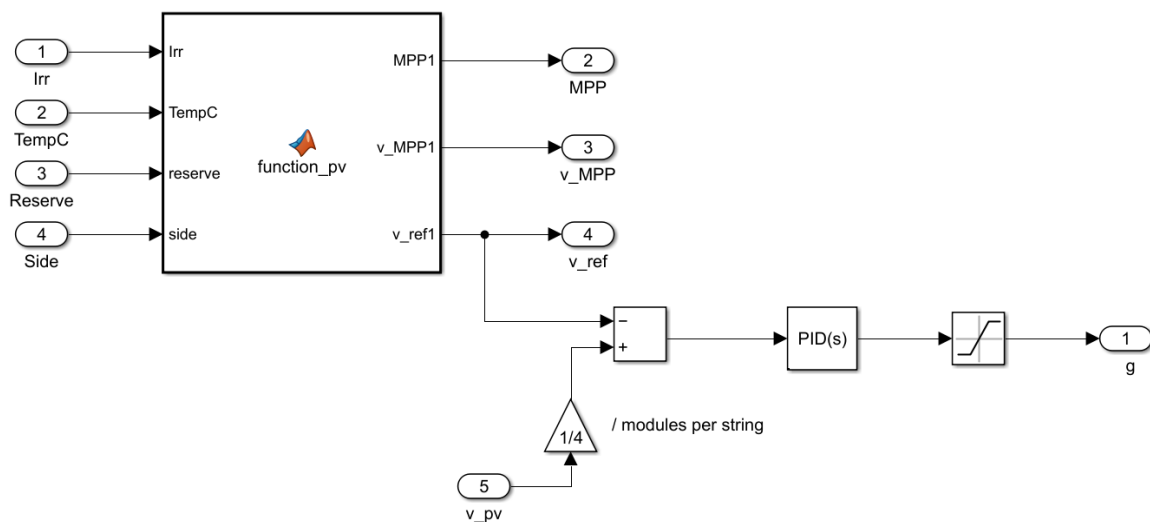


Figure 4.4: voltage control subsystem

It is mainly composed by a MATLAB function block and by a PID controller.

The function *function_PV* calculates the P-V curve and the output voltages already mentioned. To be able to solve it, it has been figured out that, due to Simulink memory overwriting errors, it is necessary to run it in the MATLAB environment, calling the actual function (which is *fcn_pv_mod*) using the `coder.extrinsic` command:

```

1 function [MPP1, v_MPP1, v_ref1] = function_pv(Irr, TempC, reserve, side)
2     MPP1 = 1;
3     v_MPP1 = 1;
4     v_ref1 = 1;
5     coder.extrinsic('fcn_pv_mod');
6     [MPP1, v_MPP1, v_ref1] = fcn_pv_mod(Irr,TempC,reserve,side);
7     end

```

Figure 4.5: *function_PV* body

Furthermore, to make Simulink able to capture that the output signals are scalar values, it is necessary to initialize them as scalars, differently from what happens in the classic MATLAB environment, which automatically understands the type of the output variables, since it does not have to handle signals.

Basically, continuously with time, *function_PV* is called and in turn it calls in the MATLAB environment the *fcn_pv_mod*, which calculates the outputs.

The fcn_pv_mod , for this reason, can be considered the “core” of the control system. Consequently, it is proposed a complete study of its body, which is fundamental to understand the photovoltaic system operation.

First of all, the selected PV module is the SOLARTECH POWER SPM210P, which is also present on Simulink database. The fundamental characteristics of the module are shown in Figure 4.6.

Module data	
Module:	Solartech Power SPM210P
Maximum Power (W)	209.916
Cells per module (Ncell)	60
Open circuit voltage Voc (V)	38.1
Short-circuit current Isc (A)	8.12
Voltage at maximum power point Vmp (V)	29.4
Current at maximum power point Imp (A)	7.14
Temperature coefficient of Voc (%/deg.C)	-0.36403
Temperature coefficient of Isc (%/deg.C)	0.051121

Figure 4.6: Solartech Power SPM210P datas

The first part of the function consists in initializing these module datas, as well as some useful constants as the elementary charge (q), the Boltzmann’s constant (k) and the reference irradiance and cell temperature:

```
function [MPP, v_MPP, v_ref] = fcn_pv_mod(Irr, TempC, reserve, side)
coder.extrinsic('fcn_pv_mod');
% Module: Solartech Power SPM210P

q = 1.60217662e-19; %elementary charge
k = 1.38064852e-23; %Boltzmanns constant
I_sc_ref = 8.12; % I_sc @Tcell,ref (TempC_ref)
V_oc_ref = 38.1; % V_oc @Tcell,ref
I_MPP = 7.14; % [A]
V_MPP = 29.4; % [V]
Irr_ref = 1000; % Reference irradiance
alpha_sc = 0.00051121; % temperature coefficient for the current
TempC_ref = 25; % Reference T cell
beta_oc = -0.0036403; % temperature coefficient for the voltage
Ns = 4; % number of modules in series (60 cells per module * 4 modules in series)
Nc = 60; % number of cells per module
```

Figure 4.7: fcn_pv_mod body - initialization

Since the modules would almost never work at the nominal ambient conditions, it is required to calculate the short circuit current and the open circuit voltage to the actual

irradiance and temperature conditions. The equations that describe this dependence are reviewed in [51].

Between the proposed correlations, they have been chosen the following two:

$$I_{sc} = I_{sc,ref} \frac{G}{G_{ref}} [1 + \alpha_{sc}(T_{cell} - T_{cell,ref})] \quad (4.4)$$

$$\begin{aligned} V_{oc} = & V_{oc,ref} * [1 + beta_{oc} * (T_{cell} - T_{cell,ref})] + 5.468511 * 10^{-2} \\ & * \log\left(\frac{G}{G_{ref}}\right) + 5.973869 * 10^{-3} * \log\left(\frac{G}{G_{ref}}\right)^2 \\ & + 7.616178 * 10^{-4} * \log\left(\frac{G}{G_{ref}}\right)^3 \end{aligned} \quad (4.5)$$

The corresponding implementation in *fcn_pv_mod* is obtained as in Figure 4.8.

The first aim of the function is to create two vectors, one containing the discretized voltages between 0 and V_{oc} , and one with the same length containing the P values corresponding to those voltage values.

From Equation (4.5) it is evident that the open circuit voltage varies with G and T_{cell} , and so the voltages vector. The dimension adaptation of the voltage vector in each practical situation is implemented in the function, as in Figure 4.8.

```
V_oc = V_oc_ref * (1+ beta_oc*(TempC-TempC_ref)) + 5.468511e-2*log(Irr/Irr_ref)+
5.973869e-3*log(Irr/Irr_ref)^2+ 7.616178e-4*log(Irr/Irr_ref)^3 ; % actual open
circuit voltage
I_sc = I_sc_ref * Irr/Irr_ref * (1+alpha_sc*(TempC-TempC_ref));
V = 0:0.01:ceil(V_oc); % discretized voltage vector going from 0 to V_oc
% to not have the vector P in the PV system varying its size at every
% iteration I can put as maximum the V_oc at a very low T (maximum V_oc),
% for example 45 V
```

Figure 4.8: *fcn_pv_mod* body – part 2

For the functioning of the algorithm, it is not necessary to produce the P-V curve as one of the outputs of the system, since the interesting value is just the reference voltage. The fact to exclude the P-V curve from the outputs could seem indifferent, but in practice, due to the variable size of the voltages vector (and so of the power vector), it creates a lot of troubles for Simulink, since it would be a signal with changing size at each instant. This is why in the outputs of the function is not present the P-V curve. In the present work the discretization of the voltage has been taken equal to 0.01 V, as a compromise between accuracy and solving time.

Going on in the explanation of the *fcn_pv_mod* body, it is at this point important to summarize the importance of the characteristic parameters of the module model, which are essential to derive the I-V curve.

In the work has been adopted the *Single-Diode Model* (SDM) of the photovoltaic cell, characterized by the equivalent circuit in Figure 4.9.

The characteristic parameters are shown in Figure 4.9: $I_{ph,cell}$ (also called I_L) is the photocurrent, $I_{s,cell}$ is the saturation current of the diode (also called I_0), n is the diode ideality factor, and $R_{s,cell}$ and $R_{sh,cell}$ are the series and shunt resistance, respectively. The electrical variables of interest are the PV cell terminal voltage ($V_{pv,cell}$) and current ($I_{pv,cell}$).

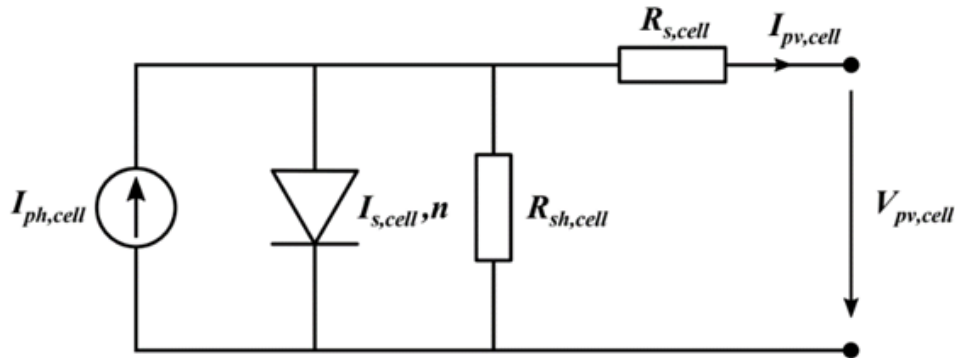


Figure 4.9: single-diode model for the photovoltaic cell

The parameters allow to solve the implicit equation describing the I-V characteristic of the cell (which is extendable to the module) [52]:

$$I = I_L - I_0 \left[\exp\left(\frac{V + I R_s}{n V_{th}}\right) - 1 \right] - \frac{V + I R_s}{R_{sh}} \quad (4.6)$$

in which V_t is the thermal voltage.

In principle, all the parameters necessary to solve the equation can be calculated analytically but, during the development of the work, it has been figured out that the coherent results with the electrical model of the Solartech Power module present in Simulink are obtained with the procedure described in the following.

First of all, R_s , R_{sh} and n are imposed equal to the ones automatically calculated by the Simulink module interface (Figure 4.10).

Diode ideality factor	<input type="text" value="1.0333"/>
Shunt resistance Rsh (ohms)	<input type="text" value="51.3726"/>
Series resistance Rs (ohms)	<input type="text" value="0.57569"/>

Figure 4.10: R_s , R_{sh} and n parameters

Knowing these, it is possible to determine analytically I_L and I_0 [52].

$$I_L \approx I_{sc} \frac{R_s + R_{sh}}{R_{sh}} \quad (4.7)$$

$$I_0 \approx \frac{I_{sc}(R_s + R_{sh}) - V_{oc}}{R_{sh}} \exp\left(-\frac{V_{oc}}{n V_{th}}\right) \quad (4.8)$$

These calculations are implemented in the function as in Figure 4.11.

```
% Parameters taken from simulink estimation
Rs = 0.57569;
Rsh = 51.3726;
n_ref = 1.0333;
V_t = Nc*k*(TempC+273.15)/q ;
V_t_ref = Nc*k*(TempC_ref+273.15)/q ;

% [Rs,Rsh,n_ref] = PV_parameters(I_sc_ref,V_oc_ref,I_MPP,V_MPP,V_t);

I_L = I_sc*(Rs+Rsh)/Rsh;
% I0 = ((I_sc-I_MPP)*(Rsh+Rs)-V_MPP)/Rsh * exp(-(V_MPP+I_MPP*Rs)/(n_ref*V_t));
I0 = (I_sc*(Rs+Rsh)-V_oc)*exp(-V_oc/(n_ref*V_t))/Rsh;
```

Figure 4.11: *fcn_pv_mod* body – characteristic parameters

The implicit solving function to obtain the I-V characteristic (Equation (4.6)) can be solved thanks to the MATLAB function *fzero*, applied to each voltage value, as in Figure 4.12.

```
%% solving equation for IV curve

I = zeros(1,length(V));
for ii = 1:length(V)
    fcn = @(x) x - I_L + I0 * (exp((V(ii)+x*Rs)/(n_ref*V_t))-1) + (V(ii)+x*Rs)/Rsh ;
    I(ii) = fzero(fcn,1);
    if I(ii) < 0
        I(ii) = 0;
    end
end
end
```

Figure 4.12: *fcn_pv_mod* body – I-V characteristic

The result is a vector *I* containing the current value corresponding to each discretized voltage value.

To obtain the power vector (i.e. the P-V curve) it is sufficient to multiply each element of the current vector to the corresponding one in the voltage vector. The *coder.varsize* command would be necessary to set a maximum size for the power vector, but, as already stated, since it is not an output the problem is not existing anymore.

```

%% PV curve
coder.varsize('PV_curve', [6000 1]);
PV_curve = I.*V ; % vector representing the PV_curve with a step of 0.01 V
% coder.varsize('PV_curve', [600 1]);

```

Figure 4.13: *fcn_pv_mod* body – P-V curve

Once the power-voltage characteristic is known, it can be easily extracted the maximum power point, as well as the corresponding voltage level. Indeed, the MPP is found as the maximum of the P-V curve. By finding its index in the power vector, it is possible to extract the corresponding voltage v_{MPP} .

```

%% MPP tracking
[MPP, pos_MPP] = max(PV_curve);
v_MPP = V(pos_MPP);

```

Figure 4.14: *fcn_pv_mod* body: MPP

In the last part of the function it is found the reference voltage for the power reserve control. In particular, knowing the desired reserve amount, it is possible to calculate the corresponding power. Once this is known, an operational side of the power curve is imposed through an external signal, allowing to determine the reference voltage (v_{ref}) thanks to a simple minimization problem, finding the voltage vector element on the desired side which is corresponding to the calculated curtailed power.

```

%% operational voltage
P_ref = MPP*(1-reserve);
pos_ref = 1;
if side == 0
P_vec = PV_curve(1:pos_MPP);
[~, pos_ref] = min(abs(P_vec-P_ref));
v_ref = V(pos_ref);
else
P_vec = PV_curve(pos_MPP:end);
[~, pos_ref] = min(abs(P_vec-P_ref));
v_ref = V(pos_ref);
end

```

Figure 4.15: *fcn_pv_mod* body: reference voltage for PRC

By comparing the maximum power point voltage in standard test conditions (1000 W/m², 25°C) calculated through the *fcn_pv_mod* function and the one taken from the datasheet, they have correctly the same value, equal to 29.4 V.

In **Errore. L'origine riferimento non è stata trovata.** it is shown the calculated P-V curve of the module Solartech Power SPM210P in standard test conditions, including the MPP and the curtailed operating condition in the hypothesis of left side operation.

The reference voltage signal is then compared with the actual voltage applied to the module, producing an input for the PI controller, which imposes the second one to be equal to the first. It is important to notice that the voltage v_{pv} coming from the electrical

model of the photovoltaic plant is the one referred to the entire series of four modules, thus it has to be divided by four to obtain the voltage applied to the single module.

The PI constants are reported in:

Proportional (P)	0.03
Integral (I)	1

Table 4.1: voltage control PI controller constants

These values have been chosen in order to limit the oscillations of voltage during the initialization transient, i.e. minimizing the initialization time.

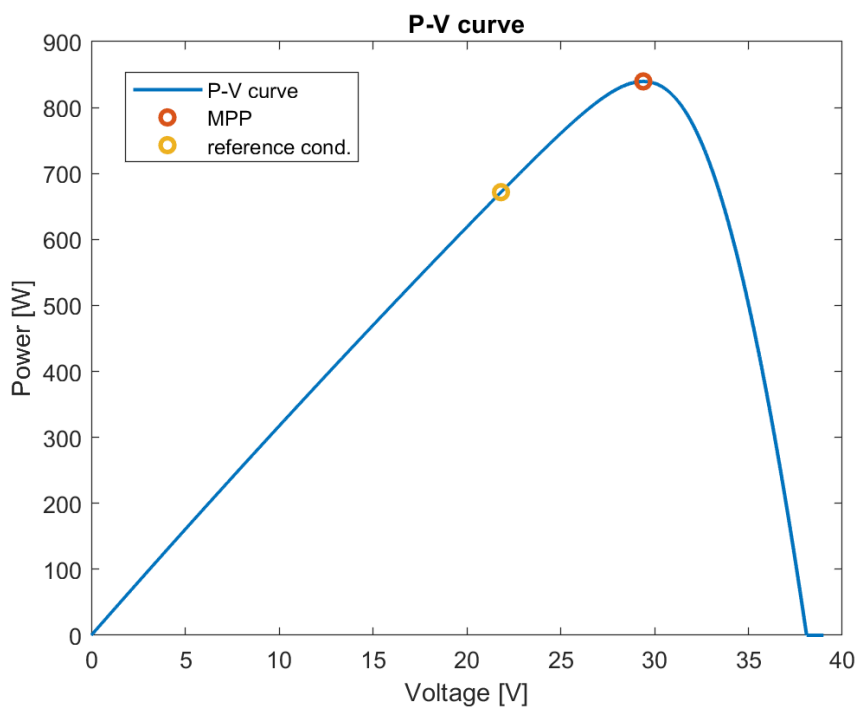


Figure 4.16: example of resulting P-V curve with MPP and reference condition

Then, since the duty cycle signal has to be limited to values between 0 and 1, a saturation block is inserted after the PI controller.

The output signal of the voltage control subsystem is then the duty cycle, which is imposed to the DC-DC boost converter in order to set the module (the series) voltage to the desired value. This is better explained in the next subsection, in which the subsystem containing the electrical model of the PV series is described.

4.3.2. Electrical model of the PV module subsystem

The second subsystem forming the photovoltaic system block is the one containing its electrical model, which is in practice the object of the control subsystem's operation.

This is way more complex in terms of layout with respect to the voltage control one, but at the same time it is less challenging to be implemented.

Indeed, it is basically composed by a predefined PV Array Simulink block in parallel with a capacitor, then a series inductor and a boost converter block (which does not contain the inductor, this is why it is needed to insert it separately). The DC-DC converter connects these ones to a DC-link, whose voltage for the aims of this work is assumed to be fixed to 230 V, as common practice in the literature when studying the power reserve control of a PV system [10]. In practice, it has been used the Single-Stage PV model already mentioned in subchapter 2.4.

The subsystem scheme is presented in Figure 4.17.

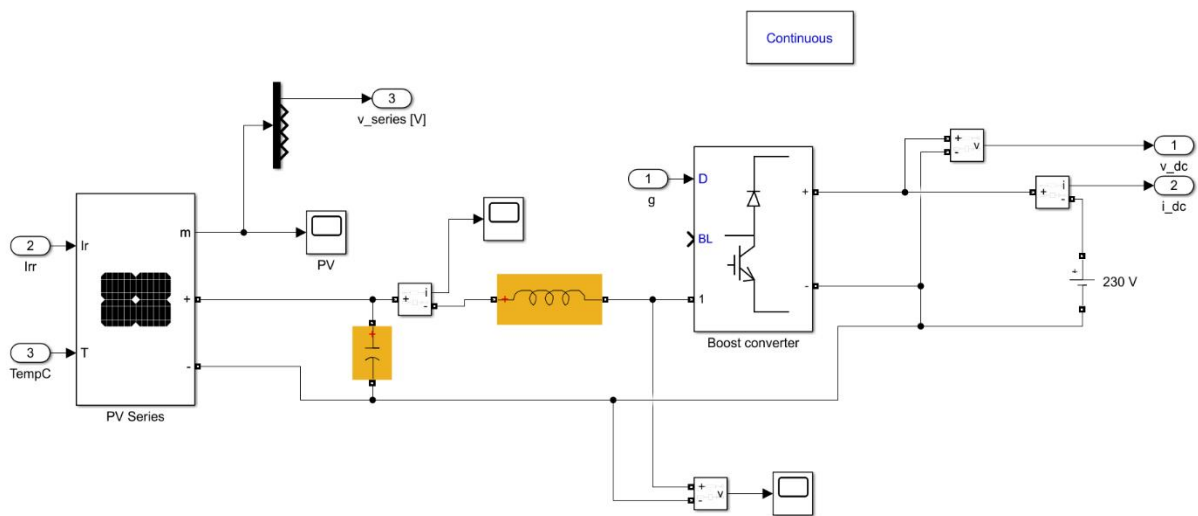


Figure 4.17: PV electrical scheme subsystem

The PV series is composed of four modules Solartech Power SPM210P. The datas of the module have been already presented in the previous subsection. The output of the predefined Simulink PV block is a five-element vector, containing five measured parameters, indicated with m : PV array voltage, PV array current, diode current, irradiance and temperature. The block is electrically connected with a capacitor and a boost converter (i.e. inductor + boost converter block).

The parameters of the capacitor and of the inductor are summarized in Table 4.2: capacitor and inductor parameters:

Capacitor capacitance [F]	100e-6
Inductor inductance [H]	10e-3
Capacitor initial voltage [V]	To be initialized
Inductor initial current [A]	To be initialized

Table 4.2: capacitor and inductor parameters

The values of capacitance and inductance have been set in order to reduce the initialization transient time (i.e. the time to reach the initial regime condition), which is one of the main issues of the present model.

The initial values of voltage and current have to be set during the initialization procedure explained at the end of this chapter. Also in this case the target is to reduce the initial transient time, which has been figured out to be strongly dependent on the initialization values assigned in various parts of the model.

The boost converter block has been used with default settings: average model (which enables the operation controlled by a duty cycle signal) and predefined parameter values. It receives the duty cycle signal coming from the voltage control block, which dictates the operation of the block. It is fundamental to not provide as input the signal containing BL , because this will hinder the pulses of the Pulse Width Modulation (PWM) generator.

The boost converter is interfaced with a DC voltage source, whose value is fixed to 230 V. Since the boost converter can only step-up the voltage, it is important to check that the voltage applied to the PV string is always lower than this value. This is why, given the characteristics of the Solartech module, it has been selected four as number of modules in series. Indeed, even if they operate at their maximum voltage (V_{oc}), they are not reached 230 V.

Two measurements of voltage and current are present on this side of the boost converter: the voltage of course is fixed to 230 V, and the current varies. The two are the outputs of the subsystem, which are then multiplied each other to obtain the power of the PV string. The other output of the subsystem is the voltage applied to the string, which is extracted from the m vector output of the PV array block and sent to the voltage control block as v_{pv} .

Returning to Figure 4.3, it can be seen the product between the voltage and the current to obtain the power of a string, and the subsequent gain block that multiplies it by the number of strings present in the power system to obtain the overall photovoltaic power.

In this sense, it is important to recall the assumptions of this model: the PV modules operate all under the same irradiance and temperature conditions and are all grouped in strings formed by four modules. In the conclusions about this work, they are presented proposals for future developments, including a more detailed layout allowing, for example, the accounting of shadowing and different irradiance conditions between the strings.

4.3.3. Reserve adaptation to frequency changes

To fully describe the photovoltaic system, it is necessary to specify another aspect: how the adaptation of the active power output happens in response to a frequency change.

This of course is implemented partially in the voltage control block, but to close the loop it is important to notice how the *reserve* input signal is generated.

The reserve adaptation block scheme is represented in Figure 4.18:

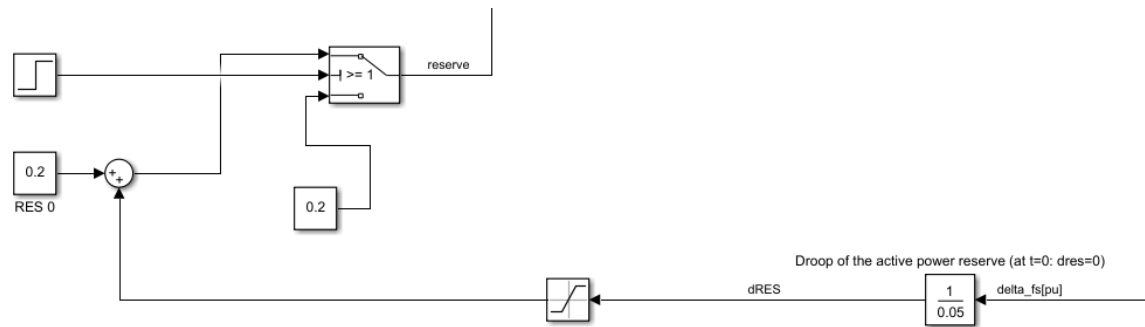


Figure 4.18: reserve adaptation scheme

The input signal contains the per unit frequency deviation. It has been decided to adapt the reserve through a droop characteristic. In practice, as happens for the traditional droop control, the output variable is changed proportionally to the input one. In this case the reserve is increased if the frequency increases, i.e. the power produced is reduced working further from the MPP.

It is fundamental to set a proper droop value. To do so, they have been performed a lot of tests during the development of this work. On one hand a too high droop constant means that the reserve varies very slightly, providing insufficient help to the primary frequency control. On the other hand, a too low droop constant leads to a reserve depletion or to an extremely low power production. For this reason, as a compromise, it has been selected 0.05, which is identical to the droop constant of the synchronous generators presented in the following of this work.

The droop block needs to be initialized. Consequently, an initial reserve value has to be imposed. It has been decided that, in correspondence of the initial regime condition, the *reserve* signal has to be equal to 0.2, with a null *dRES*, since the frequency deviation is equal to zero before the perturbations.

To implement so it is sufficient to add a 0.2 value to the *dRES* signal, which initially is null, obtaining the desired reserve value. Since the 0.2 addition is always present during the simulation time, it is important to limit the excursion of the *dRES* value, to respect the constrain:

$$reserve \in [0; 1] \quad (4.9)$$

Therefore, it is required a saturation block limiting the *dRES* signal as:

$$dRES \in [-0.2; 0.8] \quad (4.10)$$

To complete the description of this system it is necessary to state that, in case of simulation on the PV system alone, the presence of a switch to initially provide a constant reserve value to the PV system block helps to accelerate the initialization transient, but, in case of complete system with PV, wind turbines and synchronous generators, its presence is not required.

4.4. Variable Speed Wind Turbine participating to primary frequency control model

The modelling of a variable speed wind turbine is very complex. Indeed, they are present a lot of separated components which interact each other, and this becomes even more complicated in case of inertia and primary frequency control provision.

In this model, two main references have been taken into account: [17] proposes a model for the VSWT itself, which is then used as basis for the primary frequency control studies, implementing the extended OPPT method described in [18].

Furthermore, a big challenge that has been faced concerns the initialization process: for an effective operation of the model, as happens also for the photovoltaic system, it has been crucial to develop an effective initialization procedure.

This subchapter is thus divided into two subsections: one explains the VSWT model, while the other details the frequency control participation and the model implementing it.

4.4.1. VSWT model

There are a lot of different solutions when designing a wind turbine. Indeed, for example, they do exist several types of generators that can be coupled to the rotor. In this case, it has been chosen to operate with a variable-speed wind turbine using a DFIG (*doubly-fed induction generator*) and with a pitch control enabled.

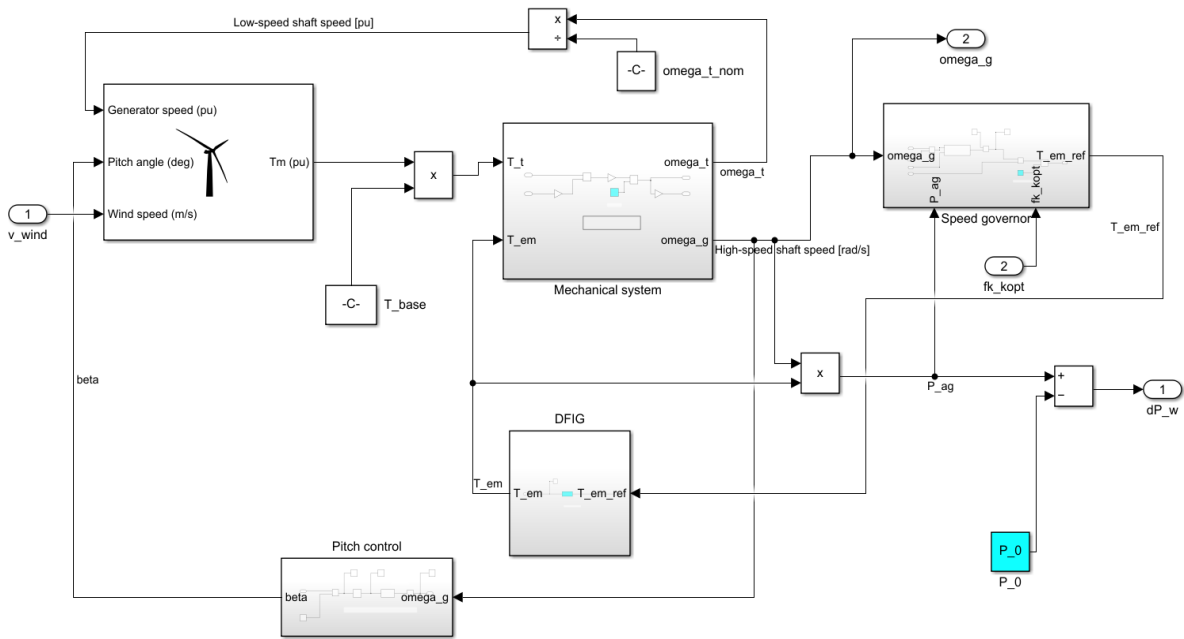


Figure 4.19: block scheme VSWT

The block scheme of the model is presented in Figure 4.19. They are present five principal blocks: the variable pitch wind turbine, the mechanical system, the speed governor, the generator and the pitch control.

To model the wind turbine it has been chosen the predefined Simulink model, filled with the datas shown in Figure 4.20. It produces better results with respect to a user defined Matlab function containing the characteristics of the wind turbine, and of course has the big advantage to be simple.

Parameters	
Nominal mechanical output power (W):	<input type="text" value="1.5e6"/>
Base power of the electrical generator (VA):	<input type="text" value="1.5e6/0.9"/>
Base wind speed (m/s):	<input type="text" value="12"/>
Maximum power at base wind speed (pu of nominal mechanical power):	<input type="text" value="0.73"/>
Base rotational speed (p.u. of base generator speed):	<input type="text" value="1.2"/>
Pitch angle beta to display wind-turbine power characteristics (beta >=0) (deg):	<input type="text" value="0"/>

Figure 4.20: Wind turbine block parameters [17]

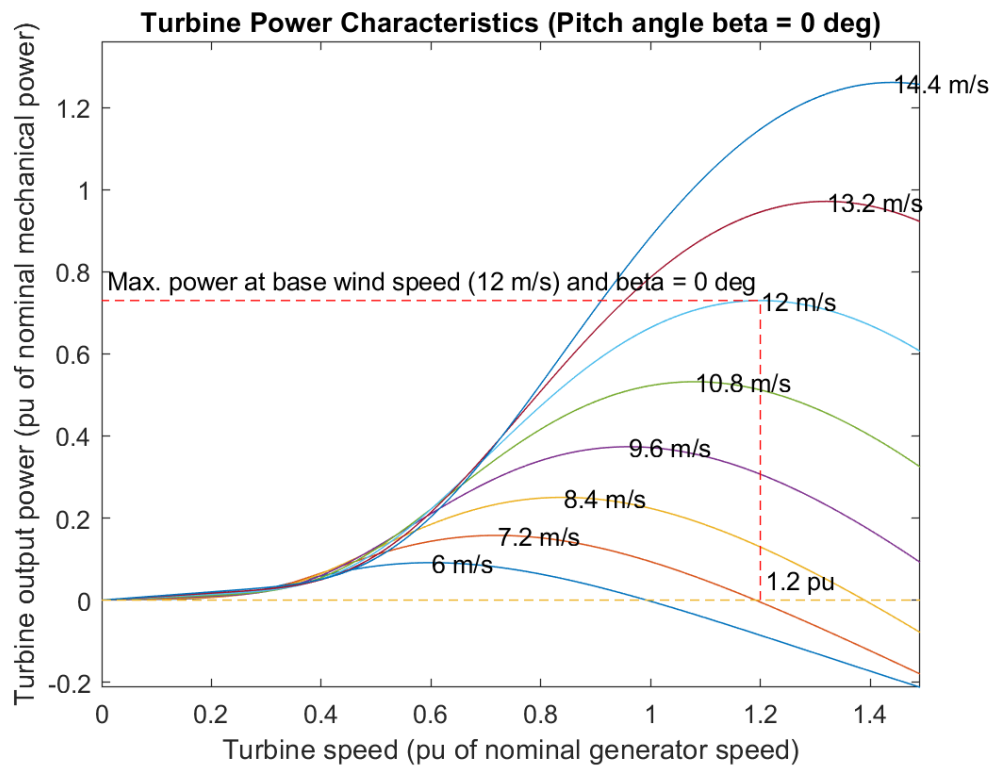


Figure 4.21: Wind turbine power characteristics

The base turbine power is set to 1.5 MW: this number is particularly significant when defining the participation factors of the three types of generator present in the model, as explained in Chapter 5.

Other characteristic parameters that are important to describe and study the wind turbine system can be calculated as in the following:

Parameter name	Value	Equation
Nominal frequency	$f = 50 \text{ Hz}$	
Pair of poles generator	$p = 2$	
Gearbox ratio	$n = 95.55$	
Base rotat. speed high-speed shaft	$\omega_{g,base} = \frac{2\pi f}{p} = 157.08 \text{ rad/s}$	(4.11)
Base rotat. speed low-speed shaft	$\omega_{t,base} = \frac{2\pi f}{n p} = 1.644 \text{ rad/s}$	(4.12)
Base torque low-speed shaft	$T_{t,base} = \frac{P_{base}}{\omega_{t,base}} = 912408.7591 \text{ Nm}$	(4.13)

Table 4.3: fundamental parameters of the wind turbine model

The turbine block receives as inputs the wind speed, the pitch angle signal and the low-speed shaft rotational speed in per unit. Basically, the block enters in the characteristics shown in **Errore. L'origine riferimento non è stata trovata.** and calculates the power in per unit, then divides it for the rotational speed to obtain the

$$T_{t[pu]} = \frac{P_{t[pu]}}{\omega_{t[pu]}} \quad (4.14)$$

torque applied to the low-speed shaft.

This torque signal is converted to absolute value multiplying for the base low-speed shaft torque and sent to the mechanical system block. It is really important to notice that, since the turbine drives a generator, the convention sets that the sign of the torque is negative: this is why the output T_m of the Simulink wind turbine block is negative. Thus, to obtain a positive value of torque to be used in the rest of the model, the base torque has to have a sign minus. If this step is not respected, the model will produce absolutely wrong results.

The mechanical system block represents the gearbox dynamics, which is coupled on one side to the rotor (low-speed side) and on the other side to the generator (high-speed side) (Figure 4.22). It is modelled as a unique mass system [53], characterized by an equivalent moment of inertia J_{eq} , given by the sum of the moments of inertia of the rotor, of the gearbox and of the generator.

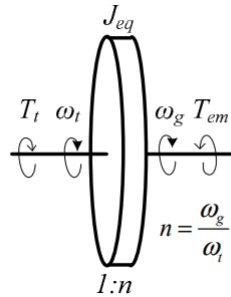


Figure 4.22: Gearbox conceptual representation

The dynamics can be described through Equation (4.15):

$$T_t - nT_{em} = J_{eq} \frac{d\omega_t}{dt} \quad (4.15)$$

with the variables expressed in their dimension, not in per unit.

Through Laplace operator it is possible to obtain the equivalent block scheme, presented in Figure 4.23.

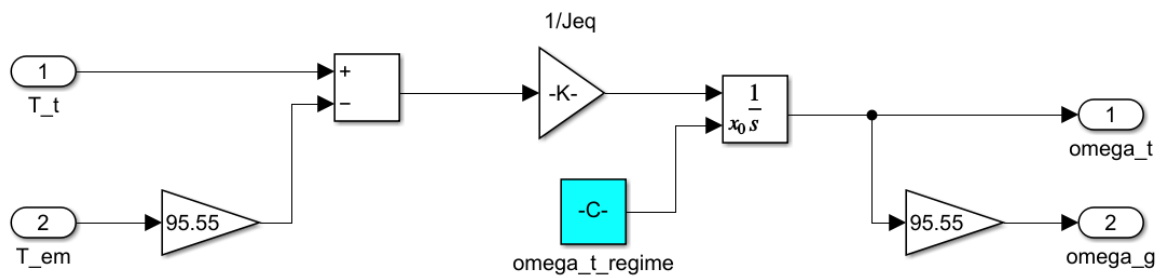


Figure 4.23: mechanical system block scheme

It is possible to observe that a difference in the torques of the two shafts causes a variation of their speed, and the moment of inertia plays the role of a proportionality constant. The output of the integrator block needs to be initialized with an external signal, named *omega_t_regime*. The initialization procedures are explained in detail at the end of this chapter.

It is also required to specify that the comparison between the torques has to take into account the gearbox ratio, represented by a gain block. The same happens on the rotational speed side, to respect the power balance in regime conditions:

$$T_t \omega_t = T_{em} \omega_g \quad (4.16)$$

The moment of inertia used in this model is obtained starting from a more common parameter, which is the equivalent inertia constant H_{eq} , through Equation:

$$\frac{1}{J_{eq}} = \frac{1}{2} \frac{\omega_{t,base}^2}{H_{eq} P_{base}} \quad (4.17)$$

with $H_{eq} = 5.29$ s (one mass model) [17].

The low-speed shaft rotational speed signal returns to the Simulink wind turbine block, while the high-speed shaft one is used as input for the speed governor block, represented in Figure 4.24.

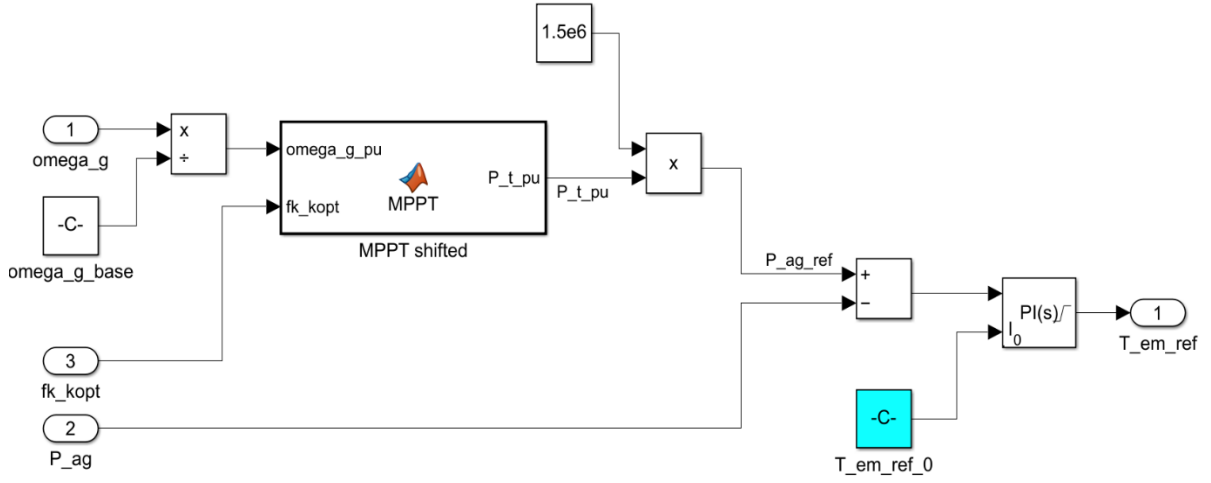


Figure 4.24: speed-governor block scheme

It is composed of two subsequent operations: first of all, a reference power signal is produced through a customized MATLAB function; then, the reference signal of power and the actual power are compared and an electromagnetic torque reference signal is calculated thanks to a PI controller.

The MATLAB function enables the frequency control participation of the wind turbine. In this sense, it can be considered one of the core components of the system. Indeed, it contains the power characteristic of the wind turbine, i.e. the power produced as a function of the ω_{g_pu} . As intuitive by its name, *MPPT shifted* is however modified with respect to the maximum power point characteristic.

To understand this modification, it is necessary to take a look at the function body (Figure 4.25).

They do exist four characteristic rotational speed values that define the characteristic shape of the $P-\omega$ function, which is described by:

$$P(\omega_{g[pu]}) = \begin{cases} K_{opt}\omega_0^3 \frac{\omega_g - \omega_{min}}{\omega_0 - \omega_{min}}, & \omega_{min} < \omega_g < \omega_0 \\ K_{opt}\omega_g^3, & \omega_0 < \omega_g < \omega_1 \\ P_{max} + (P_{max} - K_{opt}\omega_g^3) \frac{\omega_g - \omega_{max}}{\omega_{max} - \omega_1}, & \omega_1 < \omega_g < \omega_{max} \\ P_{max}, & \omega_g \geq \omega_{max} \end{cases} \quad (4.18)$$

With respect to this base case, by looking at the function body it is evident the presence of a factor called fk_kopt that substitutes the K_{opt} factor. This number is calculated in the synthetic inertia subsystem and allows to shift the “classical” characteristic curve in order to exploit the inertia of the wind turbine and to participate to the frequency control tasks.

```

function P_t_pu = MPPT(omega_g_pu, fk_kopt)
P_t_pu = 0;
omega_0 = 0.71;
omega_min = 0.7;
omega_1 = 1.2;
omega_max = 1.21;
P_max = 1;
if omega_g_pu > omega_min && omega_g_pu < omega_0
    P_t_pu = fk_kopt*(omega_0)^3*(omega_g_pu-omega_min)/(omega_0-omega_min);
elseif omega_g_pu > omega_0 && omega_g_pu < omega_1
    P_t_pu = fk_kopt*omega_g_pu^3;
elseif omega_g_pu > omega_1 && omega_g_pu < omega_max
    P_t_pu = (P_max-fk_kopt*omega_1^3)/(omega_max-omega_1)*(omega_g_pu-omega_max)+P_max;
elseif omega_g_pu >= omega_max
    P_t_pu = P_max;
elseif omega_g_pu < omega_min
    P_t_pu = 0;
end
end

```

Figure 4.25: MPPT shifted body

Actually, as better explained in the next subsection, fk_{kopt} is the result of the multiplication:

$$fk_{kopt} = f_{kopt} K_{opt} \quad (4.19)$$

To better understand the role of this factor, it is useful to observe its influence on the characteristic curve on a graph:

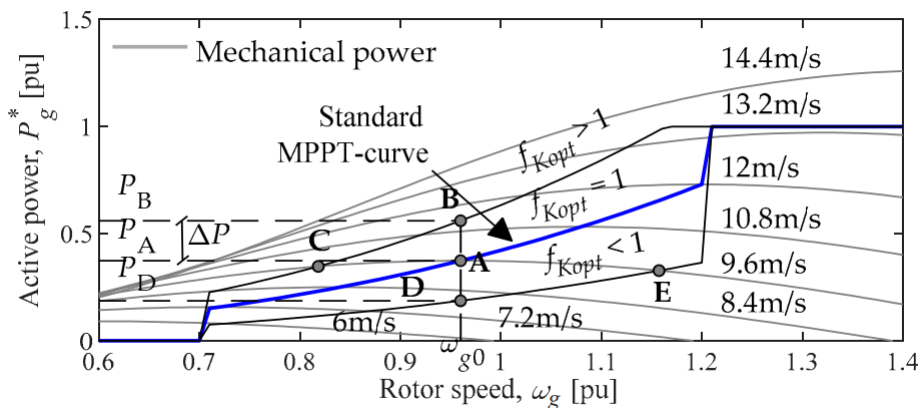


Figure 4.26: Mechanics of the method based on virtual inertia control [18]

This kind of control is called Extended OPPT Method, and its implementation will be better described in the next subsection. For now, it is sufficient to know that its action to counter a frequency deviation depends both on the system frequency variation itself (Δf_s) and on the system frequency derivative (df_s/dt).

Looking at the P - ω chart in Figure 4.26, it is possible to understand the functioning of the OPPT algorithm. Under the hypothesis of constant wind speed and normal

operating conditions, the generator will deliver a power P_A , associated with a rotational speed ω_{g0} . If it happens an underfrequency event, caused for example by a mismatch between the injected and the consumed power in the system, it will be required an increase in the power output of the turbine to reduce as much as possible the frequency oscillation. In particular, the non-null value of Δf_s and df_s/dt will activate the inertial response emulation of the wind turbine, with a consequent shift of the MPPT curve upwards (A \rightarrow B). The higher the severity of the underfrequency event (and so the magnitude of Δf_s and df_s/dt), the higher will be the value assumed by P_B . In this situation, the unbalancing between the active power extracted from the electric generator and the mechanical power delivered at the turbine shaft will cause a deceleration of the rotating masses of the turbine, testifying the exploitation of the turbine kinetic energy. This deceleration moves the operational point on the left (B \rightarrow C), reaching a new equilibrium condition when P_C coincides with P_A , situation that corresponds to a balance between the mechanical power delivered by the turbine and the active power extracted by the generator (P_C). When the support is not anymore necessary, the system returns to the initial state (C \rightarrow A), preparing it for future requirements [18].

The final output of the *MPPT shifted* function is the reference power. Then, the difference between this signal and the actual power one is used as input for a PI controller having the settings proposed in Table 4.4, that have been taken from [17] to be coherent with the other values assigned to the model.

Proportional constant (P)	3
Integral constant (I)	80

Table 4.4: speed governor PI controller parameters

This governor produces as output a signal containing the reference electromagnetic torque to be fed to the DFIG block ($T_{em,ref}$). The output of the PI controller is part of the parameters that need to be initialized before starting the simulation, as explained later on.

The DFIG block is relatively simple, due to the hypothesis that, for primary frequency control studies, the generator and all the electronic converters related to it can be modelled as a unique actuator, which receives a reference torque signal and adapts its output (i.e. its actual torque) to this input value following the dynamics of a first order system characterized by a time constant τ_c [54] [55] [56].

The corresponding block scheme can be seen in Figure 4.27.

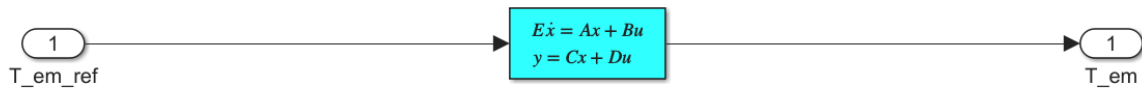


Figure 4.27: DFIG block scheme

To express the dynamics it has been chosen a state-space model, using the following constants, with $\tau_c = 0.02$:

Descriptor state-space model:	
$E\dot{x}/dt = Ax + Bu$	
$y = Cx + Du$	
Parameters	
E:	<input type="text" value="tau_C"/>
A:	<input type="text" value="-1"/>
B:	<input type="text" value="1"/>
C:	<input type="text" value="1"/>
D:	<input type="text" value="0"/>

Figure 4.28: DFIG dynamics state space model constants

It has been decided to use a state-space model since, with respect to a transfer function block, it allows to initialize the output signal.

To develop it the starting point is the corresponding transfer function:

$$T_{em} = \frac{1}{1 + \tau_c s} T_{em,ref} \quad (4.20)$$

By rearranging and imposing:

$$\begin{cases} x = T_{em,ref} \\ u = T_{em} \end{cases} \quad (4.21)$$

it is found:

$$\tau_c \dot{x} = -x + u \quad (4.22)$$

from which $E = \tau_c$, $A = -1$, $B = 1$. Furthermore, since $y = x$ is imposed (y is not needed to model the DFIG), $C = 1$.

It has also to be noticed that the produced torque is another variable to be initialized.

The signal of T_{em} coming from the DFIG returns to the mechanical system block, closing a loop. At this point, they are available all the elements required to calculate the active power produced by the turbine. In fact:

$$P_{ag} = T_{em} \omega_g \quad (4.23)$$

One last block is remaining, which is the pitch control subsystem (Figure 4.29).

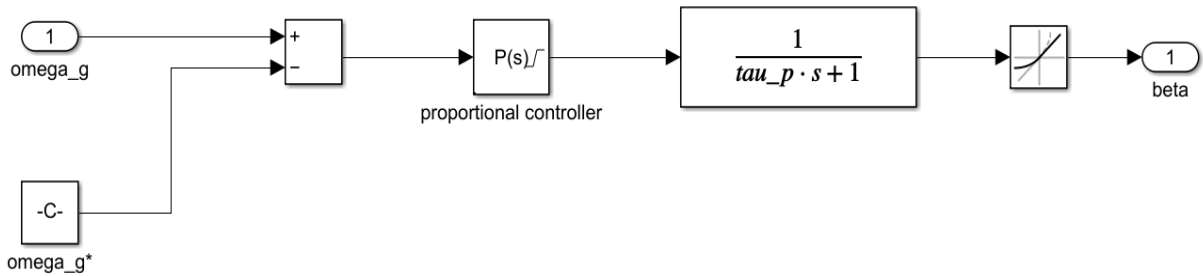


Figure 4.29: pitch control block scheme

The aim of the pitch control block is to limit the output power to the maximum value for wind speeds higher than the nominal one. To do so, the blade is rotated around its axis to modify the pitch angle (β) and reducing the coefficient of performance.

Inside it, the high-speed shaft rotational speed is compared with the maximum speed, and the difference is sent to a proportional controller, having the proportional constant equal to 500 [17]. The output signal is then fed to a transfer function, representing the dynamics of the mechanism to physically operate the blade rotation, which has been assumed to be a first order type [17].

Of course, the proportional controller has to take into account the physical limits of the pitch angle, which has to be comprised between 0° and 45° .

The first order dynamics is represented through a transfer function block, in which τ_p is equal to 0 s, i.e. the pitch variation is instantaneous. To limit the rate of variation of the pitch angle a rate limiter has been inserted to the block scheme.

The produced beta signal is sent to the Simulink wind turbine block, closing another loop.

This completes the description of the wind turbine system model. However, as already stated, to participate to the frequency control tasks, i.e. to enable the Extended OPPT Method, it is necessary to calculate the f_{k_kopt} factor, which introduces the capability to be sensible to frequency variations. This is why, in the next subsection, it is presented in detail the inertial control subsystem, which provides the f_{k_kopt} signal to the wind turbine speed governor.

4.4.2. Inertia control subsystem

In wind turbines there are vast amounts of inertia available, but they cannot be exploited with the traditional control scheme. To make them able to provide an effective inertial response, some methods have been proposed in literature, as reviewed in 3.1. As already explained, additional control loops are necessary to modify the MPPT algorithm by introducing new power setpoints that depend on the entity of the frequency deviation.

In this work an inertial-droop method has been adopted, whose name is Extended OPPT Method (*Extended Optimized Power Point Tracking*) [18]. As already seen in the previous subsection, it consist in the introduction of a *signal for the optimization zone* ($f_{k,opt}$), that allows to shift the operation of the wind turbine from the MPPT curve to other curves by exploiting the kinetic energy of the rotor.

The control function of the method is shown in Equation (4.24). As can be observed, $f_{k,opt}$ depends both on the frequency deviation and on the time derivative of the frequency. Indeed, the effectiveness of this virtual inertia algorithm depends both on the magnitude of the frequency disturbance (through Δf_s and df_s/dt) and on the initial kinetic energy stored in the rotor before the disturbance.

$$f_{Kopt} = \left(\frac{\omega_{g0[pu]}}{\omega_{g0[pu]} + k_{vir}\Delta f_{s[pu]}} \right)^3 - W_{vir} \frac{k_0}{K_{opt}\omega_{g0[pu]}^3} f_{s[pu]} \frac{df_{s[pu]}}{dt} \quad (4.24)$$

where:

$$K_0 = 2 \frac{\omega_{g0[pu]}}{\omega_{s0[pu]}} k_{vir} H_{WT} \quad (4.25)$$

with $\omega_{s0[pu]}$ that is the pre-disturbance rotational speed corresponding to the system frequency, that in per unit is equal to 1, and:

Parameter	Name	Value [18]
-----------	------	------------

k_{vir}	design constant	8
W_{vir}	weighting factor	0.2
ω_{g0}	pre disturbance ω_g	to be initialized
H_{WT}	VSWT inertia constant	5.29 s [14]

Table 4.5: Extended OPPT method parameters

The signal for the optimization zone is thus the output of the inertial control subsystem. The implementation on Simulink is relatively easy, since it almost consists in build Equation (4.24) with a block scheme, as shown in Figure 4.30.

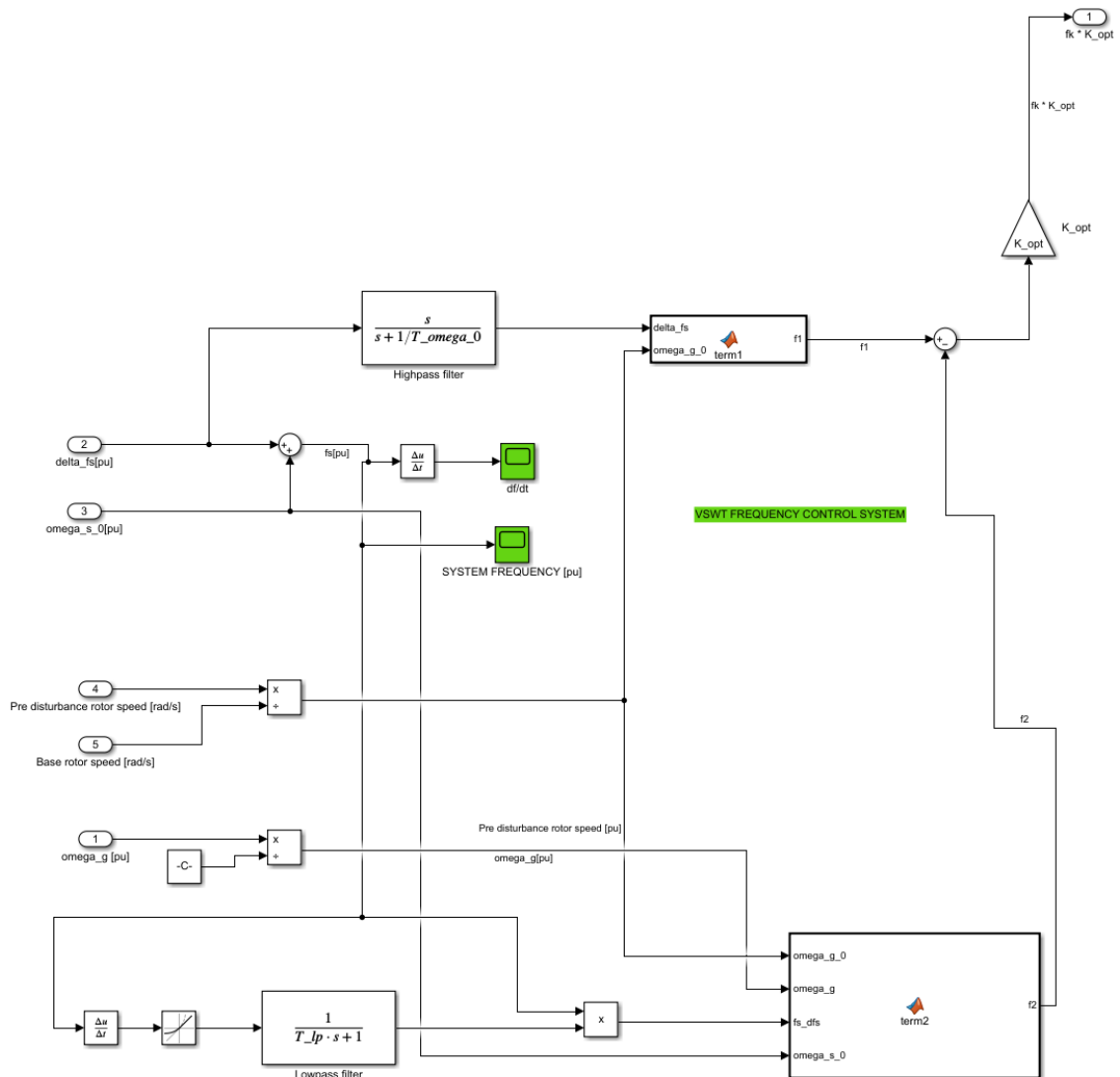


Figure 4.30: Virtual inertia control subsystem

The two Matlab functions (*term1* and *term2*) are implementing the calculation respectively of the first (*f1*) and of the second (*f2*) term that compose $f_{k,opt}$.

```
function f1 = term1(delta_fs,omega_g_0)
    k_vir = 8;
    f1 = (omega_g_0/(omega_g_0+k_vir*delta_fs))^3;
end
```

Figure 4.31: *term1* body

```
function f2 = term2(omega_g_0,omega_g,fs_dfs,omega_s_0)
    k_vir = 8;
    K_opt = 0.4225;
    W_vir = 0.2;
    H_wt = 5.29;
    K0 = 2*omega_g_0 / omega_s_0 * k_vir * H_wt ;
    f2 = W_vir*K0/(K_opt*(omega_g)^3) * fs_dfs;
end
```

Figure 4.32: *term2* body

Then, from *f1* and *f2* it is calculated $f_{k,opt}$, which is multiplied by K_{opt} to obtain the $f_{k,kopt}$ signal. This last is sent to the speed governor of the VSWT to close the loop implementing the Extended OPPT method.

4.5. Steam turbine model

The last generator present in the modelled system is a steam turbine with one reheat. It represents the generation unit that conventionally operates the frequency control in a power system. Even if the aim of this work does not include the modelling of this kind of synchronous generator, for sake of completeness it is presented its adopted block scheme, which is taken from [4], representing a linearized model of the prime mover of a steam turbine and its speed governor.

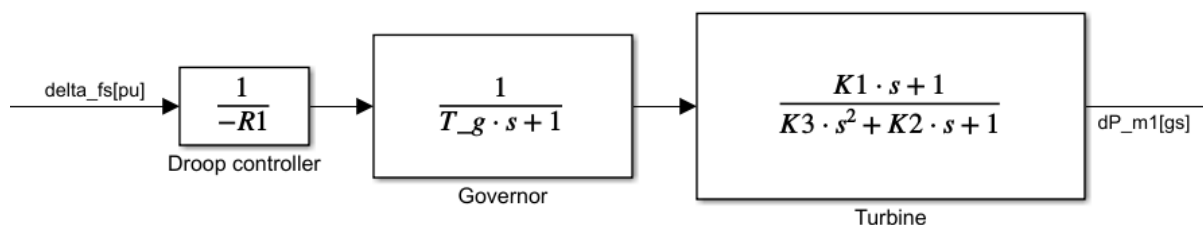


Figure 4.33: reheated steam turbine block scheme

It is important to notice that there is not the possibility to explicitly define the power of the synchronous generator (i.e. the equivalent of all the synchronous generators

present in the system). This means that its power has just to be defined through the participation factor with respect to the total base power of the system. This enhance once more the idea that in this work and in the simulations that have been performed the attention has not to be placed on the absolute values of power, but the correct way of reasoning is on relative terms (in per unit).

The parameters describing the synchronous generator model are reported in:

Parameter	Value [4] [18]
R_1	0.05
τ_g	0.2 s
K_1	1.5
K_2	5.3
K_3	2.1

Table 4.6: Synchronous generator model parameters

K_1 , K_2 and K_3 have been calculated rearranging the classical shape of the transfer function proposed in the mentioned references to better match the predefined interface of the Simulink transfer function block. In particular, from:

$$\frac{1 + F_{HP}T_{RH}S}{(1 + T_{CH}S)(1 + T_{RH}S)} \quad (4.26)$$

it has been rearranged to

$$\frac{K_1s + 1}{K_3s^2 + K_2s + 1} \quad (4.27)$$

This means that:

$$K_1 = F_{HP}T_{RH} \quad (4.28)$$

$$K_2 = T_{CH} + T_{RH} \quad (4.29)$$

$$K_3 = T_{RH}T_{CH} \quad (4.30)$$

4.6. Initialization procedure

After the description of the three equivalent generating units, it is necessary to return to the complete model and study the system initialization.

During the development of this work, it has been observed how generally the initialization problem is not addressed in the literature, even if the definition of a standardized procedure represents probably the hardest part of the modelling.

This is why it has been decided to propose a detailed description of the initialization tasks for the developed model. It is important to state that this procedure results from hundreds of simulations, in the sense that some initialization tips have been obtained from the observation of a lot of results and from the experience of working with this model.

The key issues that this subchapter wants to prevent are too long initialization times and, above all, the consistency of the results.

Basically, the initialization procedure consists in assigning initial values to some signals or variables (*state variables*) of the system, through the apposite spaces in the interface of their Simulink blocks. It is extremely important that the assigned values are coherent each other to facilitate the process and reduce the computational effort.

The first part of the discussion is thus divided for subsystems: first of all, it is explained the initialization of the photovoltaic system alone, then the one of the wind one. After that, with the observed regime values for the separated systems, it is considered the initialization of the system as a whole.

4.6.1. PV system initialization

The initialization of the photovoltaic system is the most challenging one in terms of time. This fact highlights the need of assigning proper values to the initialized variables.

First of all, they are presented the variables to be initialized:

- PV series voltage (v_{pv}) \equiv Capacitor voltage (v_C)
- Inductor current (i_L)
- PV active power (P_{PV})

The corresponding blocks in the Simulink model are coloured in orange in Figure 4.34 and Figure 4.35.

The schematics of the procedure for the PV plant is quite simple. The first step is to run a simulation on the PV system alone, without the power reserve control block and without assigning values to v_C and i_L (default inductor and capacitor blocks settings, with the initialization of the value disabled). This can be easily implemented by copying

and pasting in a blank Simulink model the PV system block, cancelling the power reserve control line, and posing as *reserve* input value a constant block of 0.2 (it has to be necessarily the initial reserve value desired for the PV in the complete model), as in Figure 4.36.

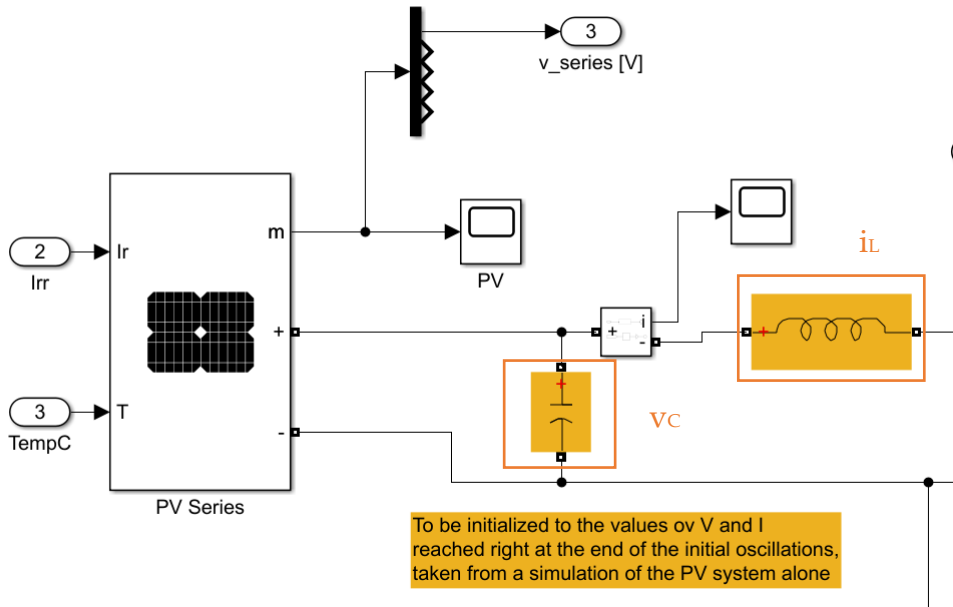


Figure 4.34: PV electrical scheme initialization variables

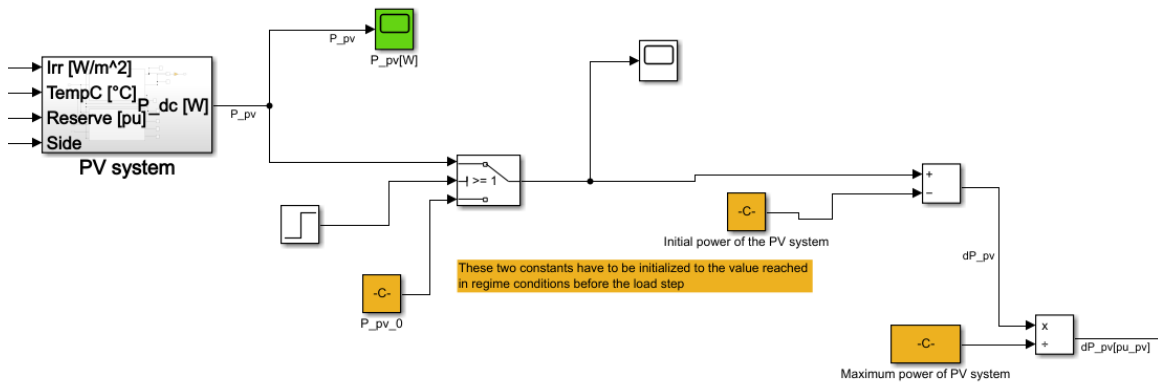


Figure 4.35: PV system power initialization

The simulation stop time has to be sufficient to reach a regime condition for the described model. Indeed, approximately, in the first second of simulation (to be conservative) it is observed a voltage and duty cycle fluctuation. After this initial period, it is reached a regime condition, i.e. PV series voltage and inductor current are constant along the time.

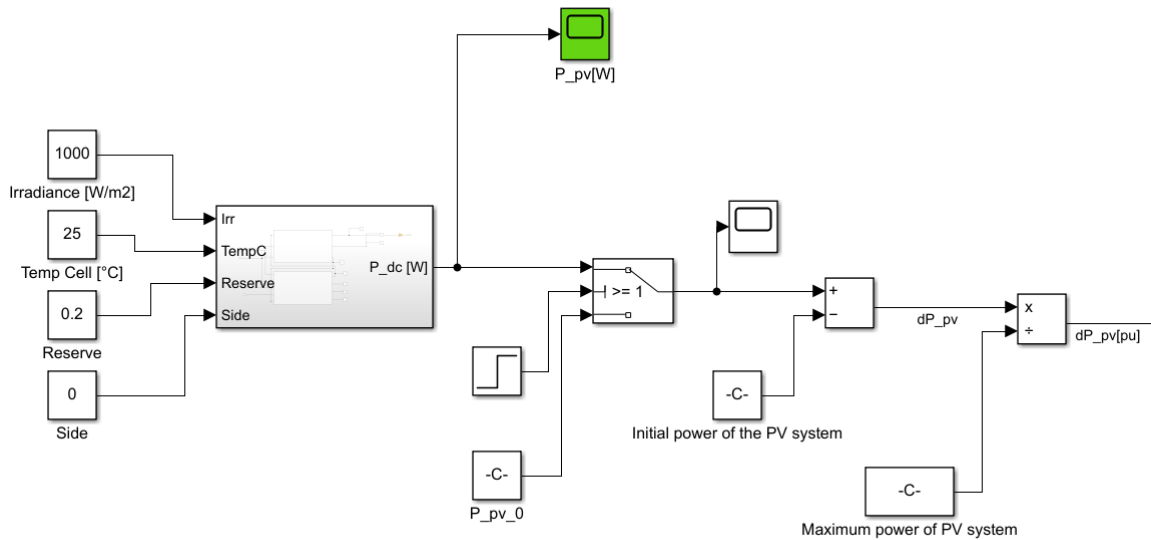


Figure 4.36: first model to be considered for PV system initialization

Arrived at this point, the issue is to select the initial values for v_c and i_L for the subsequent step. After a lot of attempts, it has been found the best option for this problem. Indeed, even if the most obvious option would be to pick the regime values, by running the simulation with them as initial values it is observed how it is not worthy in terms of time.

The characteristic shape that the voltage assumes during the initial transient is composed by an initial large and fast variation, followed by smaller and smaller oscillations, which at a certain time end. Then, the voltage still varies but without small oscillations up to a regime value, which remains constant.

The tip, as indicated in orange in Figure 4.34, is to choose as initial values for capacitor voltage and inductor current the series voltage and the inductor current reached just at the end of the small oscillations, before the regime value is reached. The initial power, instead, is simply obtained as the product between the regime current value and the regime voltage value, multiplied by the number of PV series present in the system, or, alternatively, as:

$$P_0 = P_{MPP,series}(1 - reserve)n_{series} \quad (4.31)$$

The obtained values have to be used as initial values for a PV model with power reserve control enabled (i.e. the loop between Δf_s and *reserve* is closed), still taken apart from the wind and the synchronous generators in a blank model.

In this case, it is important to insert a switch at the output of the PV system block, to allow the frequency to remain to the regime value while the PV block is being initialized (Figure 4.37).

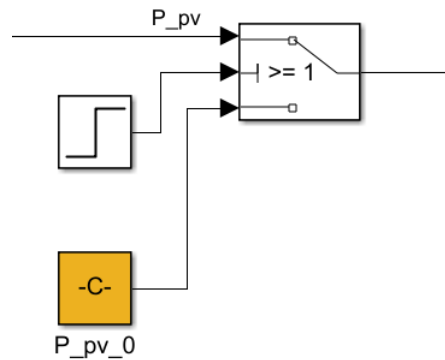


Figure 4.37: PV output power switch

The switch allows to keep the PV active power signal constant to the regime value, while in reality it is changing due to system initialization. This trick allows to keep the frequency to the regime value, which is the one desired in the simulations before a perturbation introduction, as well as to keep the reserve value fixed to the initial desired value before a perturbation (constant frequency \rightarrow constant reserve). When the PV system reaches the regime power value, the switch disconnects the block P_{pv_0} and connects the real power output signal coming from the PV block.

This can be easily implemented in Simulink by providing as input 2 to the switch a step block, that initially is null and then, after a certain time, shifts its output to one. By setting the switch block to change the output when the input 2 signal is equal or higher than 1 (Figure 4.38), at the step time it will change the output value from the one of the constant P_{pv_0} block to P_{pv} signal. If the value of P_{pv_0} is the correct one, this variation appears completely smooth and flat.

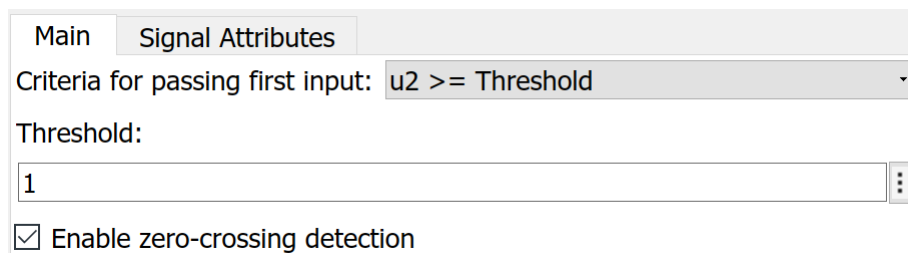


Figure 4.38: switch block settings

Another important footnote is that the step time has to be sufficiently high to make the switching happen when the initialization transient of the PV system is already finished.

The two values for v_c and i_L obtained at the end of the small initial oscillations are the ones to be inserted in the complete model to initialize it, as explained in subsection 4.6.3 .

4.6.2. Wind turbine system initialization

Before initializing the complete model, they have to be found the initial guess values also for the wind turbine system, as for the photovoltaic one.

The logic of the procedure is similar to the PV case, with some differences. Firstly, a Matlab function is run to calculate the theoretic values of the state variables for a certain initial wind speed. Then, the obtained values are inserted in the model of a wind system alone, without the frequency response capabilities. The regime values obtained from this simulation are used as initial guess in a model of wind turbine with Extended OPPT method enabled and synchronous generator. The new regime values are in turn used as initial guesses in the complete model.

In this case, the variables that need to be initialized are:

- Low-speed shaft rotational speed (ω_t)
- High-speed shaft torque (T_{em})
- High-speed shaft reference torque ($T_{em,ref}$)
- Active power (P_{ag})

Furthermore, the initial high-speed shaft rotational speed (ω_g) has to be provided to the inertial control system.

As explained before, the initial guesses of the entire procedure are calculated thanks to the following Matlab code:

```
% Initialization Wind Turbine system

v_wind_0 = 11.457; % [m/s] FILL WITH THE IMPOSED v_wind at t=0;

%% Calculation of the constant to be initialized in t=0 in Simulink model
% The results must me inserted in the corresponding constants of the model
omega_t_regime = (v_wind_0*0.1 + 0.001)*1.644; % [rad/s]
omega_g_0 = omega_t_regime * 95.55; % [rad/s]
P_0 = 0.0004*v_wind_0^2.999 * 1.5e6; % [W]
T_em_ref_0 = P_0/omega_t_regime/95.55; % [N*m] = T_em_0
```

Figure 4.39: wind system initialization code for first guess values

The algorithm is very easy: first of all, it has to be specified the wind speed at which the model has to be initialized (i.e. the initial wind speed for the regime condition before a perturbation acts on the system).

Then, a relationship between the wind speed and the ω_t has been derived from the wind turbine characteristic implemented in the VSWT Simulink block. In particular, for each of the wind speed showed in the characteristic in Figure 4.21, it does exist an optimal ω_t that maximizes the performances. By interpolation of these values against

the wind speed it is possible to find a relationship describing the optimal ω_t for any wind speed.

The same reasoning is made to find a relationship between the optimal power output and the wind speed.

v_wind [m/s]	omega_t_opt [rad/s]	P_opt [pu]
6	0.601	0.09125
7.2	0.721	0.15770
8.4	0.841	0.25040
9.6	0.961	0.37380
10.8	1.081	0.53220
12	1.201	0.73000
13.2	1.321	0.97000
14.4	1.441	1.26100

Table 4.7: VSWT Simulink block rotational speed and power characteristics

The resulting relationships are shown in Figure 4.40.

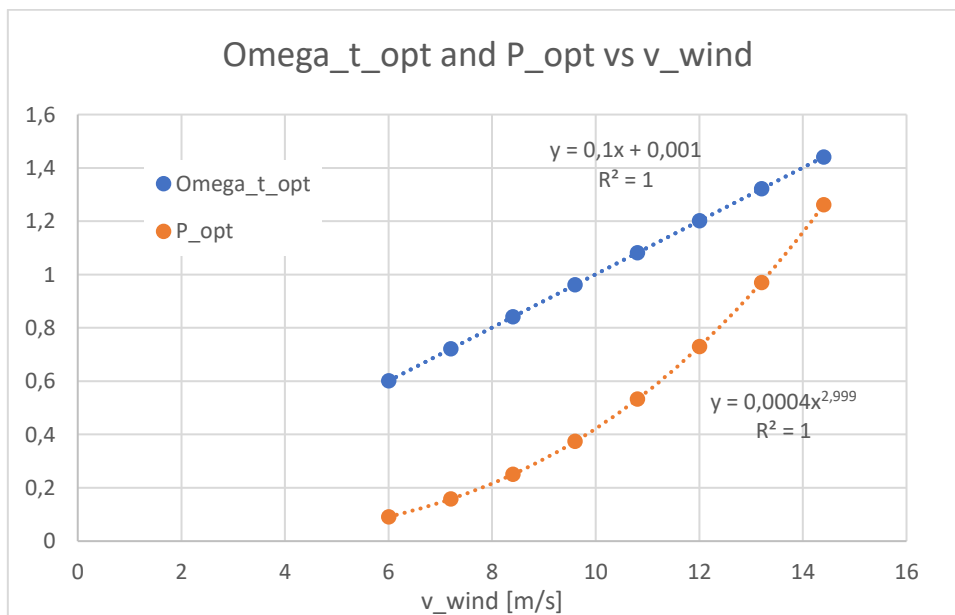


Figure 4.40: ω_{t_opt} and P_{opt} vs v_{wind} relationships

The relationships are used to find the initial guesses for the two mentioned variables. Knowing them, it is possible to easily calculate the corresponding initial conditions of the other three variables.

Once the sequence of simulations described at the start of this subsection is performed, everything is ready to initialize the complete model.

4.6.3. Complete model initialization

Once the initial guess values for the complete model variables have been found with the mentioned above procedure, it is possible to finally go through the last part of the initialization.

The conceptual scheme is right the same: after inserting the values found with the initialization procedure of PV and wind systems in the complete model, a simulation is run. For the wind subsystem, the regime values reached in this simulation are the final initial values, while for the photovoltaic system they are still chosen the values after the initial small oscillations.

An important note regards the switches present in the system. In this case, differently from the separated models, the switch time to activate the frequency response of the system has to be at $t = 0$ s. Indeed, it has been observed how the interaction between wind, PV and synchronous generators helps to make the initial transient faster and faster, producing the desired regime value with the frequency that is very close to 50 Hz (Figure 4.41), which is the aim of the initialization procedure as well as to have the differential power variation of the three units that is null (Figure 4.42). Also this last condition is accomplished using this procedure.

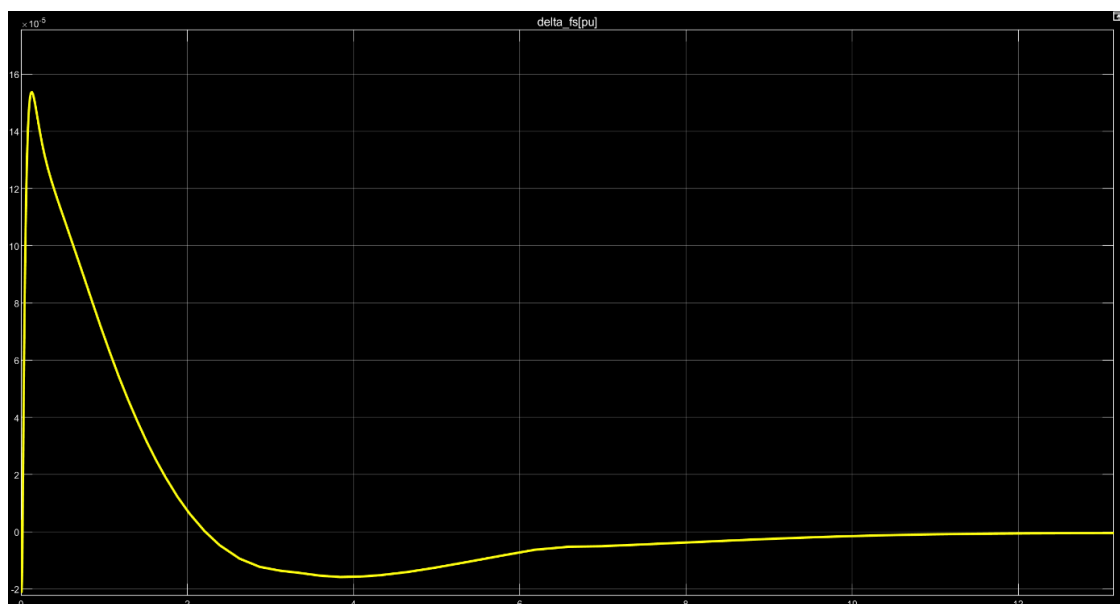


Figure 4.41: frequency trend during initial transient

The initialization in the majority of the simulations constitutes the most time requiring phase. At the same time, the studies have been performed starting from the same regime condition by changing the load variation and/or the environmental conditions and the participation factors. This is why it has been extremely important to find a way to start the simulations directly from that regime condition, i.e. from a simulation time > 0 s, to save a lot of time and produce results perfectly comparable each other.

This one and other functions available on Simulink are explained in the next chapter, together with a summary of the performed simulations, their aims and the metrics to evaluate the performances of the frequency control.

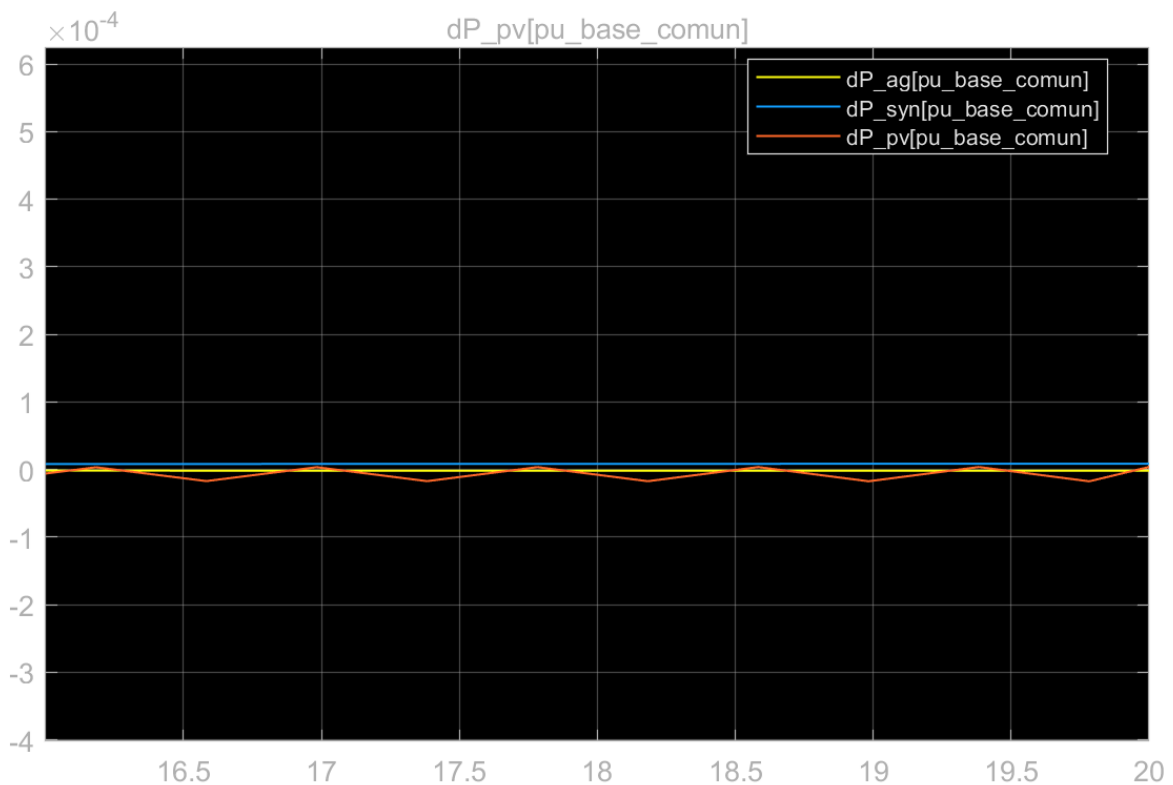


Figure 4.42: regime dP_i after the initial transient

5 Simulations summary and metrics to evaluate the results

After the description of the model developed in this work, it is necessary to explain in detail how the simulations work, and, above all, listing the simulations performed.

Furthermore, there are some useful Simulink tips that can help while using the model to run a lot of similar simulations, and, in this context, it is evaluated as really important to convey all the experience about the work on the model in this report.

Since in Chapter 6 they will be presented the results of the simulations, Chapter 5 wants also to define the metrics to evaluate them, as well as the aspects to investigate starting from the results.

It is important to remember which situation this model is describing: a small island power system, characterized by the presence of three equivalent generating units (PV, wind and synchronous generator) and an equivalent load, which can be seen as a grouping of all the smaller loads present in the island. This situation, in fact, is the one in which a mismatch between the active power produced and consumed can have more serious effects on the frequency stability, due to the small size of the power system, its lack of interconnections due to the remote geographic position, as well as the high penetration of renewable sources that usually is observed on the islands.

5.1. List of the performed simulations

The various simulations that have been performed have different aims. Instead of explaining them while looking at the results, it has been decided that, to be more clear, it is more proper to list them in advance.

They can be divided into some categories, as a function of the perturbation introduced with respect to a common reference condition. It is thus fundamental to describe this reference condition before going on.

The common reference condition that has been chosen from now on will be indicated with *"base case"*, and is characterized as follows:

- Participation factors of the three equivalent generating units respectively: $p_{wind}=0.2$; $p_{synchronous}=0.7$; $p_{pv}=0.1$ (30% of penetration of renewables on nominal power basis).
- $H_{eq} = 2.88$ s [18]; $D = 1$ [4]
- Incoming wind speed at $t = 0$ s: 9.6 m/s for constant wind simulations; 11.457 m/s for real wind profile simulations
- Irradiance at $t = 0$ s: 1000 W/m²
- Cell temperature: 25 °C
- Constant load power requirement

In each simulation, a modification with respect to this base case is introduced to study different aspects linked to the frequency stability.

As stated before, the simulations can be grouped as a function of the perturbation introduced. In particular, they have been studied these situations:

Simulation group	Aim
Load active power step up/down	Observing the frequency response of the system after a sudden variation of the load power for different step magnitudes
Small sinusoidal oscillations + step of load active power	Observing the frequency response of the system to small and continuous variations of the load, i.e. similar to the real behaviour, and to a step if a part of the reserve is already in use to balance the small variations
Variable environmental conditions (real wind speed profile, irradiance variations)	Understanding how the system responds to environmental conditions changes, as well as to a sudden load power variation in such a situation
Variable participation factors	Understanding which is the impact of an increasing penetration of renewable sources on the system's frequency stability

Table 5.1: simulations groups and aims

Furthermore, to have other points of view on the system, each simulation is performed on four different versions of the complete system:

- Primary frequency control operated only by the synchronous generators (wind turbines without virtual inertia control, PV without power reserve control)
- Primary frequency control operated by synchronous generators and wind turbines (Extended OPPT Method enabled)
- Primary frequency control operated by synchronous generators and photovoltaic strings (Power Reserve Control enabled)
- All the generators participate to the primary frequency control

The first scenario is representing the current situation in most of the power systems, since the renewables are mostly operated in their MPP condition. The fourth scenario, on the other hand, could represent a future situation in which renewables are flexible and able to help synchronous generators (or displace them) in balancing the frequency of a power system. This allows to catch the interaction between the various controllers, the help that the renewables controlled with the updated logics can give to the system, the impact of each technology in the frequency stabilization.

The final summary of the simulations performed on the model is reported in Table 5.2 and Table 5.3. A number has been used to indicate each of them, so that the results can be commented in a clearer way.

N° simulation	Features
1	Step up $P_{load} +1\%$
2	Step down $P_{load} -1\%$
3	Step down $P_{load} -2\%$
4	Step down $P_{load} -10\%$
5	Small sinusoidal variation of P_{load} (amplitude 5‰) + step down $P_{load} -10\%$
6	Real wind profile
7	Real wind profile + step down $P_{load} -10\%$
8	Steep irradiance ramp up – ramp down

Table 5.2: summary simulations 1-8

For what concerns the simulations at different participation factors combinations, there are some further specifications that have to be mentioned.

Indeed, modifying the participation factors requires attention: each combination includes a variation of power of the three generating units. Even if, as already anticipated, the results have to be observed under a relative point of view, to properly set the model for the simulations some parameters have to be adapted as a function of the participation factors. Thus, it is important to explain the link between power and participation factors in the model.

First of all, the three participation factors have to be set. Studying the base case, for example, they are equal to: $p_{wind}=0.2$; $p_{synchronous}=0.7$; $p_{pv}=0.1$.

The reference for the powers setting is the base power of the wind turbine, equal to 1.5 MW. Then, the power of the other two generators can be found as:

$$P_{base,pv} = P_{base,wind} \frac{p_{pv}}{p_{wind}} \quad (5.1)$$

$$P_{base,syn} = P_{base,wind} \frac{p_{syn}}{p_{wind}} \quad (5.2)$$

This kind of reference implies that, for the different simulations, the base power of the wind generator remains constant, while the base powers of the other two varies. Since the system is observed on the basis of the relative weights of the three generators, this is not a problem. In any case, to scale up in absolute terms the system or to vary the power of the wind generator is sufficient to insert a gain block after the wind turbine subsystem.

To complete the model setting for a certain combination of participation factors, it is required to insert the number of PV strings needed to reach the defined PV base power (Figure 5.1).

This number can be simply obtained as:

$$n_{series} = \frac{P_{base,pv}}{P_{max,series}} \quad (5.3)$$

Once this number is set, the model is updated for the set of participation factors selected, and ready for the initialization. In reality, if the ambient conditions are similar between different simulations, the initial value of the power of the PV system ($P_{pv,0}$) can be simply found scaling it on the base of the number of PV strings, as follows:

$$P'_{pv,0} = P_{pv,0} \frac{n'_{pv}}{n_{pv}} \quad (5.4)$$

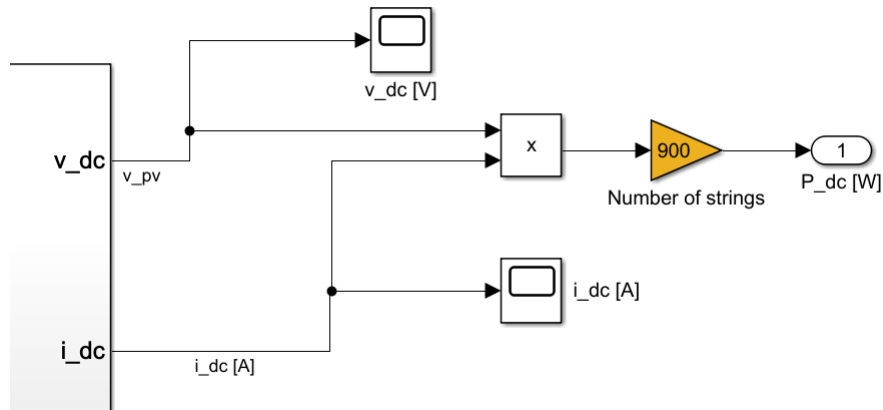


Figure 5.1: number of PV strings

The combinations of participation factors that have been tested are summarized in Table 5.3, where they are also divided into three categories: increasing wind penetration, increasing PV penetration and increasing both.

N° simulation	p_{wind}	$p_{synchronous}$	p_{pv}
9	0.3	0.6	0.1
10	0.4	0.5	0.1
11	0.5	0.4	0.1
12	0.2	0.6	0.2
13	0.2	0.5	0.3
14	0.2	0.4	0.4
15	0.3	0.5	0.2
16	0.4	0.3	0.3
17	0.4	0.2	0.4

Table 5.3: summary simulations 9-17

As probably noticed, in this work is not analysed the case of a generation loss. Indeed, this kind of model is not capable to catch that kind of event, excluded a loss of a part of the photovoltaic generation. This is intrinsic to the model developed for the system, in which the generators have to be intended as an “equivalent” of all the similar generating units present in the system. With any modifications, it is just possible to model the loss of the entire fleet of wind or synchronous generators, while for PV, since it is present a gain block at the output of the subsystem, it could be possible to

reduce with a switch the number of parallel strings to model a partial loss of generation.

In any case, in future developments of this work it could be easily implemented also this kind of analysis.

5.2. Tips to reduce the simulation time

As presented in the previous subchapter, a considerable number of simulations has to be performed. Indeed, each of the eighteen has to be carried out in four different scenarios of the complete model, for a total of seventy-two simulations.

For this reason, finding out methods to reduce the total simulation time and the computational effort has been a fundamental part of this work.

The biggest help in this sense arrived from the possibility that Simulink gives to start the simulations from an already saved state, called *Initial State*. In fact, some simulations are characterized by the same regime condition, and the only modification between one and the others happens after the regime condition is reached, simply modifying, for example, the amplitude of a perturbation.

Referring to the first group, for example, all the simulations have the same initial state, and they differ just for the amplitude of the step of load active power. In this case, it is extremely useful to run the initialization (which is the most time expensive part of the simulations) just one time, saving the regime condition as a Simulink state of the model (i.e. Simulink saves the values of all the signals at the defined time instant), and then starting all the simulations from this common initial state.

To save the final state (i.e. the regime one) of a simulation, it has to be followed this procedure, indicated in [57]:

1. Select the Configuration Parameters > Data Import/Export > Final states check box.
2. Also in the Data Import/Export pane, select the Save final operating point parameter.
3. In the edit box next to the Save final operating point parameter, enter a variable name for the *ModelOperatingPoint* object and click Apply.
4. Simulate the model.

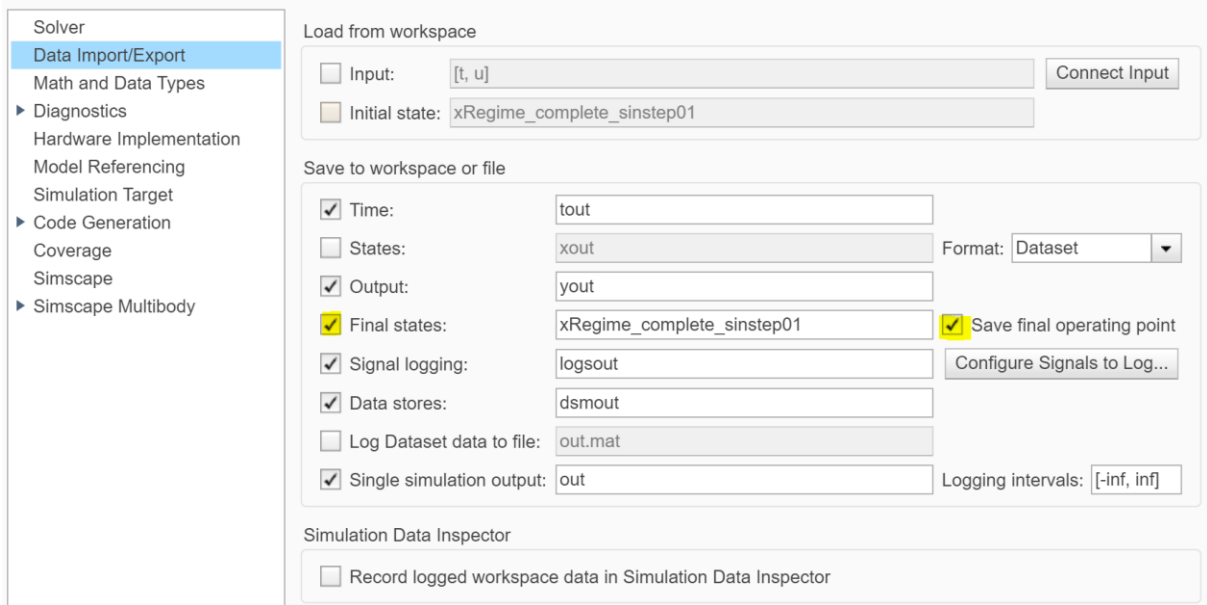


Figure 5.2: saving final state

In the Matlab workspace will appear the name of the state. It can be saved with the corresponding name, so that it remains available for all the simulations simply loading it on the Matlab workspace.

Then, to start the simulations from that initial state it is sufficient to disable the Final States check box and activate the Initial State one, inserting the name of the saved state.

Another useful tip can be used to export some signals to plot them on Matlab. To do so, it can be followed this procedure:

1. To send a signal to the Matlab workspace, it has to be added in the model in correspondence of the desired signal a block called "to Workspace".
2. In the block it has to be written the name of the signal with an "out." in the front.

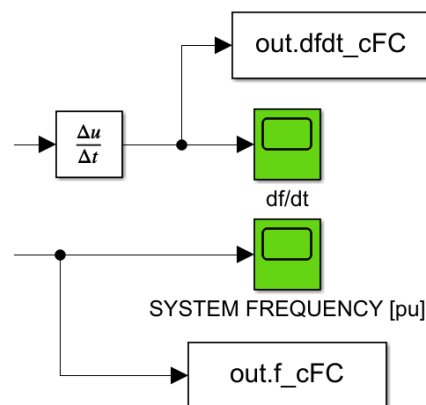
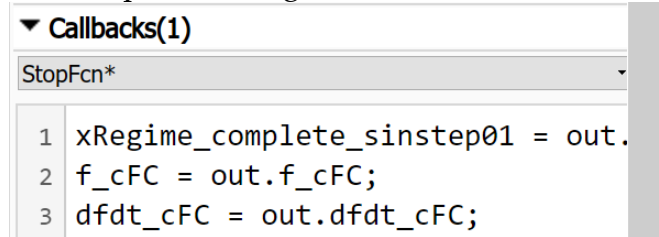


Figure 5.3: "to Workspace" block

3. Going to Modelling > Property Inspector > Properties > Callbacks, it has to be selected the callback StopFcn.
4. In the text box it has to be assigned to a variable the name of the output signal arriving from the “to Workspace” block. For example, the signals in Figure 5.3 can be sent to the workspace writing:



```

▼ Callbacks(1)
StopFcn*
1 xRegime_complete_sinstep01 = out.
2 f_cFC = out.f_cFC;
3 dfdt_cFC = out.dfdt_cFC;

```

Figure 5.4: callbacks for signal exporting to workspace

5. Start the simulation

By doing so, the signal variables will appear at the end of the simulation in the Matlab workspace. This allows to plot them in a customized Matlab plot, making the representation clearer.

5.3. Metrics to evaluate the primary frequency control adequacy

Before presenting simulation results, it is important to define quantitative instruments that can help in interpreting them. Indeed, in next chapter, they are developed both qualitative analysis on the results plot shape and quantitative observations to catch some important concepts.

It is first of all required to report a definition of primary frequency adequacy. As stated in [58], a primary frequency control is adequate if is able to ensure an uninterrupted delivery of electricity after a sudden unbalance between generation and demand, i.e. if it is capable of arresting and stabilizing the frequency deviation without exceeding the limits imposed in the grid codes.

In this work, they are used as metrics the following parameters:

- Frequency nadir [Hz]: it is a direct measure of the primary frequency control adequacy. It is calculated as the maximum/minimum value of frequency deviation occurring after an active power unbalance. The closer it is to the nominal frequency, the better.
- RoCoF [Hz/s]: it is the time derivative of the system’s frequency. The smaller it is, the better is for the system.
- *Nadir-based frequency response*: it expresses how good the primary frequency control has performed in stabilizing the frequency after a perturbation. It can be calculated as [58]:

$$\text{nadir based frequency response} = \frac{\Delta P_{\text{perturbation}}}{\Delta f_{\text{nadir}}} \quad (5.5)$$

Once defined the metrics it is possible to observe and comment the results of the simulations, which are reported in the next chapter.

5.4. Solver selection

When solving a numerical problem, the selection of the solver represents a crucial choice. In this case, when building up the model, it has been understood how important the solver is in obtaining reliable results.

Indeed, some solvers are really slow in simulating some kinds of problem, while others produce results that are far from the expected ones, due to their mathematical features.

The image shows a software interface for solver selection. At the top, there is a section titled "Solver selection" with two dropdown menus: "Type" set to "Variable-step" and "Solver" set to "ode23t (mod. stiff/Trapezoidal)". Below this is a section titled "Solver details" which is expanded. It contains several input fields and a checkbox: "Max step size" (auto), "Min step size" (auto), "Initial step size" (auto), "Relative tolerance" (1e-3), "Absolute tolerance" (auto), a checked checkbox for "Auto scale absolute tolerance", and "Solver reset method" (Fast).

Figure 5.5: solver settings pane

At the end, most proper solver has resulted to be the variable step *ode23t* (mod. Stiff/Trapezoidal), that combines a fast solution and at the same time is capable to catch some dynamics (especially for the wind system, for which the stiffness has been found out to be fundamental) that other solvers are not able to catch.

The relative tolerance and the other setting can be left in their default options, as in Figure 5.5.

6 Simulation results

As the model has been presented in detail, it is now possible to finally match the modelling part with the conceptual one. Indeed, in all the previous chapters has not been addressed with quantitative and qualitative considerations the core of this work. It is interesting to approach the problem about the primary frequency control with some major questions: how the increasing penetration of renewable generators affects it? The possibility to include them in the participation to the provision of this ancillary service is effectively helping the system, encouraging the displacement of conventional ones?

This chapter is trying to answer to these questions both qualitatively, commenting some graphs, and quantitatively, thanks to the metrics proposed earlier in Chapter 5.3.

To be clearer, the results are divided and commented by groups of simulations, since as part of a group they are united by the same aims.

6.1. Load active power step up/down

The first and simpler test to analyse the frequency response of a dynamic system is obtained by observing its behaviour after a step perturbation. In this case, the step is obtained through an instantaneous change of the load power (P_{load}). This situation is extremely simplified with respect to what happens during the normal operation of a power system, but nevertheless this test is really important to take a first look to the effectiveness of the ability of the primary frequency control in stabilizing the frequency.

Imagining the small island system that is described here through a LFC approach, i.e. its response is characterized by a transfer function and through the automatic modulation of power of the generators, a sudden step change of the load power is more likely to happen as a reduction. In other words, it is for sure more common that the load decreases suddenly (for example due to a disconnection of an industrial user) than the vice versa. This is why the maximum amplitude tested for the steps in reduction is higher than the one of step up of the load power.

The first plot reported regards simulation 1, in which the load increases suddenly its power by the 1%. In Figure 6.1 is reported the frequency oscillation of the system due to the consequent unbalance between generation power and load power.

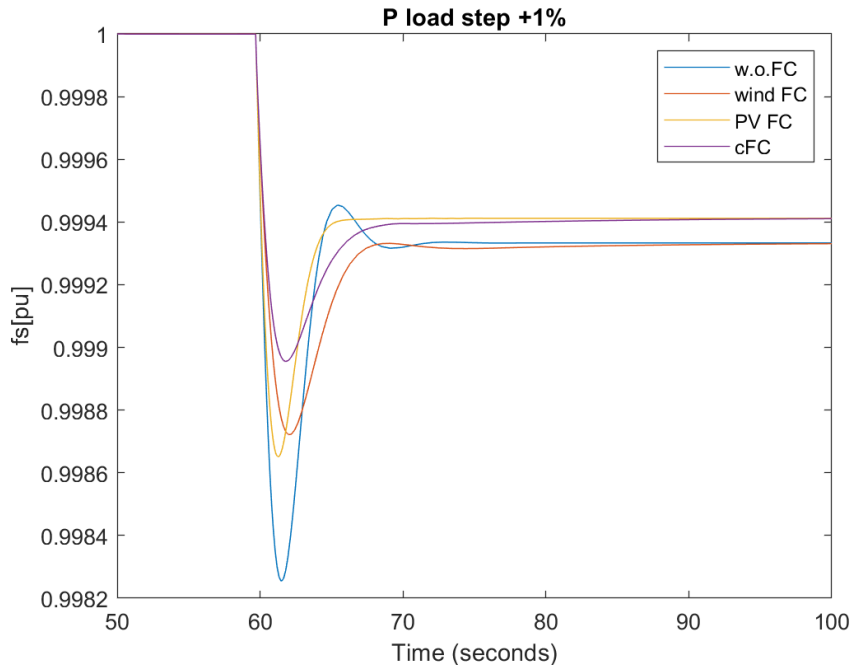


Figure 6.1: simulation 1 frequency trend

First of all, it can be observed that an increase of the load power is traduced in a decrease of the frequency. This behaviour is conceptually similar to the one of a water tank: if, in a certain instant, the flow rate exiting the tank becomes greater than the one arriving at the tank, the water level will decrease.

As observed in Figure 1.3, the frequency nadir can be easily individuated as the minimum of the frequency in the time plot. Observing it in the four scenarios: as expected, in absence of frequency response capabilities from the renewable sources, it is lower than in the other three scenarios. Indeed, it is equal to 0.9983 pu (49.915 Hz) against the 0.9990 pu (49.95 Hz) in case all the generators participate to the primary control. It is evident how the intervention of wind and photovoltaic generators in stabilizing the frequency is helping the system, since they allow to reduce the magnitude of the nadir and, after few instants, they also reduce the oscillations of the system's frequency and the stabilization time. The superposition of their effects lead to the behaviour in purple, which is the one of the scenarios in *complete FC*, i.e. all the generators participate to the primary frequency control.

Of course, since this work focuses just on the primary (and inertial) frequency control, the final value of frequency is not the nominal one, that requires also the actions of secondary and tertiary control to be restored.

Looking at the RoCoF plot in Figure 6.2, it can be seen that the PV system produces oscillations which increase the RoCoF in proximity of the step. This is a negative fact,

which would require an additional PRRC to be solved, reflects also on the *complete FC* scenario. After the peak of RoCoF, anyway, the scenario for which it is higher is the one without frequency control. This allows to understand that PRC for the PV system is capable to contain the frequency and the RoCoF in the instants after a sudden variation in the load power. On the other hand, the wind virtual inertia is operating really well both during and after the load power step.

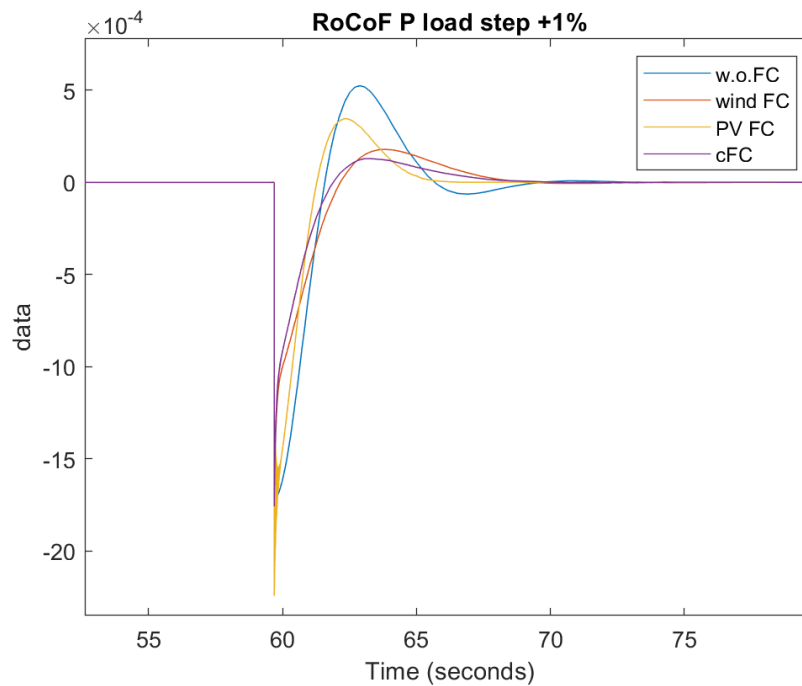


Figure 6.2: simulation 1 RoCoF

Remarkably similar results are obtained from simulation 2: a negative step of load power of the same amplitude produce the same identical behaviour of the frequency but mirrored to an increase in frequency Figure 6.3.

The nadir is also simply mirrored upwards with respect to simulation 1: in the scenario with the renewables with disabled frequency control it is equal to 1.0017 pu, while for the *complete FC* it is equal to 1.0010 pu.

In the other simulations, larger steps are introduced. Due to the similarity already discussed between the first two, they are expected to produce a frequency waveform with the same shape but different amplitude (dilated by a factor 2 and 10 respectively).

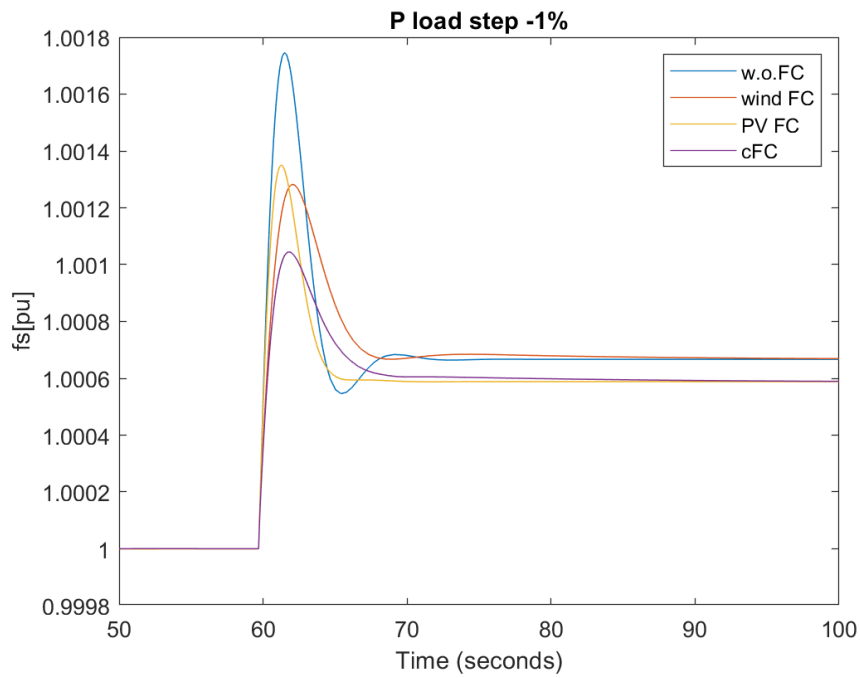


Figure 6.3: simulation 2 frequency trend

Looking at the results for simulation 3, this expectation is confirmed. This behaviour is caused by the constancy of the load damping constant and of the inertia of the synchronous generator, which do not depend on the step amplitude.

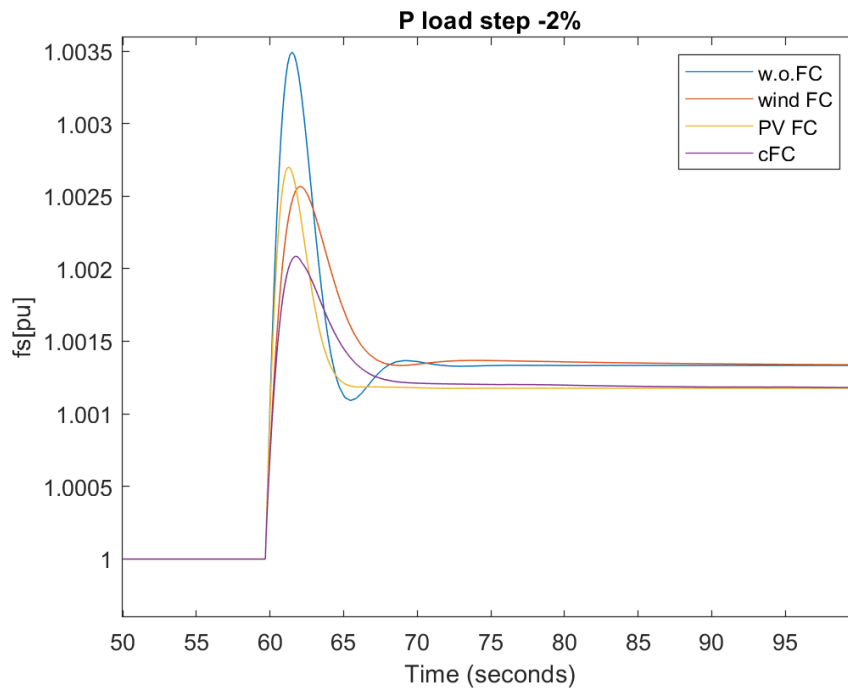


Figure 6.4: simulation 3 frequency trend

It can be also observed that the time required to stabilize the frequency is practically independent on the step amplitude, since in all the simulations the new “regime” condition after the load power step is reached almost at the same time instant.

This kind of results are coherent also with the plots for simulation 4. In this case, such a large loss of load could be associated with the disconnection of an industrial user, and it is evident how large is the frequency variation associated with this loss (**Errore. L'origine riferimento non è stata trovata.**).

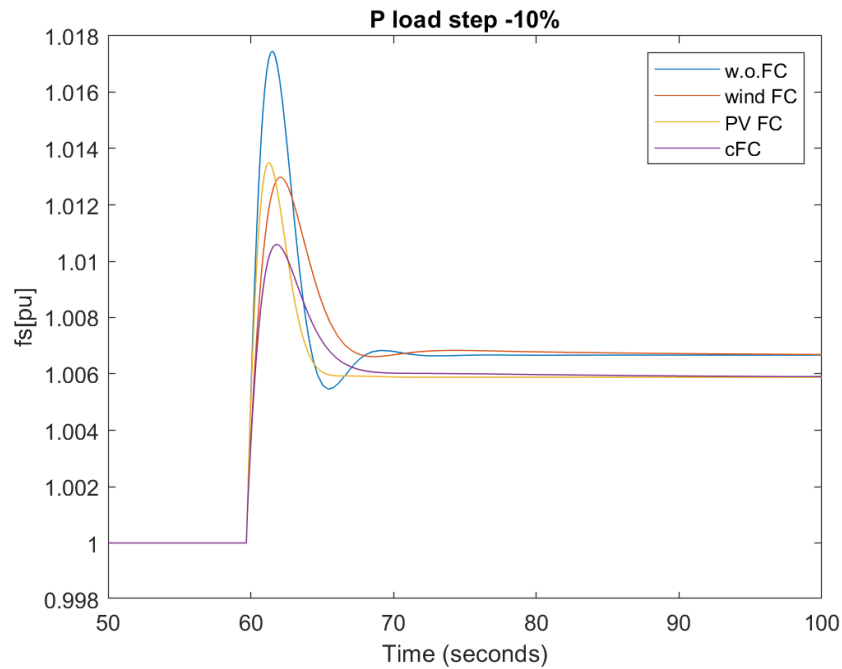


Figure 6.5: simulation 4 frequency trend

It is very interesting to observe how the different generators contribute to the frequency control by adapting their power (Figure 6.6).

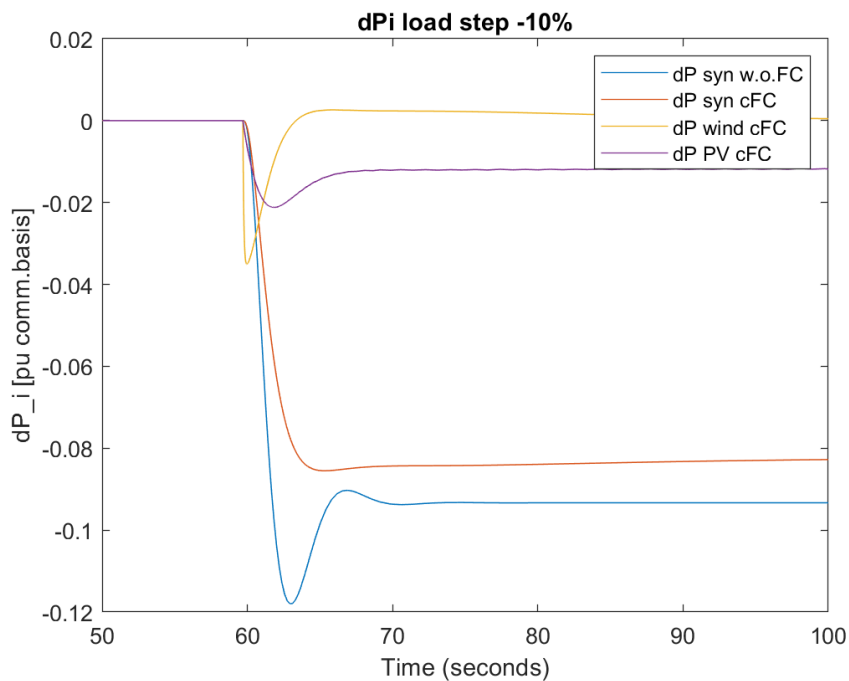


Figure 6.6: simulation 4 dP generators

It is well visible how the two renewables reduce their power to face a decrease in load one. This helps a lot the synchronous generator in containing the frequency increase: it can be seen that the steam turbine power reduction in case of *complete FC* is less intense than in case of frequency control operated just by themselves. The stabilization effect is also emphasized by the reduction of the oscillations after the nadir, that further facilitates the intervention of the synchronous generator.

The nadir reached in this extreme case is equal to 1.0175 pu (50.875 Hz), which is not compliant with many grid codes, for the “traditional” renewables control scenario. In case of updated control, on the other hand, the nadir is equal to 1.0106 pu (50.53 Hz), which also exceeds the upper frequency limit but is lower than the previous, highlighting the huge benefit introduced.

Considering the third metric (nadir-based frequency response), it has been demonstrated with these numerical results that it is practically the same in all the four simulations for what concerns the conventional scenario, while in case of *complete FC* it is a little bit lower increasing the step magnitude.

6.2. Small sinusoidal oscillations and step down load active power

In the previous case before the perturbation the reserve was entirely available to stabilize the frequency due to load power constancy. This is of course very far from the reality of a power system: the load continuously oscillates, entailing that a part of reserve is already involved in the stabilization of the frequency. This means that, if a sudden perturbation of the load power happens, the system has less reserve available to face the variation.

The aim of this second kind of simulation is exactly to address how the continuous and small variability of the load affects the primary frequency control and its capability to face in such a situation a step in load power, as well as to understand if the designed control for renewables is able to catch and follow these small load oscillations.

The load power oscillations introduced in this simulation have an amplitude of 0.005 pu.

The resulting frequency of simulation 5 is presented in Figure 6.7.

It can be observed that the system with *complete FC* needs some seconds to adapt to the sinusoidal variation of the load, but then it is able to follow it without problems. It is also possible to appreciate the huge reduction of the frequency nadir with respect to the base scenario, fact that testifies one more time the effectiveness of the updated control of the renewable generators. After the frequency peak, both the systems are able to

follow the sinusoidal oscillations of the load, but of course in the *complete FC* scenario the stabilization of the frequency is more evident and requires less time to be reached.

This simulation is particularly important for the validation of the innovative control of the renewables, since it is close to the normal behaviour of the load power, as explained previously. These results, in this sense, are really positive.

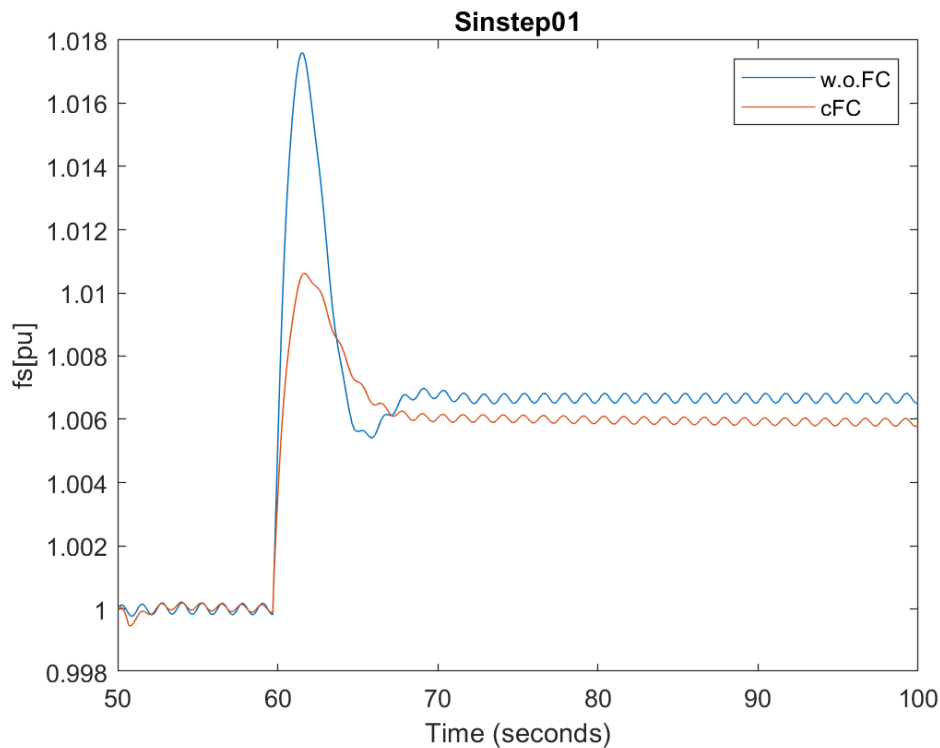


Figure 6.7: simulation 5 frequency trend

6.3. Variable environmental conditions

Two of the major drawbacks of renewables are the difficult predictability and the high variability of their primary resources, i.e. the wind and the solar irradiance.

In the field of the primary frequency control, which takes place in the time window of few seconds after a disturbance, this variability for sure affects their response, especially for what concerns the wind energy. If the sun variations are fast but occur less frequently, the wind variations are huge and occur continuously.

In this sense, the most critical situation is represented by windy days with some small clouds, in which both the wind and the irradiance are very variable.

The aim of these tests is to understand how much the variability of the renewable source affects the primary frequency control if the renewables are rigid and they do

not participate to it, and on the other hand in the case they are able to modulate their power output to smooth their power variations. Furthermore, as for the second group, a part of reserve will be already occupied to balance the natural variability of the resource, so, in case of a perturbation of the load, the reserve level could be less than the nominal amount.

The first analysis regards the most critical of the two resources: the wind. In simulation 6 and 7 the system is tested in the four scenarios with a real high variable wind profile.

The wind profile has been downloaded from a DTU database of measurements in [59], and has the following shape:

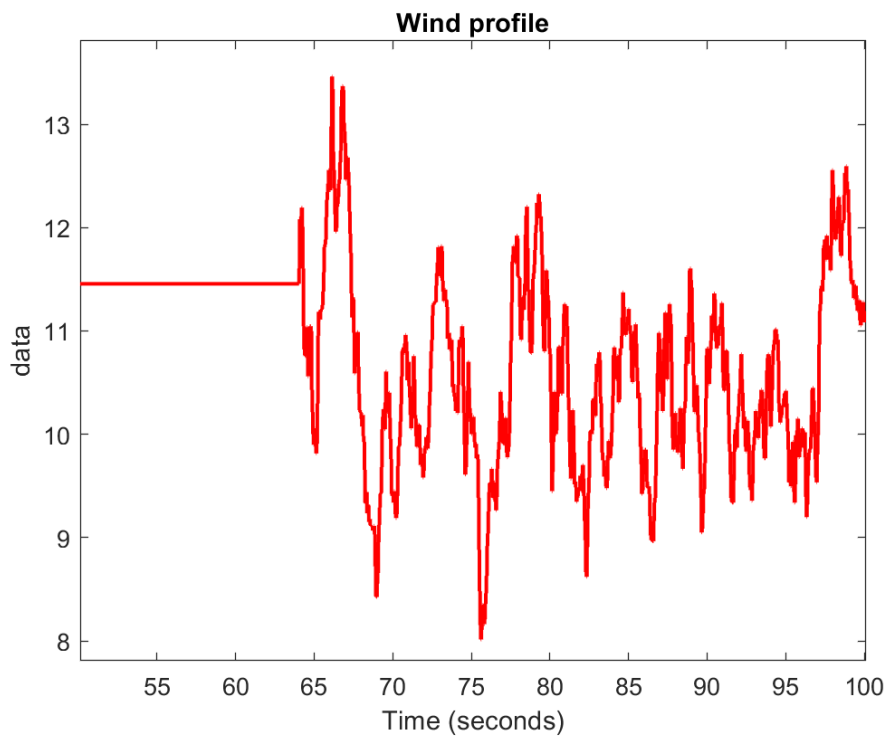


Figure 6.8: wind profile

The profile has been used as input for the wind turbine system, which is not anymore free to adapt its output only to balance the frequency: now it has also to face a variable availability of the wind resource. This means that a part of the reserve could be already involved in the balancing of the frequency consequent to a wind speed variation, reducing the capability to counter a step of load power.

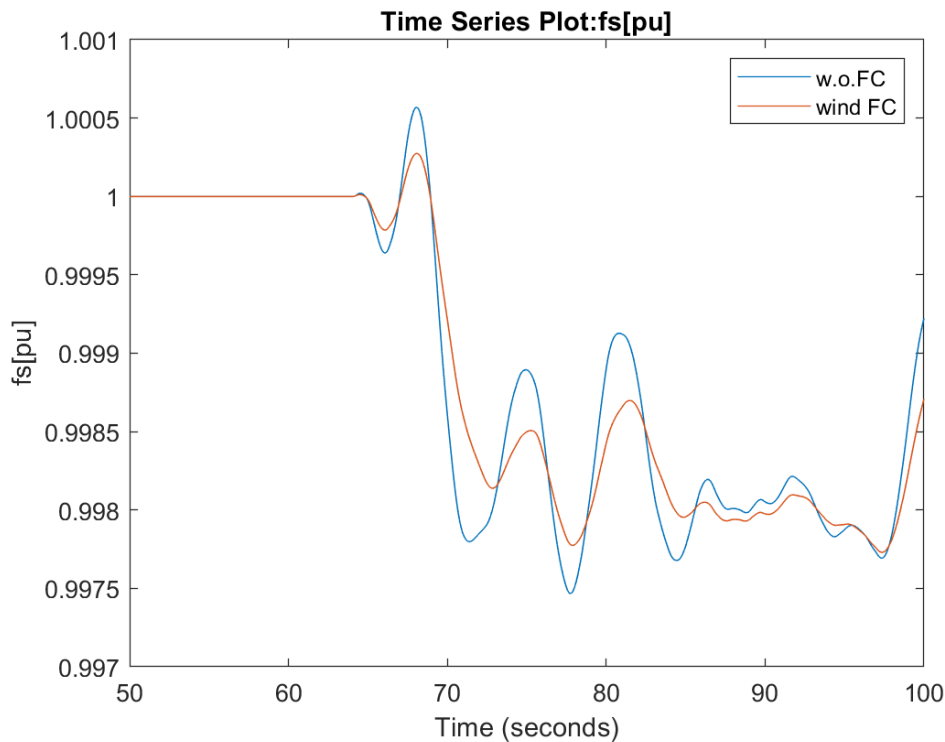


Figure 6.9: simulation 6 frequency trend

Simulation 6 studies the effect of the variable wind profile on the frequency. In particular, it is interesting to observe the response in case of wind turbine with virtual inertia control enabled compared with the base case without frequency response capabilities. The results are shown in Figure 6.9. In this simulation the variability of the wind has been introduced after 64 seconds, so that its effects are more visible starting from a regime condition.

In the base case without frequency control enabled, the wind turbines modulate their power to produce always at their maximum. This means that they do not detect that their behaviour is making the system's frequency oscillating a lot. It is possible to observe, indeed, that the frequency has a number of peaks in correspondence of the peaks of wind speed. This trend will stress a lot the system, requiring a huge control action by the synchronous generators.

On the other hand, if the wind turbines are able to exploit their kinetic energy using the Extended OPPT method, it is evident how they smooth their power variation, producing lower peaks and stressing very less the power system.

Looking at the largest nadir reached in the variable wind period, in the first scenario it is equal to 0.9975 pu (49.875 Hz), while in the updated scenario is 0.9977 pu (49.885 Hz). The reduction of the nadir is not so pronounced between the two, but the benefits consequent to the introduction of the Extended OPPT Method are evident considering the trend of frequency, since the amplitude of each oscillation is lowered. This fact is

confirmed by the plot of the RoCoF, that highlights how the rate of variation of frequency is slower and smoother in the second scenario (Figure 6.10).

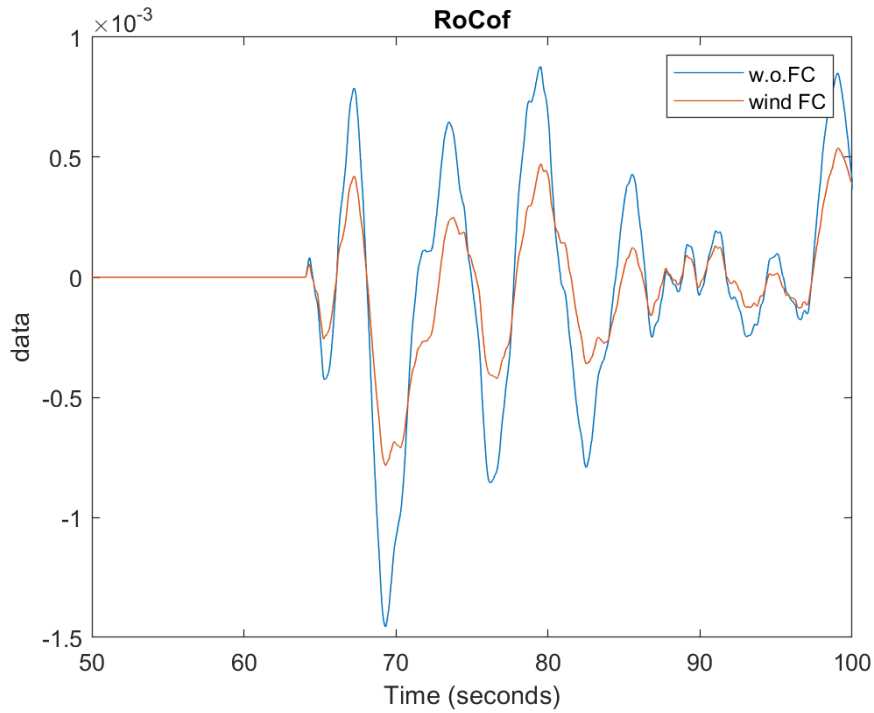


Figure 6.10: simulation 6 RoCoF

For what concerns the irradiance variation, simulation 8 has been inspired by the dynamic EN50530 test that is recognized as one of the techniques to evaluate the MPP tracking effectiveness [44]. It consists in a sequence of ramping up, constancy and ramping-down of the solar irradiance hitting the module.

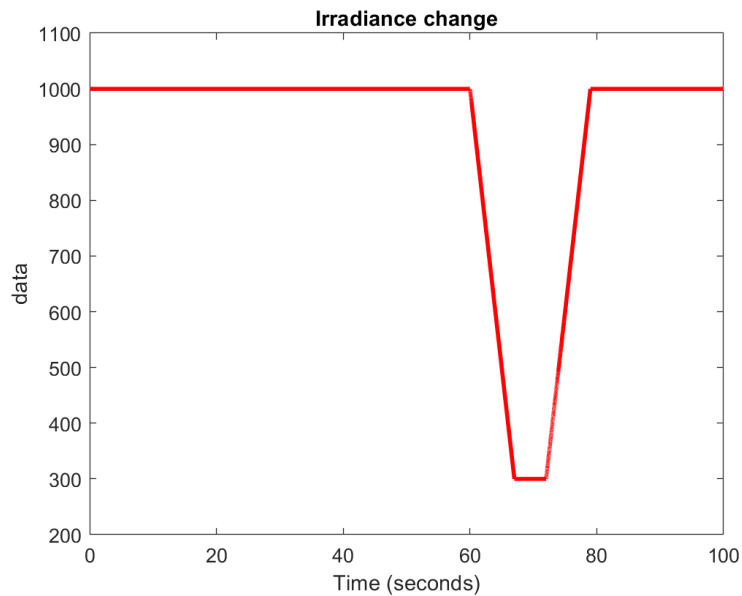


Figure 6.11: simulation 8 irradiance profile

In this case it has been adapted to model the shading of the PV modules consequent to the passage of a small cloud. As can be seen in Figure 6.11, it consists in a steep ramping down ($100 \text{ W/m}^2/\text{s}$) from the nominal irradiance of 1000 W/m^2 to 300 W/m^2 . Then, for few seconds, the irradiance remains low due to the shading, and then it increases with the same steepness again to its nominal value. This trend can be simply obtained on Simulink by using a switch to shift from a ramp-down block to a ramp-up block and inserting a saturation block at the outlet of the switch.

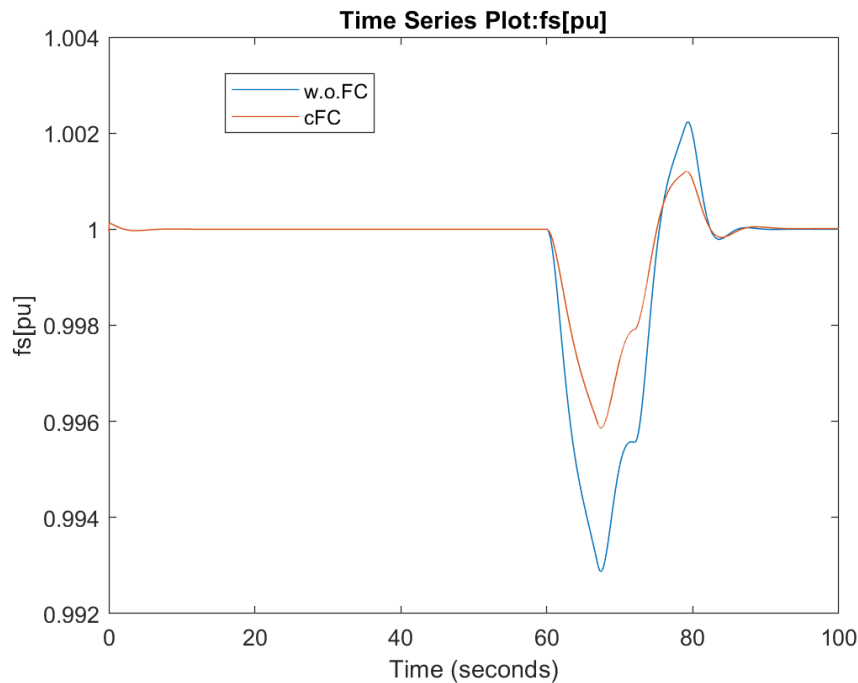


Figure 6.12: simulation 7 frequency trend

The system with the renewables participating in the primary frequency control shows also for variable irradiance to be more stable in terms of frequency, as depicted in Figure 6.12.

6.4. Increasing renewables penetration

The last scenario that this work wants to study is the more interesting in a long-time perspective. As explained in the introduction, in the future it is expected a large spread of renewable sources that will displace the conventional ones. In these simulations it is addressed the effect of such increase on the frequency stability, both in case of absence of frequency response capability by renewables and in presence of advanced controls implemented in this work.

It is important to remember the expected result of the tests in this first scenario: the increase of renewables penetration, due to their unpredictability and non-dispatchability, requires an increase in the reserve level, and at the same time displaces

the conventional plants which are responsible to operate the primary frequency control and contribute to system's inertia. Due to these facts, the magnitude of frequency nadir consequent to a perturbation is expected to increase as the penetration of renewables increases. The aim of the advanced controls, on the other hand, is to allow the substitution of the conventional fleet of generators with renewable ones without losing the ability to control the frequency. This is why, in the second case, smaller frequency nadir and frequency oscillations are expected.

When adapting the participation factors, it is really important to take into account that the displacement of synchronous generators causes a reduction of the system's equivalent inertia. In this work, it has been decided to vary it linearly with the synchronous generator participation factor. This means, for example, that if the participation factor of the equivalent steam turbine passes from 0.7 to 0.35, the equivalent inertia constant will be halved.

The first group of simulations regards an increase in VSWT penetration, whose results are shown in Figure 6.13.

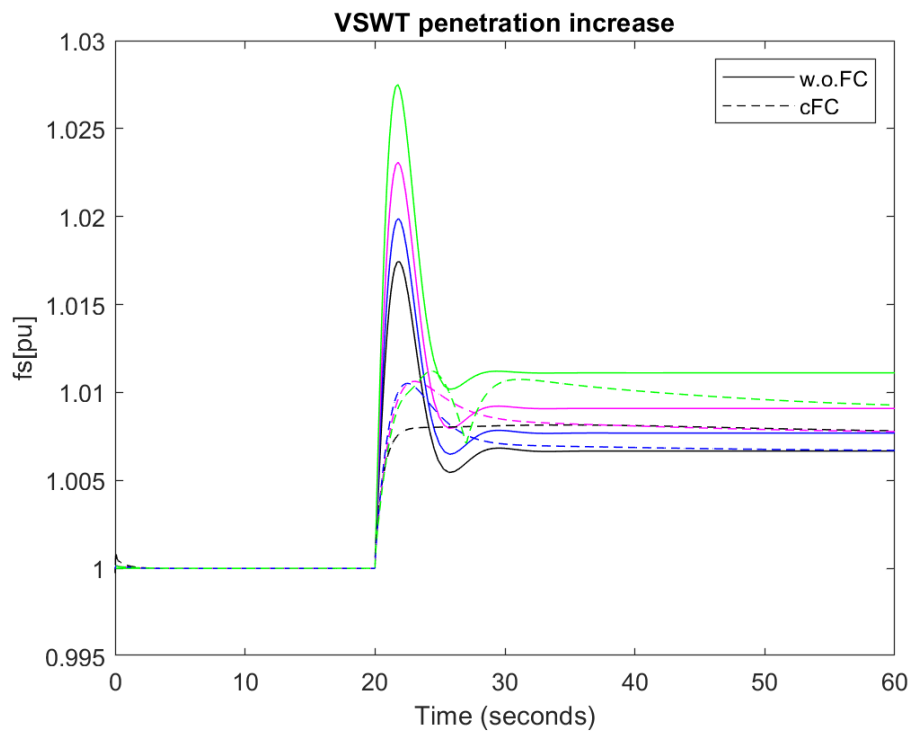


Figure 6.13: VSWT penetration increase

The continuous lines are representing the frequency variation consequent to a negative load power step of -10% in the scenario of primary frequency control operated just with synchronous generators, while the dashed lines are resulting from the scenario with *complete FC*. Taking a first look to the plot, it is immediately clear the negative effect of the increasing penetration of renewables if they are not able to participate to the primary frequency control. Indeed, for the same step of load power the nadir increases from 1.0174 pu of the base case (20% wind, 10% PV) to the 1.0275 pu in the

most extreme case (50% wind, 10% PV). Furthermore, the difference in terms of nadir between one curve and the other is not equal: increasing the wind penetration, the increase of nadir is larger and larger from one curve to the next one. This happens because there is not just an effect due to the reduction in the synchronous generator power variation weight, but also of the system's inertia.

Once stated this, it can be seen how large is the benefit associated to the introduction of the frequency response capability in renewables: the nadir is much lower than in the first scenario, and, as the penetration of VSWT increases, the mismatch between the two scenarios is way more evident. Unlikely to what happens in the first scenario, the nadir difference between the various curves in the second scenario reduces as the wind turbine penetration increases, witnessing that the provision of this service from renewables (in this case of course it prevails the effect of the wind turbines inertial control since their weight is dominant) is able to “cover” the reduction in system's inertia, improving the frequency stability.

The same kind of observations discerns from the other simulations, which regard an increase in PV penetration.

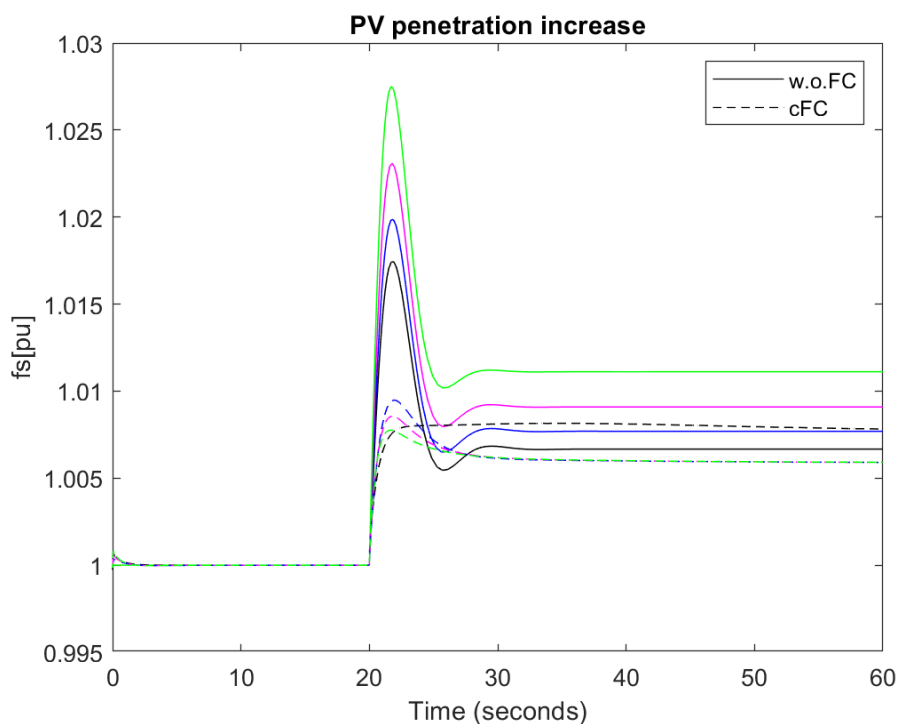


Figure 6.14: PV penetration increase

In this case the benefit is even larger, since, after a certain value of p_{pv} , the nadir even reduces as the penetration of photovoltaic increases. For example, in the most extreme case (40% PV, 20% wind), the nadir is lower than in the less PV-penetrated systems (10% PV, 20% PV and 30% PV).

In a future scenario it is not difficult to imagine power systems which are even largely penetrated by renewables. This case is studied in simulation 17, with the 80% of renewable participation. The correspondent results are shown in Figure 6.15.

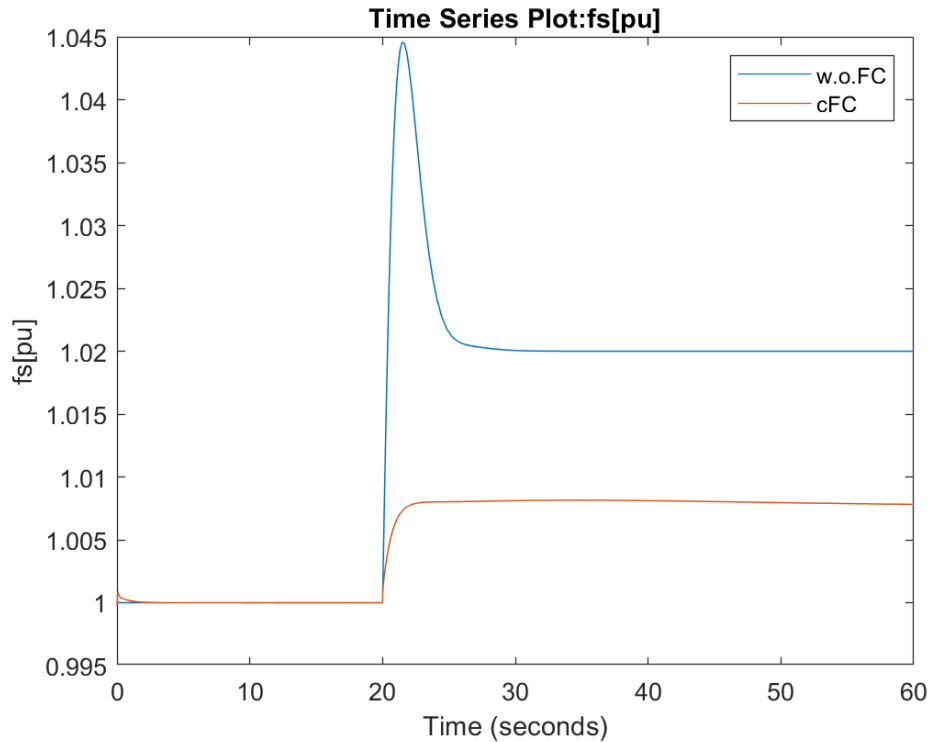


Figure 6.15: simulation 17 frequency trend

It is evident and huge the benefit obtained by the synergy between the Extended OPPT Method and the Power Reserve Control on the frequency stability. With such a renewables penetration the system's inertia is really small (-72% with respect to the base case), and at the same time a variation of power of the synchronous generator has just a small influence on the overall active power balance, accounting just for the 20% of the per unit common basis power. The consequence to a drop of load power is potentially critical: a frequency nadir of 1.0446 pu corresponds to 52.23 Hz, which is an incredibly large frequency deviation.

On the other hand, the introduction of renewables updated controls and their coordination allows to limit the nadir to 1.0082 pu (50.41 Hz), which is a perfectly acceptable value even facing an exceptionally strong perturbation event. By looking to the results of the two simulations (11 and 15) in which respectively wind and PV penetration are equal to 40% as in simulation 17, it can be observed that, if taken singularly, the frequency nadir is more accentuated, while in the seventeenth the trend of frequency is very flat. This fact enhances the idea that the two controls do not just act individually, but they support each other in the frequency control task, due to their different response rates but that integrate very well each other (Figure 6.16), obtaining a very smooth frequency trend and a satisfying frequency containment and stabilization.

Finally, it is really interesting to observe the effect of this control in a more dynamic situation. In particular, combining simulation 6 (variable wind profile + load power step -10%) with simulation 17 (40% wind, 40% PV) it is obtained the frequency profile shown in (Figure 6.17).

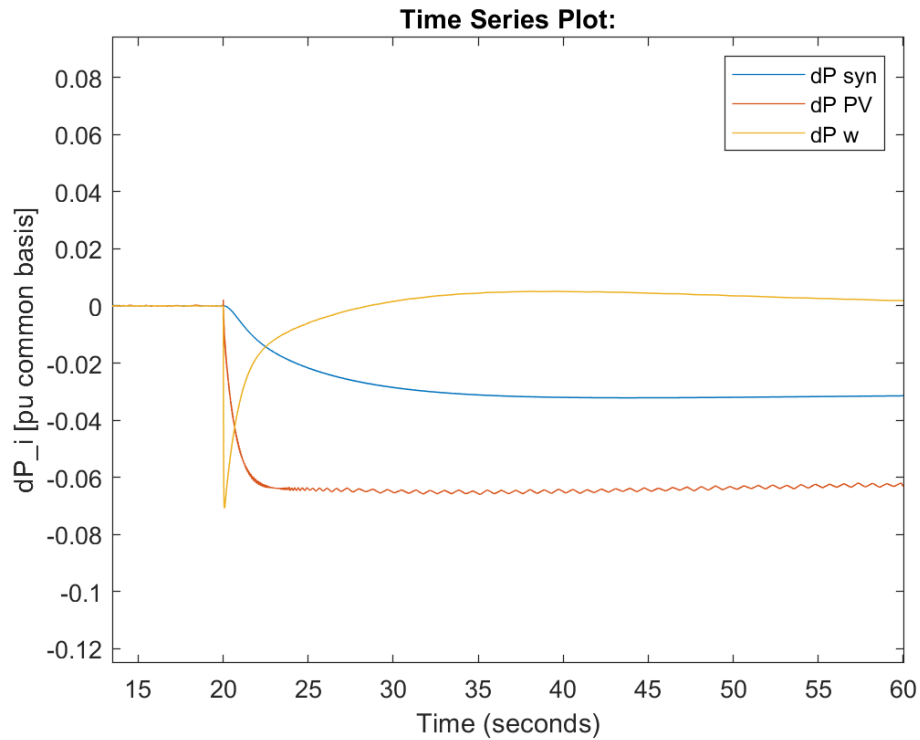


Figure 6.16: simulation 18 power variations

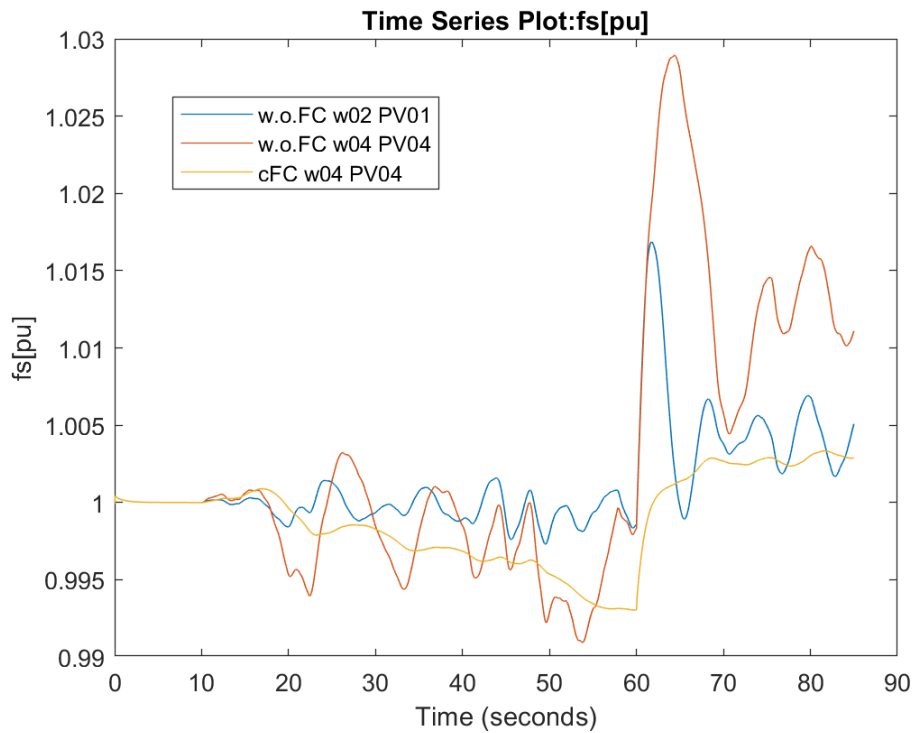


Figure 6.17: simulation 6 for different scenarios frequency trend

It can be observed that the variability of the wind, as already demonstrated, has an increasing effect on the frequency instability if the penetration of PV and wind turbine increases. If the system's inertia decreases, indeed, the system frequency is more sensible to the perturbation, included the step introduced at time 60 s. In case of updated control of renewables, when they are constituting the large majority of the generation fleet it is evident how good they control the frequency in case of variable wind profile, smoothing almost all the peaks produced. In this case the load step helps the system, together with an average wind speed increase, in keeping the frequency to proper values.

7 Conclusions and future developments proposals

After the detailed analysis of the results of the simulations of developed model shown in Chapter 6, it is possible to take stock of the work that has been carried out.

Looking ahead to a future in which renewables will be increasingly relevant in the energy mix, they have been implemented two strategies starting from the literature proposed models to make them able to help (or substitute) conventional generators in keeping the power system stable. In particular, Power Reserve Control and Extended OPPT Method have been adopted in this work aiming in allowing respectively photovoltaic modules and variable-speed wind turbines to participate to the primary frequency control. Indeed, the challenge of providing with non-programmable renewable generators the services that nowadays are operated by fossil fuelled plants will become more and more central as their presence will increase to a more significant level.

In this sense, the results obtained in this work, especially when the two controls coexist, are encouraging. Indeed, even if the Power Reserve Control introduces a very small increase of the RoCoF in the very few instants after a strong and sudden perturbation, the frequency nadir is reduced with respect to the case in which the frequency is not supported by renewables, especially in a future scenario in which they are massively present in the power system.

The model and the results rely on some simplifications, which make them general but at the same time lacking in detail. For this reason, there is open field for future developments of the present work in some areas.

One of the possible fields of improvement is the modelling of the photovoltaic system, in particular for what concerns the shading conditions and the inequality in the sun resource distribution among the modules. Indeed, this would allow a deeper study about the capability of photovoltaic systems in supporting the system's frequency in more realistic situations.

Another possible improvement regards the modelling of the load. Indeed, it could be really interesting to better characterize its active power demand profile in case of a small island, to make the study even more realistic and fitted on real field situations.

The last and more challenging proposal for future developments would be to model node by node a small system as the one studied in an overall way with the LFC approach in this work. This of course will make it completely fitted to a specific practical situation, allowing to catch some details that for sure with a general approach are invisible; at the same time, the adaptation to a very specific contest removes one of the biggest advantages of the LFC approach, which is the generality and the versatility of the developed model. Nevertheless, since the results obtained are promising, such improvements are for sure interesting and can add a lot of cues to go deeper in the knowledge of this argument that in the future will be at the centre of the scientific focus.

Bibliography

- [1] IEA. [Online]. Available: <https://www.iea.org/data-and-statistics/data-browser?country=WORLD&fuel=CO2%20emissions&indicator=CO2BySector>.
- [2] A. Mazur, "Does increasing energy or electricity consumption improve quality of life in industrial nations?", 2011.
- [3] IRENA, "Global Energy Transformation - a roadmap to 2050," 2019.
- [4] P. Kundur, Power System Stability and Control, electric Power Research Institute.
- [5] F. Díaz-González, M. Hau, A. Sumper, O. Gomis-Bellmunt, "Participation of wind power plants in system frequency control: Review of grid code requirements and control methods", 2014.
- [6] E.I. Batzelis, G.E. Kampitsis, S.A. Papathanassiou, " Power Reserves Control for PV Systems With Real-Time MPP Estimation via Curve Fitting", 2017.
- [7] A. Sangwongwanich, Y. Yang, F. Blaabjerg, D. Sera, "Delta Power Control Strategy for Multi-String Grid-Connected PV Inverters", 2017.
- [8] X. Li, H. Wen, Y. Zhu, L. Jiang, J. Hu, W. Xiao, "A Novel Sensorless Photovoltaic Power Reserve Control With Simple Real-Time MPP Estimation".
- [9] A. Hoke, S. Chakraborty, M. Shirazi, E. Muljadi, "Rapid Active Power Control of Photovoltaic Systems for Grid Frequency Support", 2017.
- [10] J. M. Riquelme-Dominguez, S. Martínez, "A Photovoltaic Power Curtailment Method for Operation on Both Sides of the Power-Voltage Curve," 2020.
- [11] A. Aziz, A. T. Oo, A. Stojcevski, "Frequency regulation capabilities in wind power plant", 2018.

- [12] K. Clark, N.W. Miller, J.J. Sanchez-Gasca, "Modelling of GE wind turbine-generators", 2010.
- [13] S. Engelken, A. Mendonca, M. Fischer, " Inertial response with improved variable recovery behaviour provided by type 4 WTs", 2017.
- [14] D. Ochoa, S. Martínez, "Fast-Frequency Response Provided by DFIG-Wind Turbines and its Impact on the Grid", 2017.
- [15] Y.-K. Wu, W.-H. Shu, T.-Y. Hsieh, T.-C. Lee, "Review of Inertial Control Methods for DFIG Based Wind Turbines", 2015.
- [16] G. Martínez-Lucas, J. I. Sarasua, J. I. Perez-Diaz, S. Martinez, D. Ochoa, "Analysis of the Implementation of the Primary and/or Inertial Frequency Control in Variable Speed Wind Turbines in an Isolated Power System with High Renewable Penetration. Case Study: El Hierro Power System", 2020.
- [17] D. Ochoa, S. Martínez, "A Simplified Electro-Mechanical Model of a DFIG-based Wind Turbine for Primary Frequency Control Studies".
- [18] D. Ochoa, S. Martínez, "Analytical Approach to Understanding the Effects of Implementing Fast-Frequency Response by Wind Turbines on the Short-Term Operation of Power Systems", 2021.
- [19] E. Council. [Online]. Available: <https://www.consilium.europa.eu/en/policies/climate-change/paris-agreement/>.
- [20] UNFCCC. [Online]. Available: <https://unfccc.int/process-and-meetings/the-paris-agreement/the-paris-agreement>.
- [21] European Environment Agency. [Online]. Available: <https://www.eea.europa.eu/ims/share-of-energy-consumption-from>.
- [22] IRENA, "Grid Codes for Renewable Powered Systems," 2022.
- [23] Fainan Hassan, Math Bollen, "Integration of the Distributed Generation in the Power System", IEEE Press, 2011.
- [24] Chin Kim Gan, Bashar Sabeeh Abdulraheem, "Power System Frequency Control Survey", 2016.

- [25] J. Paserba, V. Ajarapu, G. Andersson, P. Kundur et al., "Definition and Classification of Power System", IEEE, 2004.
- [26] A. Sguarezi, J. Stanley Bryant, M. Gu, E. R. Conde D., L. Meegahapola, "Power System Stability with Power-Electronic Converter Interfaced Renewable Power Generation: Present Issues and Future Trends", 2020.
- [27] UCTE, "P1 – Policy 1: Load-Frequency Control and Performance," 2009.
- [28] B. P. e. a. M. Saeedian, "Emulating Rotational Inertia of Synchronous Machines by a New Control Technique in Grid-Interactive Converters," 2020.
- [29] ENEA [Online]. Available: <https://www.energiaenergetica.enea.it/glossario-efficienza-energetica/lettera-p/potenza-efficiente-di-un-impianto-di-generazione.html#:~:text=Massima%20potenza%20elettrica%20erogabile%20per,efficienza%20e%20nelle%20condizioni%20ottimali..>
- [30] Terna, "Codice di rete - Capitolo 4 - Regole per il dispacciamento".
- [31] Terna, "PARTECIPAZIONE ALLA REGOLAZIONE DI FREQUENZA E FREQUENZA-POTENZA," 2008.
- [32] A. Kinshin, N. Ruban, A. Gusev, "Review of Grid Codes: Ranges of Frequency Variation".
- [33] R. Rajan, F. M. Fernandez, Y. Yang, "Primary frequency control techniques for large-scale PV-integrated power systems: A review".
- [34] Y. G. Rebours, D. S. Kirschen, M. Trotignon, S. Rossignol, "A Survey of Frequency and Voltage Control Ancillary Services—Part II: Economic Features", 2007.
- [35] O. Gandhi, D. Sampath Kumar, D. Rodriguez-Gallegos, D. Srinivasan, "Review of power system impacts at high PV penetration Part I: Factors limiting PV penetration".
- [36] J. M. Riquelme-Dominguez, F. De Paula Garcia-Lopez, S. Martínez, "Power Ramp-Rate Control via power regulation for storageless grid-connected photovoltaic systems".

- [37] A. Sangwongwanich, Y. Yang, F. Blaabjerg, "Development of Flexible Active Power Control Strategies for Grid-Connected Photovoltaic Inverters by Modifying MPPT Algorithms".
- [38] E.I., Batzelis, G.E., Kampitsis, S.A., Papathanassiou, " Power Reserves Control for PV Systems With Real-Time MPP Estimation via Curve Fitting", 2017.
- [39] G. Angenendt, S. Zurmuhlen, J. Figgner, K. Kairies, D. Uwe Sauer, "Providing frequency control reserve with photovoltaic battery energy storage systems and power-to-heat coupling," 2020.
- [40] C. Brivio, S. Mandelli, M. Merlo, "Battery energy storage system for primary control reserve and energy arbitrage".
- [41] National Renewable Energy Laboratory, "On the path to sunshot: The role of advancements in solar photovoltaic efficiency, reliability, and costs", 2016.
- [42] A.A. Solomon, D. Bogdanov, C. Breyer, "Curtailment-storage-penetration nexus in the energy transition", 2019.
- [43] S. Nanou, A. Papakonstantinou, S. Papathanassiou, "A generic model of two-stage grid-connected PV systems with primary frequency response and inertia emulation", 2015.
- [44] J.M. Riquelme-Dominguez, S. Martínez, "Systematic Evaluation of Photovoltaic MPPT Algorithms Using State-Space Models Under Different Dynamic Test Procedures", 2022.
- [45] K.V. Vidyandandan, N. Senroy, " Primary frequency regulation by deloaded wind turbines using variable droop", 2013.
- [46] M. Hwang, E. Muljadi, J.W. Park, P. Sorensen, T.C. Kang, "Dynamic droop-based inertial control of a doubly-fed induction generator", 2016.
- [47] P. Fairley, "Can Synthetic Inertia from Wind Power Stabilize Grids?," *IEEE Spectrum*, 2016.
- [48] Y. Fu, X. Zhang, Y. Hei, H. Wang, "Active participation of variable speed wind turbine in inertial and primary frequency regulations", 2017.

- [49] J. O’Sullivan, A. Rogers, D. Flynn, P. Smith, A. Mullane, M. O’Malley, “Studying the maximum instantaneous non-synchronous generation in an island system – Frequency stability challenges in Ireland”, 2014.
- [50] S. Li, C. Deng, Z. Shu, et al., “Equivalent inertial time constant of doubly fed induction generator considering synthetic inertial control”, 2016.
- [51] H. Ibrahim, N. Anani, “Variations of PV module parameters with irradiance and temperature”, 2017.
- [52] C. Carrero, D. Ramirez, J. Rodriguez, C.A. Platero, “Accurate and fast convergence method for parameter estimation of PV generators based on three main points of the I-V curve”, 2011.
- [53] T. Hardy, W. Jewell, “Emulation of a 1.5MW wind turbine with a DC motor”.
- [54] N. W. Miller, J. J. Sanchez-Gasca, W. W. Price, R. W. Delmerico, “Dynamic modeling of GE 1.5 and 3.6 MW wind turbine-generators”, 2003.
- [55] N. R. Ullah, T. Thiringer, D. Karlsson, “Temporary Primary Frequency Control Support by Variable Speed Wind Turbines- Potential and Applications”, 2008.
- [56] K. Clark, N. W. Miller, J. J. Sánchez-Gasca, “Modeling of GE wind turbine-generators for grid studies”, 2010.
- [57] Mathworks, “Mathworks,” [Online]. Available: <https://it.mathworks.com/help/simulink/ug/save-state-information.html#:~:text=To%20save%20just%20the%20logged,use%20the%20default%20xFinal%20variable..>
- [58] J. U. e. a. J. H. Eto, “Use of Frequency Response Metrics to Assess the Planning and Operating Requirements for Reliable Integration of Variable Renewable Generation”, Ernest Orlando Lawrence Berkeley National Laboratory, 2010.
- [59] DTU, “dtu.dk,” [Online]. Available: <https://gitlab.windenergy.dtu.dk/fair-data/winddata-revamp/winddata-documentation/-/blob/master/readme.md/>.
- [60] “<https://support.microsoft.com/en-us/word>”, [Online].

List of Figures

Figure 1.1: principle of primary frequency control.	8
Figure 1.2: impact of system inertia on frequency response.	10
Figure 1.3: Primary, secondary, and tertiary frequency control response.	11
Figure 1.4: proper dead band compensation for droop controllers.	13
Errore. L'origine riferimento non è stata trovata.	18
Figure 2.2: issues for high PV penetration related to this work topics.	19
Figure 2.3: P-V curve for a photovoltaic module for two different values of irradiance.	20
Figure 2.4: Power to frequency characteristic (P-f characteristics) for BESS providing FCR on the Central European market.	23
Figure 2.5: two-stage grid-connected PV system	25
Figure 2.6: single-stage grid-connected PV system.	25
Figure 2.7: indicative scenario of least squares curve fitting MPP estimation	26
Figure 3.1: Active power frequency control research study line in wind based power plants	30
Figure 3.2: Power rotor-speed curves for different values of pitch angle and deloaded options for a 1.5 MW wind turbine (wind speed: 10 m/s)	33
Figure 4.1: Typical time ranges in which the phenomena involved in the operation and control of a power system take place	36
Figure 4.2: developed model simplified scheme.	39
Figure 4.3: photovoltaic system model, including the electrical model (upper subsystem) and the voltage control (bottom subsystem).	40
Figure 4.4: voltage control subsystem.	41
Figure 4.5: <i>function_PV</i> body.	41
Figure 4.6: Solartech Power SPM210P datas.	42
Figure 4.7: <i>fcn_pv_mod</i> body - initialization.	42
Figure 4.8: <i>fcn_pv_mod</i> body – part 2.	43

Figure 4.9: single-diode model for the photovoltaic cell.	44
Figure 4.10: R_s , R_{sh} and n parameters.	44
Figure 4.11: <i>fcn_pv_mod</i> body – characteristic parameters.	45
Figure 4.12: <i>fcn_pv_mod</i> body – I-V characteristic.	45
Figure 4.13: <i>fcn_pv_mod</i> body – P-V curve.	46
Figure 4.14: <i>fcn_pv_mod</i> body: MPP.	46
Figure 4.15: <i>fcn_pv_mod</i> body: reference voltage for PRC.	46
Figure 4.16: example of resulting P-V curve with MPP and reference condition...	47
Figure 4.17: PV electrical scheme subsystem.	48
Figure 4.18: reserve adaptation scheme.	50
Figure 4.19: block scheme VSWT.	52
Figure 4.20: Wind turbine block parameters	52
Figure 4.21: Wind turbine power characteristics.	53
Figure 4.22: Gearbox conceptual representation.	54
Figure 4.23: mechanical system block scheme.	55
Figure 4.24: speed-governor block scheme.	56
Figure 4.25: <i>MPPT shifted</i> body.	57
Figure 4.26: Mechanics of the method based on virtual inertia control	57
Figure 4.27: DFIG block scheme.	59
Figure 4.28: DFIG dynamics state space model constants.	59
Figure 4.29: pitch control block scheme.	60
Figure 4.30: Virtual inertia control subsystem.	62
Figure 4.31: <i>term1</i> body.	63
Figure 4.32: <i>term2</i> body.	63
Figure 4.33: reheated steam turbine block scheme.	63
Figure 4.34: PV electrical scheme initialization variables.	66
Figure 4.35: PV system power initialization.	66
Figure 4.36: first model to be considered for PV system initialization.	67
Figure 4.37: PV output power switch.	68
Figure 4.38: switch block settings.	68
Figure 4.39: wind system initialization code for first guess values.	69

Figure 4.40: ω_{t_opt} and P_{opt} vs v_{wind} relationships.	70
Figure 4.41: frequency trend during initial transient.	71
Figure 4.42: regime dP_i after the initial transient.	72
Figure 5.1: number of PV strings.....	77
Figure 5.2: saving final state.	79
Figure 5.3: “to Workspace” block.....	79
Figure 5.4: callbacks for signal exporting to workspace.....	80
Figure 5.5: solver settings pane.	81
Figure 6.1: simulation 1 frequency trend.	84
Figure 6.2: simulation 1 RoCoF.	85
Figure 6.3: simulation 2 frequency trend.	86
Figure 6.4: simulation 3 frequency trend.	86
Figure 6.5: simulation 4 frequency trend.	87
Figure 6.6: simulation 4 dP generators.....	87
Figure 6.7: simulation 5 frequency trend.	89
Figure 6.8: wind profile.	90
Figure 6.9: simulation 6 frequency trend.	91
Figure 6.10: simulation 6 RoCoF.	92
Figure 6.11: simulation 8 irradiance profile.....	92
Figure 6.12: simulation 7 frequency trend.	93
Figure 6.13: VSWT penetration increase.	95
Figure 6.14: PV penetration increase.	95
Figure 6.15: simulation 17 frequency trend.	96
Figure 6.16: simulation 18 power variations.	97
Figure 6.17: simulation 6 for different scenarios frequency trend.	98

List of Tables

Table 1.1: European grid codes: frequency variation.....	14
Table 1.2: RoCoF limits.	14
Table 2.1: reviewed models for PV power reserve control.	24
Table 4.1: voltage control PI controller constants.	47
Table 4.2: capacitor and inductor parameters.	49
Table 4.3: fundamental parameters of the wind turbine model.	54
Table 4.4: speed governor PI controller parameters.....	58
Table 4.5: Extended OPPT method parameters.	62
Table 4.6: Synchronous generator model parameters.....	64
Table 4.7: VSWT Simulink block rotational speed and power characteristics.	70
Table 5.1: simulations groups and aims.	74
Table 5.2: summary simulations 1-8.	75
Table 5.3: summary simulations 9-17.	77

List of symbols

Variable	Description	SI unit
f	Frequency	Hz
t	Time	s
P	Power	W
H	Equivalent inertia constant	s
\mathcal{E}_{kin}	Kinetic energy	J
J	Moment of inertia	kg m ²
ω	Rotational speed	s ⁻¹
R	Droop constant	-
v	Voltage	V
i	Current	A
C_p	Coefficient of performance	-
λ	Tip speed ratio	-
ρ	Density	kg m ⁻³
β	Pitch angle	°
p_i	Participation factor	-
G	Irradiance	W m ⁻²
T	Temperature	K
R_s	Series resistance	Ω
R_{sh}	Shunt resistance	Ω
T_t	Low-speed shaft torque	N m
T_{em}	High-speed shaft torque	N m
K_i	Generic constant	-
D	Load damping const.	-
v_{wind}	Wind speed	m s ⁻¹

Acknowledgments

First of all, I would really like to thank the person who helped me developing this thesis, with a lot of patience, time and passion. Muchísimas gracias Profesor Martínez! I will be forever grateful to him for his support, not only technical but also personal. I also would like to thank my advisor in PoliMi, Professor Merlo, who has been always available in these months with his precious advices.

Thanks to my parents, who silently have been always on my side along this path that now comes to an end. I still can see all the anxiety and the difficulties of my studies, and in every second they were ready to support me.

Thanks also to my granparents, who hosted me in Milan in these years. One of the most valuable things that this experience gave me is the chance I had to know them deeper.

At the end I would like to thank my friends, the new and the old ones. To Salvatore and Giacomo in particular: we went together through thousands of battles and adventures, of coffees and jokes. Without good friends (almost brothers) it would be impossible to face small great challenges.

I would like to thank my university for the knowledges it gave me but even more for the people I met during this journey.

At the end, thanks to Oreste and Giovanni, who have always been a shoulder on which leaning and an incitement to discover new things.

